UNIVERSITY OF SÃO PAULO

GEOSCIENCE INSTITUTE

CO_2 mineralization process in basalt rocks: study case, Serra Geral Formation, Paraná sedimentary Basin, São Paulo state

VALENTINA ALZATE RUBIO

Master thesis presented to the Geosciences Program of Geochemistry and Geotectonic for obtaining the title of Master in Science

Concentration area: Geochemistry of exogenous processes.

Advisor: Prof. PhD. Colombo Celso Gaeta Tassinari

São Paulo

2023

Serviço de Biblioteca e Documentação do IGc/USP
Ficha catalográfica gerada automaticamente com dados fornecidos pelo(a) autor(a)
via programa desenvolvido pela Seção Técnica de Informática do ICMC/USP

Bibliotecários responsáveis pela estrutura de catalogação da publicação:
Sonia Regina Yole Guerra - CRB-8/4208 | Anderson de Santana - CRB-8/6658

Alzate Rubio, Valentina
CO2 mineralization process in basalt rocks: study case, Serra Geral Formation, Paraná sedimentary Basin, São Paulo state / Valentina Alzate Rubio; orientador Colombo Celso Gaeta Tassinari. -- São Paulo, 2024.
112 p.

Dissertação (Mestrado - Programa de Pós-Graduação em Geoquímica e Geotectônica) -- Instituto de Geociências, Universidade de São Paulo, 2024.

1. Basalt's petrography. 2. Whole rock geochemistry. 3. Carbon mineralization. 4. Carbon capture and geological storage. 5. Petrography . I. Gaeta Tassinari, Colombo Celso , orient. II. Título.

UNIVERSIDADE DE SÃO PAULO
INSTITUTO DE GEOCIÊNCIAS

CO2 mineralization processes in basalt rocks: Study case, Serra Geral Formation, Paraná sedimentary basin, São Paulo state

VALENTINA ALZATE RUBIO

Orientador: Prof. Dr. Colombo Celso Gaeta Tassinari

Dissertação de Mestrado

Nº 929

COMISSÃO JULGADORA

Dr.Colombo Celso Gaeta Tassinari

Dra.Haline de Vasconcellos Rocha

Dr.Alanielson da Câmara Dantas Ferreira

SÃO PAULO
2024

Dedication

To my beloved parents and Fabi,

This thesis is dedicated to you, with immeasurable gratitude and profound love. Your unwavering support, encouragement, and sacrifice have been the bedrock upon which my academic journey has been built. Your faith in me, even during my moments of doubt, has been a constant source of inspiration. Your sacrifice has allowed me to pursue my dreams with unrelenting determination. I am eternally grateful for it.

This thesis stands as a testament to the love and support you have generously bestowed upon me. It is a reflection of the values and principles you instilled in me, and a tribute to the incredible parents who have always believed in my potential, even when I haven't myself.

With all my heart, I dedicate this thesis to you, my pillars of strength, my mentors, and my greatest supporters. Thank you for being the wind beneath my wings, propelling me toward academic achievement and personal growth.

With deepest love and gratitude,

Valentina

Acknowledgments

I would like to express my heartfelt gratitude to all those who have been instrumental in the successful completion of my master journey. Without your support, guidance, and encouragement, this accomplishment would not have been possible.

First and foremost, I extend my sincere appreciation to my advisor Colombo, whose unwavering dedication, expertise, and invaluable insights have been the cornerstone of this research. Your mentorship has not only enriched my academic experience but also inspired me to push the boundaries of knowledge.

I am deeply indebted to the entire IGc – Geoscience Institute and IEE – Energy and Environment Institute for fostering an intellectually stimulating environment that nurtured my research endeavors. The collaborative spirit and resources provided by the institutes played a fundamental role in shaping the outcome of this thesis.

My gratitude extends across borders to my friends from another life, you have been a source of camaraderie, support, and moments of respite throughout this journey. Your presence, both in the academic and personal spheres, has made this experience all the more enriching.

To my friends in Brazil, o meu bloquinho de meninas, who have offered friendship, cultural exchange, unwavering encouragement and warm hugs. Your diverse perspectives and love have broadened my horizons and enriched my life.

Lastly, I would like to acknowledge all the individuals, institutions, and resources that have contributed to this thesis as well: The amazing technical support from Samuca from LTA laboratory, the Scanning electron microscopy laboratory, in charge of Eng. Isaac, the X-ray fluorescence laboratory and help of tec. José Paulo Sertek and the Optical microscopy laboratories of the IGc. I am also grateful for the support of the RCGI – Research Centre for Gas Innovation and sponsorship of Repsol Sinopec Brazil through the FUSP – Support Funding to the University of São Paulo Project 3801.

Thank you from the bottom of my heart.

Sincerely,

Valentina

Epigraphe

“I don’t wish you all sort of gifts.
I just wish you what most people don’t have:
I wish you the time to be happy and to laugh
and if you use it wisely, you can make something out of it.
I wish you the time for your actions and reflections,
time not only for yourself, but also to give away to others.
I wish you the time – not to hustle and run
but the time to be content.
I wish you the time – not to simply let it pass
I wish that you have enough time to be amazed and to trust,
and not simply to look at the watch.
I wish you the time to reach for the stars
and the time to grow, to mature
I wish you the time to hope and to love
It makes no sense to postpone this time.
I wish you the time to find yourself
to see happiness in each day and each hour.
I wish you the time also to forgive.
I wish you the time to live.”

- *ELLI MICHLER*

Resumo

Os basaltos da Formação Serra Geral, proeminentes na bacia do Paraná, são caracterizados pelo conteúdo mineral de Ca-plagioclásio, Ca-clinopiroxênio e vidro vulcânico, que liberam cátions Ca, Mg e Fe durante a hidrólise, facilitando a formação de carbonato nos poros da rocha. Este processo natural é usado na captura e armazenamento de carbono para remover permanentemente o dióxido de carbono e armazená-lo em reservatórios ígneos.

As indústrias do estado de São Paulo contribuem com 25% das emissões de gases de efeito estufa do Brasil, ressaltando a importância da implementação de estratégias de CCS. Este estudo tem como foco a região de Ribeirão Preto-Reginópolis, no estado de São Paulo, caracterizando a composição mineralógica e geoquímica dos basaltos da Fm. Serra Geral utilizando técnicas como petrografia óptica, fluorescência de raios X e MEV. Os resultados destacam dimensões favoráveis dos derrames basálticos para captura mineral, dominados por fácies pahoehoe simples e pahoehoe *pounded*, com conteúdo significativo de Ca-plagioclásio, Ca-clinopiroxênio e celadonita.

Apesar das variações geológicas, as formações basálticas apresentam potencial de mineralização consistente nos experimentos, enfatizando a aptidão do estado de São Paulo para projetos de injeção de CO_2 e mineralização de carbono. Portanto, essas descobertas sugerem perspectivas promissoras para a utilização de derrames basálticos como reservatório ígneo em iniciativas de CCS, dadas as suas características geoquímicas e texturais favoráveis, incluindo boas concentrações de cátions-chave e texturas litológicas propícias à mineralização de carbono.

Abstract

The Serra Geral Formation basalts, prominent within the Paraná basin, are characterized by mineral content of Ca-plagioclase, Ca-clinopyroxene, and volcanic glass, which release Ca, Mg, and Fe cations during hydrolysis, facilitating carbonate formation within the rock's pores. This natural process is used in Carbon Capture and Storage to permanently remove carbon dioxide and store it within igneous reservoirs.

Industries in São Paulo state contribute 25% of Brazil's greenhouse gas emissions, underscoring the importance of implementing CCS strategies. This study focuses on the Ribeirão Preto-Reginópolis region of São Paulo state, characterizing the mineralogical and geochemical composition of Serra Geral basalts using techniques like optical petrography, X-ray fluorescence and SEM. Results highlight favorable dimensions of basaltic flows for mineral trapping, dominated by simple pahoehoe and pounded pahoehoe facies, with significant Ca-plagioclase, Ca-clinopyroxene, and celadonite content.

Despite geological variations, the basalt formations exhibit consistent mineralization potential in the experiments, emphasizing São Paulo state's suitability for CO_2 injection and carbon mineralization projects. Therefore, these findings suggest promising prospects for utilizing basaltic flows in CCS initiatives, given their favorable geochemical and textural characteristics, including good concentrations of key cations and lithological textures conducive to carbon mineralization.

Table of Content

List of figures

List of tables

List of maps

1 Introduction

Mafic rocks, particularly basaltic formations, are highly favorable for Carbon Capture and Storage (CCS) (Gislason et al., 2010; Marieni and Oelkers, 2018; Clark et al., 2020). The mineralogy of basaltic formations primarily comprises Ca-plagioclase, Ca-clinopyroxene, and volcanic glass (Haldar and Tišljar, 2014). These minerals release Ca, Mg, and Fe cations when exposed to dissolved CO_2 in water due to their high reactivity during hydrolysis (Berger et al., 1994; Blum and Stillings, 1995; Oelkers and Gislason, 2001). The rich fluid transports dissolved chemical species, which then precipitate in the form of carbonates within the porous spaces of the rock, effectively fixing CO_2 within the atomic arrangement of the mineral crystals (Matter et al., 2011; Schaef et al., 2011).

Projects such as Carbfix in Iceland and Wallula in the United States demonstrate the feasibility of carbon mineralization through CO_2 injection in basalts. By 2024, Carbfix has captured and stored over 100,000 metric tons of carbon dioxide (CO_2) since its inception in 2014 (Carbfix, 2024). Wallula injected over 1000 tons of CO_2 in a supercritical state mineralizing 90% of it (McGrail et al., 2017b).

Understanding the mineralization process of carbonates includes the study of dissolution rates and alterations of these minerals (Cao et al., 2023). It is essential to determine optimal conditions such as temperature, pressure, and pH for maximizing cation release (Oelkers, 2001; Gislason and Oelkers, 2003; Gudbrandsson et al., 2011). The presence of acidic, gas-charged water accelerates the release of these ions and promotes the formation of carbonate minerals such as calcite, magnesite, and siderite, which preferentially consume the cations mentioned before (Snæbjörnsdóttir et al., 2017).

The Serra Geral Formation basalts in the Paraná Basin constitute one of the largest continental flood basalts globally (Rämö et al., 2016). This basin has an area of about 1700km^2 and reach depths of 6km in the basin center (Cañón-Tapia, 2018), it also has a sedimentary and magmatic record of more than 400 million years, containing important reserves of raw and secondary materials as well as the presence of two aquifer systems with water for public supply (Gastmans et al., 2013, 2016).

The Serra Geral Formation basalts have experienced long-term chemical and physical weathering due to their age of more than 135 million years (Rämö et al., 2016; Rossetti et al., 2018; Giovanardi et al., 2022). However, the secondary minerals resulting from hydrothermal alteration serve as indicators of the rocks' mineralizing capacity (Marieni and Oelkers, 2018), representing the desired outcome of CCS: carbonate minerals precipitated within vesicles and fractures of the basalt formation through the influence of CO_2-rich fluids (Rasool et al., 2023).

On the other hand, the São Paulo state industries, located in the western part of the Paraná basin, make up more than 25% of the greenhouse gasses emissions of the entire country (Medina Ketzer et al., 2015). By 2021, these emissions reached up 2.42 billion tons of equivalent CO_2 (Grattan, 2022), positioning Brazil as the fifth-largest emitter of greenhouse gas in the world. Therefore, deployment of CCGS in the Serra Geral Formation basalts would generate a positive effect on the diminution of those emissions and improvement in the strategies for climate change mitigation.

Carbon mineralization in basalts is still in the developmental stage in Brazil, with no operational projects and very few published works (Carneiro et al., 2013; Silva Ramos et al., 2023). Ongoing investigations and efforts are focused on enhanced oil recovery (EOR) in sedimentary sequences at the offshore petroliferous fields (Junior et al., 2023).

This study aims to characterize the overall mineralogical and geochemical composition of the Serra Geral Formation basalts in the Ribeirão Preto-Reginópolis region of the São Paulo state, before perform CO_2 injection experiments. Using traditional mineralogical and geochemical laboratory techniques, such as optical petrography, X-ray fluorescence and scanning electron microscopy, primary and secondary minerals will be identified along the geochemical bulk composition of the basalts.

With the acknowledge of the mineralogical and chemical composition of the basalts, will be possible to establish their potential for carbon mineralization (Schaef et al., 2010; McGrail et al., 2017a; Pogge von Strandmann et al., 2019) and to elaborate geochemical prospectivity maps for the Paraná basin as part of the conditioning layers for site selection of CO_2 injection. This geological characterization makes part of the Pre CO_2 injection phase of the MINE.CO_2 Project by Repsol Sinopec Brazil.

2 Literature Review

This chapter presents a brief review of the literature on geological carbon capture and storage, focused especially on the process of carbon mineralization in basalts and the efforts of global projects that are in operation. Then, it is presented a review of the geochemical context of the reactions that participate in the formation of carbonates by injection of CO_2, such as the dissolution rates of the main mineral phases that form basalt and give it its reactive character. Finally, the geological context of the Paraná sedimentary Basin is also described with interest in the basalts of the Serra Geral Formation.

2.1 Carbon capture and geological storage

Carbon capture and storage (CCS) technology is a crucial solution for mitigating climate change by removing CO_2 from industrial sources and the atmosphere and storing it permanently underground, commonly within geological formations (Raza et al., 2022). It is estimated that between 100 and 1000 gigatons (Gt) of CO_2 will be captured and stored by the end of the century (Van Pham et al., 2012; Romanak and Dixon, 2022; Ratouis et al., 2022). The use of saline aquifers and basalt formations in CCGS (Carbon Capture and Geological Storage) projects like Sleipner, Wallula, and CarbFix enables effective carbon mineralization (Michael et al., 2010; Peuble et al., 2015).

The urgency of CCS technology is underscored by the alarming rise in global CO_2 emissions, which remained over 30 Gt/year in recent years (Jackson and Garthwaite, 2023). The average annual CO_2 concentration in the atmosphere reached 419 ppm in 2023, nearly 51% above the level of the XVIII century, when the Industrial Revolution started (NOAA, 2023). In response to this crisis, the Paris Agreement was signed by 196 parties, aiming to limit global warming to 2°C and striving to keep it below 1.5°C compared to preindustrial levels, as outlined by the United Nations Framework Convention on Climate Change (UNFCCC, 2015).

CCU (Carbon Capture and Utilization) and BECCS (Bioenergy with Carbon Capture and Storage) are other promising approaches to combatting climate change by capturing and either permanently storing or re-purposing CO_2 emissions in forms of construction materials or new sources of energy (IEA, 2021), which complement the efforts in CCS technology and the goals of the Paris Agreement.

2.1.1 Reservoir types

Underground geological formations are used to storage CO_2 due to their wide range of geochemical and geomechanical properties. Depleted hydrocarbon reservoirs, saline aquifers, coal seams and shale formations are the most popular geological sites for storage because they are already characterized and proved (Michael et al., 2010; Temizel et al., 2016; Askarova et al., 2023). Composition and state of the CO_2 fluid injection along injection depth is going to depend on the reservoir geological setting. However, it is recommended to inject at depths greater than 600m, especially if there's presence of aquifers (IPCC, 2005), in order to avoid CO_2 leakage and aquifer contamination.

2.1.1.1 Saline aquifers

Deep saline aquifers are promising sites for CO_2 sequestration, potentially capable of storing up to 10,000 gigatons (Gt) of CO_2 globally (IPCC, 2005; GCCSI, 2008). Several trapping processes are responsible for securely retaining CO_2 within these aquifers, including hydrodynamic and residual trapping, as well as pore-size, solubility, and mineral trapping (Liu and Grana, 2020). The dynamics of brine accumulations are significantly influenced by convection currents generated by different density and concentration gradients. Various factors, such as multiphase flow dynamics, geochemical interactions, geomechanical properties, porosity, and permeability, impact CO_2 migration in relation to brine (Al Hameli et al., 2022).

Commercial operations like Sleipner, Snhvit, and In Salah have successfully injected around 15 million tons of CO_2 between 1996 and 2007 (Eiken et al., 2011). Numerous other pilot and commercial projects, including those in Gorgon, Australia, Nagaoka, Japan, and Ketzin, Germany have been proposed (Flett et al., 2009; Martens et al., 2011; Ogawa et al., 2011). While there is some uncertainty regarding the environmental consequences of aquifer CO_2 storage, research suggests that appropriate site selection can minimize adverse effects (Michael et al., 2010). Suitable aquifers should have impermeable caps to prevent CO_2 release and high permeability ($10^{-21}m^2$ nanodarcies) and porosity (<1%) beneath the cap for even CO_2 distribution. Leakage into groundwater sources, while theoretically possible, is unlikely (Doble et al., 2023). Chemical interactions between CO_2 and surrounding rock could lead to the formation of stable carbonates, extending CO_2 storage duration (Li et al., 2020).

2.1.1.2 Depleted oil and gas reservoirs

Depleted oil and gas reservoirs are highly suitable for long-term CO_2 storage due to their proven integrity and safety, evident in the fact that oil and gas have remained trapped within

them for millions of years due to structural and stratigraphic trapping (Hannis et al., 2017). The comprehensive geological analysis and established physical attributes of these reservoirs provide a solid foundation for CO_2 geological storage. Also, oil and gas companies have developed predictive computer models for hydrocarbon transport, displacement, and entrapment. Thus, the existing infrastructure and wells can be repurposed for CO_2 storage (Raza et al., 2018). These reservoirs, primarily comprising sandstone, limestone, and dolomite, offer a wide range of porosity and permeability for substantial CO_2 injection (Hughes, 2009; Hamza et al., 2021). In addition, presence of low permeability caprocks that minimize leakage provides a major advantage (Askarova et al., 2023). Moreover, in some cases, CO_2 can enhance CH_4 recovery and may be employed in enhanced oil recovery (EOR) (Rasool et al., 2023). Nevertheless, challenges exist, including the need to assess the condition of wells and caprocks, monitor pressures, and avoid injector clogging (Gauteplass et al., 2020). Careful management is essential to ensure both reservoir integrity and caprock stability (Hughes, 2009).

2.1.1.3 Enhanced oil recovery

The application of CO_2 flooding for enhanced oil recovery (EOR) has gained significant attention due to its economic advantages in increasing oil and gas production (Lainez and Castrillon, 2018). Primary production methods typically recover only a fraction of the initial oil in situ, and secondary recovery techniques like water flooding add limited additional yields (Yang et al., 2023). EOR methods, including CO_2 injection, have exhibited substantial potential for achieving enhanced oil recovery ranging from 7% to 23% (Al Hameli et al., 2022).

Various CO_2 injection strategies have been proposed, such as continuous injection and alternating water and CO_2 injection (Al-Mutairi and Kokal, 2011; Junior et al., 2023). The effectiveness of oil displacement by CO_2 is contingent on reservoir temperature, pressure, and oil composition. Up to 67% of the injected CO_2 may return with the produced oil, with the remaining portion retained in the reservoir through various mechanisms (Jin et al., 2017).

Optimizing CO_2-EOR requires specific reservoir criteria, including a minimum depth of 600 meters (Shehata et al., 2012). The choice between immiscible and miscible flooding hinges on factors like oil properties, temperature, and CO_2 purity. Reservoir characteristics, such as thickness, permeability and rock heterogeneity, also influence the efficiency of CO_2 storage (Ampomah et al., 2017). Reservoir heterogeneity can be advantageous, facilitating the more effective spread of CO_2 and thereby improving storage capacity (Zhao et al., 2016).

2.1.1.4 Coalbed Methane

In addition to conventional oil reservoirs, CO_2 injection has also been applied to enhance coalbed methane (CBM) recovery. Enhanced CBM recovery utilizes CO_2 to improve methane retrieval from coal seams (Mazzotti et al., 2009). This approach can be cost-effective and potentially offset storage expenses (Hernandez et al., 2006). The global potential for CBM is substantial, with connected CO_2 storage capacity (Al Hameli et al., 2022). The presence of wide coalbed fracture networks enables efficient gas movement and desorption of strongly adsorbed methane (Tambaria et al., 2022), ultimately boosting recovery rates up to 90% from the traditional 50% (Zarrouk and Moore, 2009). Post- retrieval methane, the injected CO_2 is stored, particularly in coalbeds at shallower depths, relying on CO_2 adsorption (Temizel et al., 2016). Successful projects in this domain include those in the San Juan Basin, Sydney Basin, and deep coalbed methane in Alberta (Pan and Wood, 2015).

2.1.1.5 Shale Reservoirs

Shale reservoirs have also been considered for carbon storage. These unconventional reservoirs, including shale oil and shale gas, share similarities with coalbeds in terms of CO_2 adsorption processes (Jin et al., 2017). CO_2-enhanced shale gas production, akin to ECBM, may help reduce storage costs. While the current CO_2 storage potential in oil or gas shale remains uncertain, the abundance of shale resources suggests substantial storage capacity, albeit limited by poor permeability (Godec et al., 2014). Benefits include CO_2-enhanced gas recovery and low leakage risk due to shale's tight properties and strong CO_2 adsorption capabilities (Busch and Gensterblum, 2011). Multiple studies have showcased successful carbon storage in unconventional shale gas formations, highlighting the potential for simultaneous CO_2 storage and enhanced hydrocarbon recovery (e. g. Khosrokhavar et al., 2014). Substantial progress has been made in evaluating the feasibility, economic benefits, and factors influencing the recovery process in these reservoirs, offering a promising pathway for CO_2 storage while tapping into untapped oil and gas resources (Sun et al., 2020).

2.1.1.6 Igneous Reservoirs

The injection of CO_2 into basalt formations is considered advantageous for geological storage, offering significant potential storage volumes and permanent carbon fixation through mineralization. Magmatic provinces in regions like the Pacific Northwest of the USA, the Deccan Plateau in India and the Paraná Etendeka in Brazil-Africa are viewed as suitable for storage due to their internal fractures and mineralization capacity (Raza et al., 2022). Ultramafic rocks, with higher magnesium, iron and calcium content, may offer even better potential for

storage. Basalt formations are praised for their widespread distribution, mineralization capacity, reactivity, and low risk leakage (Gislason and Oelkers, 2014). Moreover, deep-sea basalt presents an option for stable carbonate formation, particularly in Central-Atlantic magmatic provinces near urban centers (Goldberg et al., 2010).

Potential of offshore injection of CO_2 into volcanic sequences within the North Atlantic Igneous Province for large-scale permanent storage via carbonate mineralization has been studied. Investigations into the Faroe Islands Basalt Group reveal a range of porosities and permeabilities, with unmineralized brecciated lava flow crusts exhibiting the highest porosity. The capillary trapping mechanism in these formations is highly efficient, significantly limiting CO_2 mobility (Rosenqvist et al., 2023).

The Wallula Pilot Sequestration Project explores borehole geophysical data and core chemistry in the Columbia River flood basalt (PNNL, 2013). It highlights the cyclic nature of basalt flows with porous flow tops and massive flow interiors. Apparent porosity in flow tops significantly overestimates effective porosity obtained from hydraulic testing, while the interiors appear pervasively fractured, as observed in borehole images (Gislason et al., 2010; Zakharova et al., 2012).

The CarbFix pilot project seeks to improve techniques for permanently storing carbon dioxide (CO_2) in the basaltic rocks of the mid-ocean ridge of Iceland (Site: Carbfix.com). The project involves capturing and separating flue gases at the Hellisheidi Geothermal Power Plant, injecting CO_2 gas dissolved in water at elevated pressures at depths of 400-800 meters, and monitoring storage (Matter et al., 2011; Kristjánsdóttir and Kristjánsdóttir, 2021).

2.1.2 Carbon trapping mechanisms and reactions

As it is explained in the work of Zhang and Song (2014) and Al Hameli et al. (2022), carbon dioxide (CO_2) mobilization within a reservoir depends on multiple factors and trapping mechanism (Figure 1.1), so the permanent storage of CO_2 can be guaranteed. Injection of supercritical CO_2 ($_{sc}CO_2$) offers more advantages due to its density properties. Being denser than gaseous CO_2 allows taking more advantage of the pore space. Also, $_{sc}CO_2$ can adapt to temperature and pressure changes by phase changing. So $_{sc}CO_2$ can be stored in supercritical phase, or in liquid or gaseous state (Prasad et al., 2023) According to the different phase changes that CO_2 can undergo, different chemical reaction will occur, leading to a specific trapping mechanism.

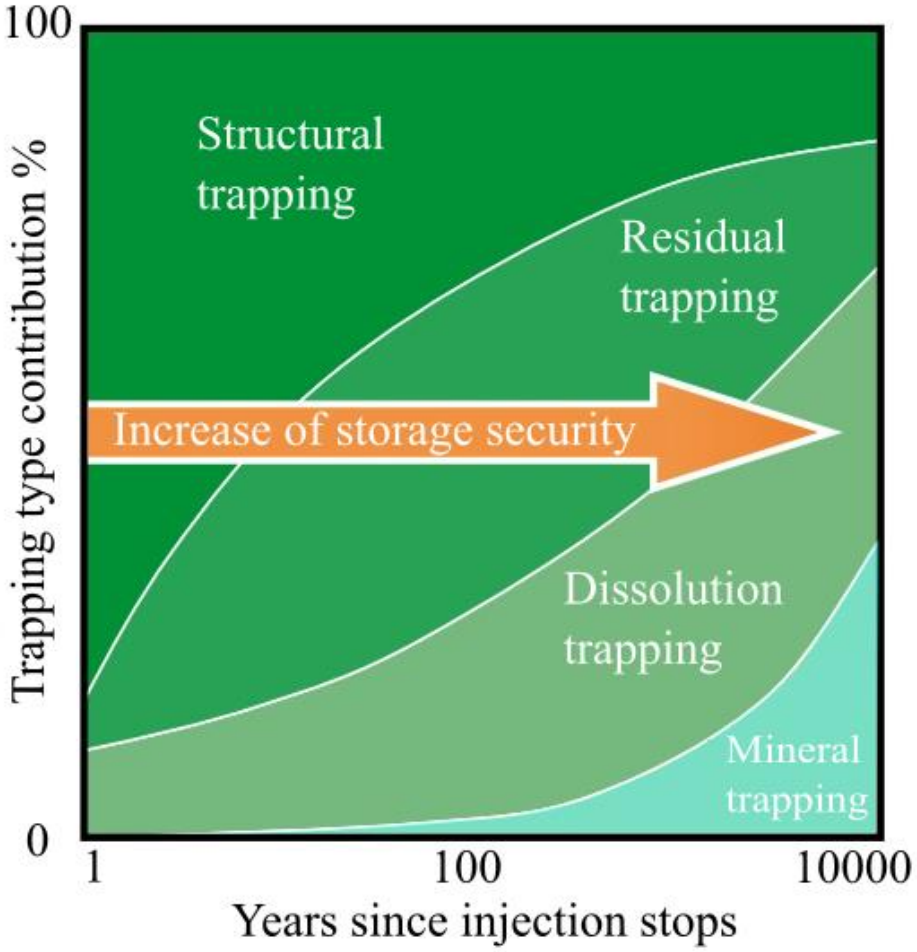

Figure 1.1 - Physical and geochemical trapping determine storage security of CO_2 within the reservoir. Being time dependent processes, mineral trapping turns into the most secure trapping mechanism. (Modified from IPCC, 2005).

2.1.2.1 Dissolution trapping

Dissolution or solubility trapping involves the dissolution of CO_2 within formation fluids, causing CO_2 to migrate upwards to the reservoir-caprock interface and then laterally beneath the caprock as a separate phase (Bolster, 2014). Upon contact with formation brine, CO_2 dissolves into the brine until an equilibrium state is achieved, dependent on factors like salinity, pressure, and temperature (Szulczewski et al., 2013). This dissolution process is slow due to molecular diffusion, taking thousands of years for complete CO_2 dissolution in brine (Figure 1). The denser CO_2-saturated brine sinks due to gravity, enhancing CO_2 trapping and increasing storage capacity (Anchliya et al., 2012). The dissolution-diffusion-convection (DDC) process is crucial for CO_2 storage efficiency, with studies showing it can improve storage capacity and

reduce CO_2 migration through caprock, impacting storage estimations and caprock integrity assessment (Pruess and Müller, 2009; Al Hameli et al., 2022).

2.1.2.2 Adsorption trapping

This mechanism involves the adsorption of CO_2 onto sandstones. limestones and dolomite reservoirs, as well as in organic materials present in coals and shales, particularly in shale gas reservoirs (Hamza et al., 2021), thanks to the clay minerals and organic particles present in the composition of these lithologies. CO_2 adsorption in the micropore surfaces of coal seams, allows greater CO_2 storage at shallower depths than in other sedimentary reservoirs (Golding et al., 2011). Gas in shale reservoirs exists in the form of free gas and adsorbed gas. The last one is highly influenced by the content of total organic carbon (TOC) and clay because of their porosity, pore volume and specific surface area, as is indicated in the work of Xie et al. (2021). Thus, at higher TOC and clay content, adsorption increases.

Adsorption, involving strong intermolecular interactions between gas molecules (typically CH_4 or CO_2) and solid shale surfaces, is an exothermic process. Desorption, conversely, is endothermic, and both play vital roles in gas generation and CO_2 sequestration in shale gas reservoirs (Dang et al., 2017). Successful hydraulic fracturing triggers desorption from shale surfaces to matrix pores and fractures, facilitating gas production (Tian et al., 2022). If CO_2 is sequestered in a shale gas reservoir, this process is reversible (Xie et al., 2021). Adsorption and desorption in nanopores are important for CO_2 injection efficiency, particularly in the presence of organic matter (Merey and Sinayuc, 2016). CO_2 adsorption process can reduce gas saturation in rock pores, being the second-order mechanism after CO_2 miscibility and dissolution in liquid. This effect is amplified in formations with higher total organic carbon (TOC), as discussed by Lashgari et al. (2019).

2.1.2.3 Structural trapping

Structural or stratigraphic trapping, represents the most common mechanism in geological sequestration and, as can be observed in Figure 1, has effectively preserved subsurface oil and gas reservoirs for centuries (Zhang and Song, 2014). As it has been stated in previous works (e.g. Bradshaw et al., 2007; Shukla et al., 2010a), this process relies on geological features like anticlines covered by impermeable caprocks and stratigraphic traps, sometimes with sealed faults, for the storage of CO_2 in either its aqueous or supercritical state. In structural trapping, CO_2 ascends to the top of geological formations beneath a non-permeable seal, where it remains trapped due to capillary pressure (Michael et al., 2010). Ensuring the optimization of this

storage mechanism is vital to maintain CO_2 injected underground for an extended period. During injection, CO_2 migration in the target formation is primarily controlled by viscosity forces and stored according to depth, existing as supercritical or gaseous phases based on specific pressures and temperatures. Once injection concludes, supercritical CO_2 has a tendency to migrate upwards due to buoyancy and laterally through preferential pathways until encountering a caprock, fault, or another sealing barrier, preventing further movement (Anchliya et al., 2012).

2.1.2.4 Hydrodynamic trapping

This physicochemical trapping is a complex mechanism for CO_2 containment in reservoirs or saline formations, bridging the gap between chemical and physical trapping. It involves a slow migration of CO_2 over an extended period, leading to entrapment through residual, solubility, or mineral mechanisms (Bachu et al., 1994). As is explained by Johnson et al. (2004), in saline formations, hydrodynamic trapping can occur gradually, displacing saline water due to CO_2 lower density. It ascends buoyantly to the formation's top, continues moving as a distinct phase, and eventually gets entrapped as residual CO_2 or within structural or stratigraphic traps within the sealing formation. Over time, CO_2 dissolves in formation water and travels with groundwater, often spanning millions of years for fluids to reach the surface. Hydrodynamic trapping essentially serves as a common link among various trapping mechanisms, ensuring long-lasting CO_2 containment in reservoirs (Wang et al., 2022).

2.1.2.5 Residual trapping

The residual capillary trapping is a key process for enhancing capacity and integrity of CO_2 storage on industrial reservoirs (Niu et al., 2015). Initially, when CO_2 is introduced into the reservoir, it displaces brine in a co-current fashion. Upon cessation of injection, due to the density contrast between CO_2 and brine, a counter-current flow ensues, causing CO_2 to migrate upward while brine moves downward (Md Yusof et al., 2022). Consequently, brine infiltrates pores, leading to CO_2 displacement and the substantial saturation of CO_2 becoming trapped in small pore clusters, often referred to as capillary or residual trapping (Suekane et al., 2008; Zhang and Song, 2014; Al Hameli et al., 2022).

The surface tension at the CO_2-brine interface raises the capillary entry pressure, effectively immobilizing CO_2 in the pores due to residual gas saturation (Rasmusson et al., 2018). This mechanism is highly efficient, restricting CO_2 mobility, and significantly impacts CO_2 migration and distribution within geological formations, subsequently affecting the

effectiveness of other trapping mechanisms (Raza et al., 2017). Experimental and numerical modeling studies have demonstrated the significant impact of capillary trapping on CO_2 storage, emphasizing its role in limiting CO_2 movement and enhancing overall trapping efficiency (Shukla et al., 2010b). Factors such as injection rates, formation pressure, and heterogeneity play critical roles in determining the final immobilized CO_2 saturation, with higher viscosity to gravity force ratios and increased heterogeneity enhancing CO_2 trapping as residual gas (Niu et al., 2015).

2.1.2.6 Mineral trapping

Mineral trapping involves the interaction of CO_2 with minerals within a geological formation, leading to gradual dissolution in formation water and initiating diverse geological reactions (Pearce et al., 2022). These reactions can either benefit the containment of CO_2 through the formation of new carbonate minerals (Iglauer, 2017; Pogge von Strandmann et al., 2019; White et al., 2020) or aid in CO_2 migration (Shabani et al., 2022), depending on the specific circumstances. The outcome hinges on the formation's structure, mineral composition, and hydrogeology. CO_2 in the aqueous phase acts as a weak acid, reacting with rock minerals to create bicarbonate ions, influenced by the formation's mineral content. The precipitation of CO_2 minerals is contingent upon the rock formation's mineralogy (Rochelle et al., 2004). In first instance, the success of CO_2 sequestration depends on accurate geochemical modeling. Factors like mineral content, gas pressure, temperature, and rock porosity significantly impact the effectiveness of the trapping process, making it a complex and context-specific mechanism (Xu et al., 2007).

2.1.3 Carbon mineralization in basalts

The carbon mineralization process involves several steps. First, CO_2 is captured from industrial sources or directly from the atmosphere. It is then pressurized and injected into deep basalt formations through wells drilled into the rock (Clark et al., 2020).. The high pressure facilitates the dissolution of CO_2 into water, which reacts with the basaltic mineralogical content (GCCSI, 2018; Ernst, 2021).

Once inside the basalt, the dissolved CO_2 undergoes a series of reactions with cations such as calcium, magnesium, and iron, forming solid carbonate minerals like calcite, magnesite, and siderite (Schaef et al., 2011; Zhang and DePaolo, 2017). These carbonates are chemically stable and can remain trapped in the rock for millions of years, effectively removing CO_2 from the

atmosphere and preventing its release back into the environment. Carbon mineralization in basalts offers several advantages as a carbon capture and storage (CCS) technique.

Basalt formations are globally abundant and can potentially store important amounts of CO_2 (White et al., 2020; Ratouis et al., 2022). The process is naturally occurring and has been observed in nature, indicating its long-term stability (Voigt et al., 2021). Additionally, the reactions occur relatively quickly, allowing for efficient capture and storage of CO_2.

However, accurately quantifying mineralization during injection remains challenging due to the intricate interplay of dissolution, precipitation, and adsorption processes (White et al., 2020). Furthermore, the influence of naturally occurring minerals adds complexity to this assessment. To tackle this, studies rely on numerical modeling, hydrological testing, and borehole data analysis to evaluate mineralization processes and mitigate potential long-term leakage risks (Fisher, 1998; Marieni and Oelkers, 2018; Mahzari et al., 2021).. Despite the pressing need for efficient carbon capture and storage strategies, determining the storage capacity equations for basalt reservoirs remains a work in progress.

One significant challenge arises from the rapid mineral carbonation occurring in basalts, which can alter storage capacity dynamically.(Okoli et al., 2024). The complex chemical reactions and physical phenomena involved, including pore throat clogging influenced by pressure, temperature, wettability, rock matrix characteristics, and fluid composition, make accurate storage capacity estimation in basalt formations a difficult task. McGrail et al. (2006) considered the Columbia River basalts and, using the volumetric method based on average parameters like thickness, porosity, and hydrostatic pressure, estimated a CO_2 storage potential exceeding 100 Gt. Nonetheless, the inherent variability and complexity of such geological systems necessitate ongoing research to refine these estimations.

2.1.4 Global CCS projects

As it was presented in the section of Igneous Reservoirs 2.1.1.6, the distribution of basaltic provinces is global. They can be found in Northmerica (CR, Keweenawan, Newark and Hartford), India and Pakistan (Decan traps), China (Emeishan and Hannuoba), Siberia (Siberian Traps) and the North Atlantic mid-ocean ridge basalts, covering areas from 500km^2 to 2200km^2 (McGRail, 2003). Basalts from these provinces has been studied and tested for

carbon mineralization in order to permanently and massively storage CO_2, being successfully in operation the CarbFix project and in proven state the Wallula Project.

Another successful operational CCS projects are found in Norway (Sleipner field) and in Brazil (Santos basin). They implement CO_2 injection in sedimentary formations such as saline aquifers and depleted reservoir to recover oil and gas, keeping a nearly neutral CO_2 emission footprint. These projects are pioneer in the CCS field due to their relation to the oil and gas industry and having developed base methodologies useful for CCS pilots in igneous reservoirs.

2.1.4.1 Carbfix

The Carbfix project is a pioneering initiative aimed at mitigating carbon dioxide (CO_2) emissions by injecting and mineralizing CO_2 in basaltic rock formations. It was initially launched in Iceland in 2007 as a collaboration between the University of Iceland, Reykjavik Energy, and other partners and it has injected more than 95000 MT (metric tons) of CO_2 since 2014 (Carbfix, 2022; Matter et al., 2011).

From the injection experience in Iceland, it is known that to achieve permanent containment of CO_2 in a geological reservoir, adequate formation porosity, permeability, and spread are required, as well as a trapping mechanism to prevent CO_2 migration and leakage (Callow et al., 2018; Ratouis et al., 2022). Numerical models are used to characterize the behavior of CO_2, its fluid path and monitoring (Mahzari et al., 2021; Raza et al., 2022). Thus, in Carbfix the dissolution of the gas in water and the rapid mineralization of the dissolved gas in stable minerals are combined for CO_2 trapping (Pogge von Strandmann et al., 2019).

Geochemical and sample monitoring and analysis are used to confirm mineralization in the reservoir (Van Pham et al., 2012; Schott et al., 2016; Snæbjörnsdóttir et al., 2017). The monitoring data is used to calibrate and create numerical models that forecast the short- and long-term injection of gasses into the reservoir. Finite volume codes, such as TOUGH2 and PHREEQ, are used for numerical simulation in porous and fractured media (Ratouis et al., 2022).

The conceptual model of the injection site integrates geological features, physical processes, and data from wells, including testing, production, and tracers (Alfredsson et al., 2013). At the Carbfix injection site, olivine basaltic and hyaloclastic sequences are found at depths of around 1000 meters, with temperatures between 220 °C and 250 °C (Snæbjörnsdóttir et al., 2017).

2.1.4.2 Wallula

The Wallula Project was a geologic carbon sequestration field demonstration led by the Pacific Northwest National Laboratory (PNNL) (White et al., 2020). The project aimed to investigate the feasibility of injecting CO_2 into basalt formations for long-term storage. The injection site was located near Wallula, Washington, in the Columbia River Basalt Group.

Approximately 1000 tons of supercritical CO_2 were injected into deep Columbia River Basalt zones. Two years after the CO_2 injection, rock core samples were extracted from the injection zone for analysis. The samples revealed the presence of authigenic carbonate mineralization. A new analysis of pre- and post-injection hydrologic tests revealed that around 60% of the injected CO_2 was mineralized within two years, occupying about 4% of the reservoir pore space (McGrail et al., 2017a; White et al., 2020). This analysis method offers a way to quantify mineralization and monitor CO_2 storage in basalt formations and other carbon storage reservoirs.

Furthermore, a detailed analysis of pre-injection and post-injection hydrologic tests was conducted (Schaef et al., 2011). This analysis leveraged the differences in fluid properties between supercritical CO_2 ($scCO_2$) and water to assess changes in near-field, wellbore, and reservoir conditions approximately two years after the injection ended (McGrail et al., 2017a).The monitoring and analysis techniques developed during the Wallula Project can also serve as valuable tools for assessing the behavior of injected CO_2 in basalt.These methods provide insights into the efficiency and effectiveness of CO_2 sequestration and can aid in the long-term monitoring and verification of storage sites.

2.1.4.3 Sleipner

The Sleipner project is a pioneering carbon capture and storage (CCS) initiative located in the North Sea, operated by Equinor (formerly Statoil) (Bickle et al., 2007; Williams and Chadwick, 2012; Furre et al., 2017). It began in 1996 and primarily focuses on the storage of CO_2 emissions from natural gas production. The project specifically targets the Sleipner West gas field, where the extracted natural gas contains high levels of CO_2. To prevent the release of CO_2 into the atmosphere, the extracted CO_2 is separated from the natural gas stream and then compressed for transportation (Van Den Broek et al., 2010). Instead of being released, the captured CO_2 is injected deep underground into the Utsira Formation, a porous sandstone layer located beneath the seabed (Pratikna et al., 2022). The Utsira Formation acts as a caprock, securing geological storage site, effectively trapping and storing the CO_2. As it is detailed in the works of Eiken et

al., (2011) and Furre et al. (2017) The Sleipner project has been successful in reducing greenhouse gas emissions, with over one million tons of CO_2 being captured and stored annually. It has played a significant role in demonstrating the technical feasibility and safety of CCS technology, showcasing that large-scale CO_2 storage can be achieved. The project has been operating for more than two decades, making it one of the longest-running CCS initiatives in the world.

2.1.4.4 Santos basin EOR

Enhanced Oil Recovery (EOR) techniques are utilized in the oil industry to maximize the extraction of hydrocarbons from reservoirs (Michael et al., 2010). The Santos Basin, located in the Brazilian offshore, is a prolific hydrocarbon producing region known for its significant offshore oil reserves (Ciotta, 2022). Different EOR methods have been employed in the Santos Basin to enhance oil recovery and optimize production (Junior et al., 2023).

One of the EOR techniques employed in the Santos Basin is gas injection, particularly carbon dioxide (CO_2) injection. CO_2 injection can improve oil recovery by reducing the oil's viscosity and swelling it, allowing for easier flow (Jamekhorshid and Azin, 2023). Additionally, CO_2 injection can lead to the extraction of additional oil through mechanisms such as miscibility, swelling, and extraction of dissolved oil (Benson and Cole, 2008). However, the availability and sourcing of CO_2 are important considerations in implementing this method. Furthermore, in the Santos Basin has been applied other EOR methods such as thermal methods, including steam injection, which can help reduce oil viscosity and enhance its mobility for improved recovery.

All 21 platforms operated by Petrobras in the pre-salt region of the Santos Basin are equipped with CCUS technology for Enhanced Oil Recovery (EOR) (Petrobras, 2022). The incorporation of this technology has led to continuous improvement in performance. By injecting CO_2 into the reservoir, Petrobras enhances the efficiency of oil production while simultaneously reducing greenhouse gas (GHG) emissions on a per-barrel basis. This approach allows Petrobras to operate with lower costs and a reduced carbon footprint, ensuring the competitiveness of the project.

In 2022, they achieved a significant milestone by injecting a record 10.6 million metric tons (MT) of CO_2 for CCUS purposes (site: Petrobras.com.br). This volume accounted for approximately 27% of the total gas injected in Petrobras' pre-salt fields and about 25% of the

total CO_2 injected by the entire industry during that year, as reported by the Global CCS Institute.

2.1.4.5 CCGS Project making and social perception

The public perception of Carbon Capture and Storage (CCS) technology is a critical aspect of its successful implementation. Diverse studies explore the significance of public engagement and social acceptance in CCS projects, emphasizing the importance of public understanding of the risks and benefits associated with the technology (e. g. L′Orange Seigo et al., 2014). Effective communication by project proponents, along with robust measures for public engagement, is crucial for fostering acceptance and trust in CCS initiatives. Furthermore, authoritative decision-making processes that transparently reflect the outcomes of public engagement are essential for building confidence in CCS among stakeholders (Netto et al., 2021).

In addition to technological, economic, and environmental considerations, social acceptance emerges as a decisive factor for the deployment of CCS technology. The study highlights the limited research on public perception of industrial CCS (iCCS) and emphasizes the need to understand the factors influencing acceptance for policy and industry decision-making (Witte, 2021). Concerns about safety, political risks, and the displacement of other climate change mitigation efforts are identified as key factors shaping public perception of CCS. Effective risk communication, early engagement of local communities, and identification of local benefits are proposed strategies to enhance acceptance and trust in CCS initiatives (Leiss and Larkin, 2019). Local communities' prior experiences, perceived fairness in decision-making processes, and identification of tangible benefits are key determinants of acceptance.

Project developers must engage with local stakeholders early in the planning stages, prioritize transparent communication, and build partnerships with trusted community organizations to address concerns and maximize social acceptance (Wallquist et al., 2012). Overall, the investigations underscore the importance of integrating social acceptance considerations into CCS planning and implementation processes to ensure its successful deployment as a climate change mitigation strategy.

2.2 Geochemical framework

To explain the reactive character of basalt, it is necessary to start by defining its composition. The types of magmas depend on each tectonic environment and the crystallization of its mineral phases. The mineral phases of basalt present different dissolution rates when they come into contact with fluids rich in CO_2. This section describes the characteristics of these processes, involved in carbon mineralization.

2.2.1 Basalt composition

Magma is a silicate melt formed due to thermal and density instabilities in the mantle and crust (Marsh, 2015). It is primarily generated through partial melting of a parent rock, regardless of its composition. This buoyant magma can ascend, leading to volcanism, or become stalled at depth, resulting in plutonism (Koppers and Sager, 2014). This overall process is known as magmatism.

Flood basalts are extensive basaltic formations that rapidly erupted onto continents, such as the Columbia River Basalts, Deccan Traps, and Paraná Etendeka Province (Cañón-Tapia, 2018; Ernst, 2021). These basalts consist mainly of tholeiitic composition and are thought to originate from mantle plumes or melting of the subcontinental lithosphere triggered by mantle plumes (Koppers and Sager, 2014).

Continental flood basalts exhibit lower levels of Mg, Fe, and other compatible elements compared to mid-ocean ridge basalts (MORB) or island basalts (Wang et al., 2015). They often display enrichment trends in Fe but can have lower Ti than other oceanic basalts. Incompatible element distributions vary widely within flood basalts, even within the same volcanic field (Macdougall, 1988).

The mineralogy of basaltic formations consists of mainly three components: Ca-plagioclase [$(Na,Ca)(Si,Al)_4O_8$], Ca-clinopyroxene [$Ca(Mg,Fe)(SiAl)_2O_6$] and volcanic glass, according to Bowen's reaction series (Figure 2.2). This composition also determines the viscosity and crystallinity of the magma (Marsh, 2015).

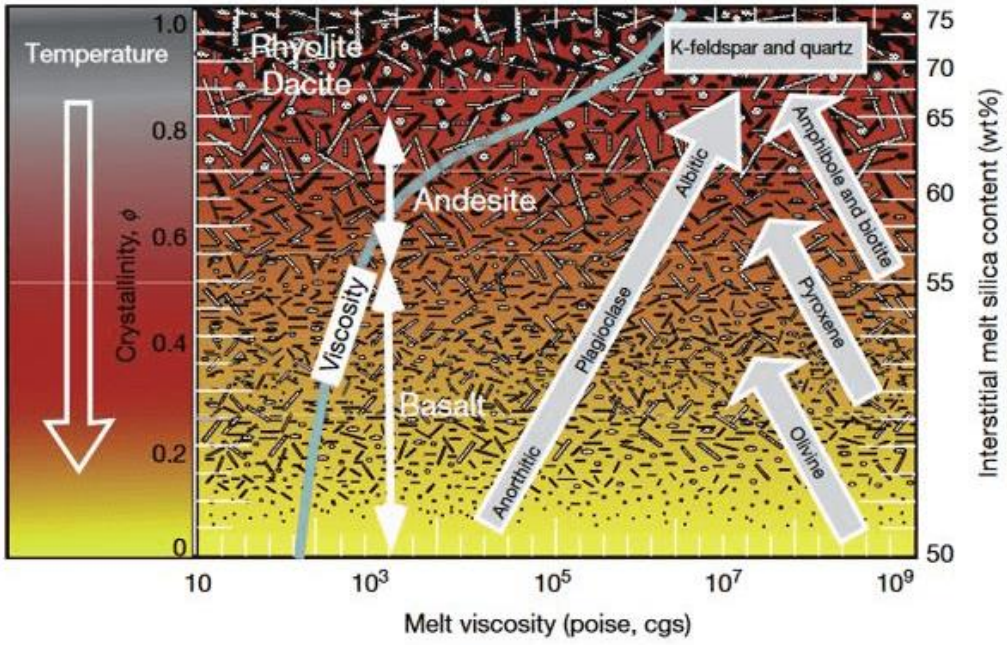

Figure 2.2 - Bowen's crystallization series from mafic to felsic minerals, including magma viscosity curve (Modified from Marsh, 2015).

2.2.2 Dissolution rates

As Giacomel et al. (2018) described, injection methodology in Carbfix consists of injecting into basalts the captured CO_2 and H_2S dissolved in water, configuring a carbonic acid. The composition of the fluid accelerates the rocks dissolution and release of divalent cations. These cations then precipitate to form stable carbonate and sulfide minerals (Snæbjörnsdóttir et al., 2017; Kristjánsdóttir and Kristjánsdóttir, 2021). Studies and experiments focused on the mineralogy and dissolution rates of crystalline basalt and basaltic glass (Gudbrandsson et al., 2011; Marieni et al., 2013; Marieni and Oelkers, 2018; Schaef et al., 2010, 2011) show that the dissolution rates of the crystalline basalt can be lower compared to the basaltic glass, despite having a comparable chemical composition and similar experimental conditions. Dissolution of pyroxene, and consequent release of Mg and Fe cations, is favored by acidic to neutral pH conditions. Dissolution of plagioclase and release of Ca and Al is favored by basic pH conditions. Furthermore, secondary minerals and alteration products were identified as potential sources of cations for mineralization due to its calcium content and reaction capacity. Therefore, understanding which mineral provides a significant number of reactive cations is crucial in establishing the appropriate conditions for mineral dissolution.

2.2.2.1 Basaltic glass

Basaltic glass is typically found as interstitial material within the rock. When considering the thermodynamic stability of major phases in basalt, volcanic glass is known to be the most reactive component, followed by pyroxene, with plagioclase being the least reactive (Oelkers and Gislason, 2001; Gislason and Oelkers, 2003). As a result, dissolution rates for basaltic glasses are faster and comparable to crystalline silicates like olivine and anorthite. Stockmann et al., (2011) conducted an experiment and found that the dissolution rates of basaltic glass remain unaffected by the precipitation of secondary $CaCO_3$. This lack of structural compatibility between glass and calcium carbonate actually promotes the nucleation and growth of discrete $CaCO_3$ crystals, rather than hindering the dissolution process (Stockmann et al., 2008).

2.2.2.2 Ca-Feldspar

Oelkers and Schott (1995) stated that the dissolution of anorthite (calcium-rich plagioclase feldspar) can be achieved by dissolving a single structural unit composed of aluminum, oxygen, and silicon (Al-O-Si). They found that the hydrolysis rates of these minerals remain unaffected by the aqueous AYSi ratio or chemical affinity, especially in far from- equilibrium conditions. The dissolution process of anorthite involves three phases: the exchange of calcium and hydrogen ions within the feldspar structure, the formation of precursor complexes on the surface through hydrogen ion adsorption, and the subsequent detachment of these precursor complexes.

In experiments conducted by Schaef et al. (2010), supercritical CO_2 was injected into basalts of different origins. It was observed that feldspar with an average composition ranging from andesine to labradorite (An_{38} to An_{57}) demonstrated increased resistance compared to pure anorthite. Consequently, it is known that reducing the calcium content in plagioclase feldspar enhances its stability, as noted by Wolff-Boenisch et al. (2006).

2.2.2.3 Ca-Clinopyroxene

Previous experiments (e. g. Wolff-Boenisch et al., 2006; Schaef et al., 2010; Zakharova et al., 2012), show that dissolution rates of augite can be higher compared to basaltic glass under certain conditions. Hoch et al. (1996) observed that the dissolution rates of augite, based on silicon release, were approximately three times greater in experiments with 1.5 ppm dissolved oxygen compared to sealed experiments. Additionally, it was noted that the presence of dissolved oxygen played a significant role in the weathering of iron-bearing pyroxenes, leading

to an enhancement of dissolution rates rather than the formation of a secondary iron mineral layer.

Regarding enstatite, Oelkers and Schott (2001) explained that the breaking of magnesium-oxygen (Mg-O) bonds in its structure occurs more rapidly than the breaking of silicon-oxygen (Si-O) bonds. However, this breaking of Mg-O bonds does not fully destroy the enstatite structure; it only partially liberates the silica tetrahedral chains. The dissolution of enstatite proceeds through magnesium releasing exchange reactions between aqueous hydrogen ions and magnesium in the enstatite structure, followed by the relatively slow detachment of silica from the partially liberated tetrahedral chains.

Experiments performed for dissolution rates of augite (Oelkers & Schott, 2001; Schott & Oelkers, 1995) show they decrease as the pH increased up to pH 5-6. However, under more basic conditions, the dissolution rates remained unaffected by the pH. The relationship between dissolution rates and pH primarily depends on the speciation of the aqueous metal in the mineral M2 site, rather than the quantity of adsorbed protons, water, or hydroxide ions on the mineral surface.

Concerning the isotopic composition of magnesium (Wimpenny et al., 2010; Ryu et al., 2016; Schott et al., 2016), weathering of igneous rocks, particularly basalts, leads to the depletion of isotopically light Mg from continental sources. The preferential removal of light Mg from solution occurs through the precipitation of chrysotile and carbonates, while the formation of clay minerals in silicate soils tends to incorporate heavier Mg isotopes.

2.2.3 Carbonates

The available cations will mix with the carbonate molecule, previously formed by the dissolution of CO_2 in water, the generation of carbonic acid, the hydrolysis of the rock, and form different types of carbonate minerals such as siderite, magnesite, calcite or dolomite. Knowing this natural process, it is possible to model the chemical reactions first using geological time and natural conditions and then changing P, T and pH to accelerate mineralization and try to predict possible products (Voigt et al., 2021).

According to the experiments performed by Giacomel et al., (2018), basalt carbonation is the result of kinetic processes involving (1) dissolution of basalt primary minerals due to interaction with acid water, (2) diffusion of the dissolved material, and (3) precipitation of carbonates. The potential for mineralization in the reservoir depends on the ratio of divalent cations in the rock

minerals to the amount of CO_2 in the pore space, as approximated by the modified formula from Zhang and DePaolo (2017). These reactions are presented in Table 1.

Table 1 - Geochemical reactions of dissolution and precipitation due to CO_2 injection in basalts (Modified from Raza, 2022).

Dissolution reactions	**Precipitation reactions**
$CO_{2(g)} + H_2O = H_2CO_3$ $H_2CO_3 = HCO_3 + H^+$ Basaltic glass + $xH^+ \rightarrow Mg^{2+} + Ca^{2+} + Fe^{2+}$ $+ 2Mg^{2+} + 2H_2O + SiO_{2(aq)}$ *Forsterite/Olivine interactions* $MgCaSi_2O_6 + 4H^+ \rightarrow Mg^{2+} + Ca^{2+} + 2H_2O + 2SiO_{2(aq)}$ *Diopside interactions* $CaAl_2Si_2O_8 + 8H^+ \rightarrow Ca^{2+} + 2Al^{3+} + 2SiO_{2(aq)} + 4H_2O$ *Ca-plagioclase*	$(Fe, Ca, Mg)^{2+} + CO_2 + H_2O \rightarrow$ $(Fe, Ca, Mg)\ CO_3 + 2H^+$ *Siderite, calcite, magnesite, ankerite, dolomite*

2.3 Geological framework

This section describes the geological context of the Paraná basin, its main characteristics, its filling history and tectonic events dating back to around 400 My. The history and characteristics of the Serra Geral Formation basalts are also presented, whose flows are interbedded with the sedimentary sequences of the basin.

2.3.1 Paraná basin

The Paraná Basin is a large sedimentary basin located in Brazil, but also extending into parts of Paraguay, Argentina, and Uruguay, covering an area of approximately 1700 km^2 (ANP, 2020).

The Paraná Basin preserves a vast record of sedimentary and volcanic deposits that span several hundred million years (Soares, 1991; Milani et al., 2007; Sant'Anna et al., 2006; Rossetti et al., 2018). It is known for its extensive sequences of sedimentary rocks, including sandstones, shales, and coal-bearing formations (Pinto, 2019). These sedimentary deposits represent various environments of deposition, such as marine, fluvial, and lacustrine settings.

One of the notable features of the Paraná basin is the presence of large-scale volcanic activity during the breakup of the supercontinent Gondwana (Pacheco et al., 2018; Rocha-Júnior et al., 2020a). The basin contains extensive basaltic lava flows, known as the Serra Geral Formation or the Paraná Continental Flood Basalt, which resulted from fissure volcanism associated with

the rifting and opening of the South Atlantic Ocean. These basalt flows can reach thicknesses of up to 2,000 meters (Fernandes et al., 2018; Machado et al., 2018). The Paraná basin is of great economic importance as it contains significant reserves of coal, oil, and natural gas. It has been an important region for mining and hydrocarbon exploration and production as well (Morelatto).

2.3.2 Tectonostratigraphy

The Paraná basin holds approximately 400 million years of geological history. It consists of several supersequences (Figure 1.3), including the Rio Ivaí, Paraná, Gondwana I, Gondwana II, Gondwana III and Bauru (Pinto, 2019). The Gondwana III Supersequence is characterized by sandstones from the Botucatu Formation and basalt spills from the Serra Geral Formation (Morelatto).

These supersequences were detailly described and reviewed in the work of Milani (1998, 2007), as it follows:

Río Ivaí Supersequence: Sedimentary sequence deposited since before the Devonian, consists of the Alto de Garcas, Iapó and Vila Maria formations. Presents intercalations of fossil shales and sandstones that record the first regressive transgressive cycle of the basin.

Paraná Supersequence: Sandstones, clays and fossil shales of the Devonian and Carboniferous. It consists of the Furnas and Ponta Grossa Formations. This supersequence represents the second transgressive regressive cycle of the basin.

Gondwana I Supersequence: It is composed by the coalbeds of the Rio Bonito Formation, Iratí Formation and the Itararé Group. It contains glaciogenic deposits, sandstones, shales and turbidites from the Permian transgression. The Gondwana I Supersequence documents a complete transgressive-regressive cycle, beginning with the Pennsylvanian glacial package, reaching conditions of maximum marine drowning in the Palermo Formation in the Artinskian, and ends in continental deposits that would bridge the syneclisis at the beginning of the Mesozoic.

Gondwana II Supersequence: The geological characteristics of this supersequence allows an interpretation of the Meso-Neo-Triassic subsidence of the Paraná Basin, wich could be related to the development of asymmetric distensional grabens, accommodating river drainage over the flexural ramp of this system , with a regional dip of the substrate to the north in the Gaucho portion and to the south in a similar Uruguayan trough, while the lacustrine pelites would have

accumulated along the more subsident portions. The cyclicity observed in this package, in which lacustrine pelites and fluvial sandstones are interspersed, would have developed in response to variations in the lake's base level due to a combined control of tectonics and climate (Milani et al. 1998).

Gondwana III supersequence: Goes from the Jurassic to the Cretaceous. Comprises the interval in the stratigraphic record of the Paraná Basin in which the aeolian sedimentites of the Botucatu Formation and the magmatites of the Serra Geral Formation are located. This section, if added to the suprabasaltic sedimentary package, will correspond to the São Bento Group, by Schneider et al. (1974). The Gondwana III Supersequence is widely distributed throughout the Paraná Basin, and its continental sedimentites are predominantly represented by aeolian facies

Bauru Supersequence: The post-basaltic opening constitutes a psammitic siliciclastic unit accumulated in semi-arid to desert conditions. It has a maximum preserved thickness of around 300 m and an occurrence area of 370,000 km^2, in the States of Minas Gerais, São Paulo, Paraná, Mato Grosso do Sul, Goiás and Mato Grosso, as well as in the Northeast of Paraguay. The Bauru Supersequence has discordant basal contact (nonconformity), especially with basalts from the Serra Geral Formation.

The basin's structural features include NNE-SSW and NW-SE lineaments related to the reactivation of transcurrent systems during the Upper Ordovician and tectonic uplift of the Western Gondwana during the Upper Triassic to Upper Jurassic (Pinto, 2019; Silva et al., 2021). East-West lineaments are associated with the movement of the South American Plate during the Late Cretaceous to the Neogene, generating right-lateral faults within the plate.

In the work of Pinto (2019), geophysical lineaments at different depths correspond to Brazilian strike-slip systems, including the Transbrasiliano, Campo do Meio, Paraíba do Sul, and Neotectonic strike-slip systems.

The basalts in the study area of Ribeirão Preto-Reginópolis region overlay the Botucatu Formation, which is younger than the Piramboia Formation (Fernandes et al., 2018). The Piramboia Formation is composed of medium to fine sandstones, deposited in a fluviolacustrine and aeolian environment (Côrtes and Perinotto, 2015). The Serra Geral Group is directly covered by other units, including the Marília and Vale do Rio do Peixe Formations of the Bauru Group (De Paula E Silva et al., 2009), the Itaqueri Formation in the Brotas region, and alluvial and colluvio-alluvial deposits in the Itirapina area (Riccomini, 1997). The Marília Formation includes fine to medium-grained sandstones, mudstones, conglomerates, and conglomeratic

sandstones (Marques Dos Santos et al., 2020). The Vale do Rio do Peixe Formation consists of fine to very fine-grained sandstones with some siltstones or sandy mudstones (Fernandes et al., 2003).

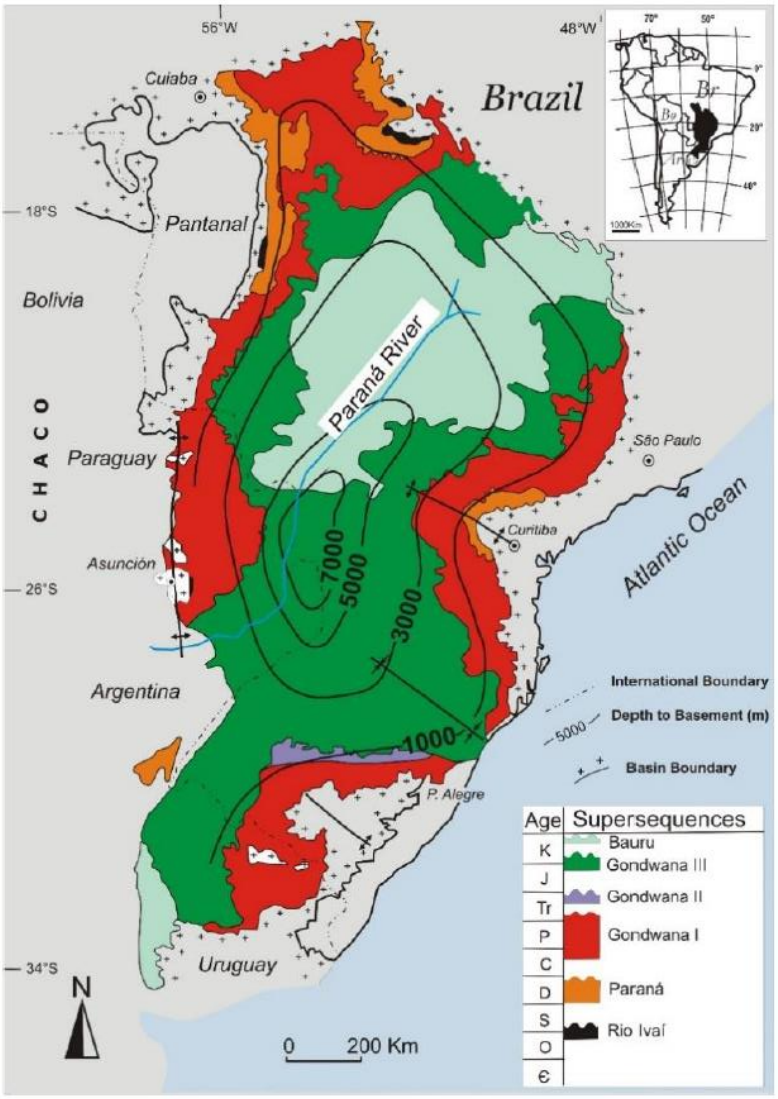

Figure 1.3 - Distribution of the sedimentary supersequences that composed the tectonostratigraphic record of the Paraná basin (Bergamaschi et al., 2016).

2.3.3 Serra Geral Formation

The Paraná-Etendeka magmatism represents a significant geological event characterized by extensive volcanic activity during the Early Cretaceous period, approximately 133 to 128 million years ago (Rämö et al., 2016; Cañón-Tapia, 2018). This magmatism occurred within the Gondwana supercontinent, primarily in the Paraná Basin in South America and the Etendeka Province in southwestern Africa. The volcanic activity resulted in the emplacement of vast flood basalts, forming one of the largest continental flood basalt provinces globally (Rocha-Júnior et al., 2020b). These basaltic lava flows, such as those from the Serra Geral Formation in Brazil,

cover extensive areas and are associated with the breakup of Gondwana and the opening of the South Atlantic Ocean (Rossetti et al., 2018). The Paraná-Etendeka magmatism is significant not only for its immense scale but also for its role in paleogeographic reconstructions and understanding the dynamics of supercontinent breakup and the opening of ocean basins during the Early Cretaceous (Pinto, 2019; Silva et al., 2021).

The Serra Geral Formation dates from approximately 135 million years ago, and consists of tholeiitic basalts with distinct geochemical characteristics. The province southern part exhibits low-TiO_2 and low incompatible element levels, while the northern portion has high TiO_2 concentrations (Pacheco et al., 2018; Machado et al., 2018; Rocha-Júnior et al., 2020a). Metasomatic processes and lithospheric refertilization contribute to geochemical variations. These rocks are basic lava flows intercalated with sediments, showing variations in P_2O_5 as well (Fernandes et al., 2018). They are enriched in Fe_2O_3 but have lower alkali and MgO content. The basalts may exhibit Pitanga, Gramado, Esmeralda or Urubici magma-types tholeiitic signature (Pacheco et al., 2018).

Fernandes et al., (2010) in their work defined four basalt spills labeled B1, B2, B3, and B4 in the Bonfim Paulista area (SP). In order of their age, B4 has mostly eroded, while B1 and B2 have average thicknesses of 45 and 55 meters, respectively. All four basalts exhibit sheet-like lobes and were likely formed through the inflation mechanism. B1 and B2 have thick upper vesicular crusts, and B2 and B3 display cooling columns, particularly noticeable in B3 due to the presence of lower columnar (B3-C) layer and overlying entablature layers (B3-E). B3 is the thickest flow, ranging from 75 to 100 meters, and contains hydraulic breccias distributed in pockets or along sub-horizontal fractures that allow fluid circulation. B3 can be clearly distinguished from B1 and B2 based on various oxides and trace elements. B1 and B2 differ primarily in the oxides P_2O_5 and TiO_2 and the elements Cu, Zn, Y, and Ni.

The province outcrop area in southern Brazil (Paraná, Santa Catarina and Rio Grande do Sul states) corresponds to the Torres Formation (TF) and Vale do Sol Formation (VSF) (Rossetti et al., 2018). TF consists of tholeiitic basalts, including lower portions of Gramado magma type lavas and compound lavas from Basic Volcanic Episode I and II. The internal structure of TF exhibits a lower crust with pipe vesicles, a massive core with segregation structures, and a vesicular upper crust. On the other hand, VSF comprises vertically stacked sheet-like lava flows of rubbly pahoehoe morphology, with an average thickness of 35-45 meters and reaching a maximum thickness of 500 meters in some areas.

2.3.3.1 Serra Geral – Guaraní Aquifers

The Serra Geral - Guarani aquifer system represents one of the largest groundwater reservoirs in South America, spanning across Brazil, Argentina, Paraguay, and Uruguay (Cunha et al., 2016; Leite et al., 2021). Comprising sedimentary and volcanic rocks, this transboundary aquifer system plays a crucial role in providing freshwater resources to millions of people in the region (Hirata and Foster, 2021). The Serra Geral Formation, characterized by basaltic rocks, acts as a protective layer overlying the Guarani Aquifer, which consists of sedimentary deposits (Gastmans et al., 2013). With its vast storage capacity and high permeability, the Guarani Aquifer serves as a vital source of drinking water, irrigation, and industrial supply for numerous communities (Bongiolo et al., 2014). However, the aquifer system faces threats from overexploitation, contamination, and climate change impacts, necessitating collaborative management and conservation efforts among the riparian countries to ensure its sustainable use for current and future generations.

.

3 Methods and samples

3.1 Field work

Field work was carried out in the first week of November, 2022. Basalt hand samples were collected from four quarries in the Ribeirão Preto – Reginópolis region, in the São Paulo state (Map 2.1). To cover the variety of basalt facies, samples were chosen from massive, tabular and fractured flows. In total 29 samples were collected, from them 16 were sent to lamination and then 11 to geochemical analysis.

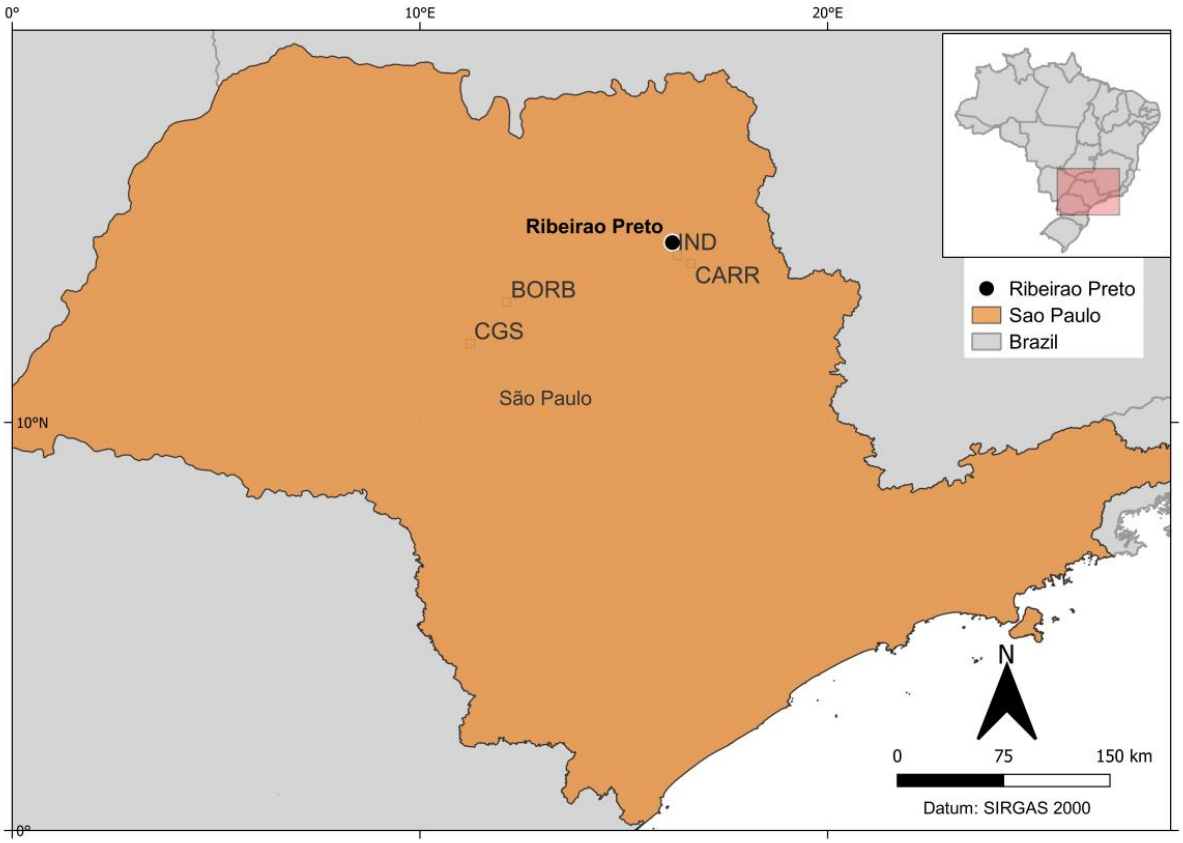

Map 3.1 - Location map of the quarries visited during field work in the Ribeirão Preto-Reginópolis region (SP).

Thin sections were elaborated in the Lamination Laboratory of GeoAnalitica facilities in the Geoscience Institute (IGc) of the University of São Paulo. Petrography was determined in the Petrographic Microscopy Laboratory of the IGc. Geochemical analysis for whole rock was carried out by the GeoAnalitica FRX laboratory, where major, minor and trace elements were analyzed. The Scanning Electron Microscopic Analyzes (SEM) were carried out in a LEO 4401 Microscope, coupled to the EDS detector (Energy Dispersive X-Ray Spectrometer), which performs qualitative and quantitative chemical analysis of the mineralogical constituents.

3.2 Petrography

Optical mineralogy focuses on studying the interaction of light with minerals, primarily through the use of a polarizing microscope. Its applications include the identification of minerals in rock thin sections or individual grains (Nehru, 1989).

The optical properties of minerals, such as refractive index and birefringence, are related to their crystal chemistry, allowing for correlations between these properties and mineral characteristics. Thin sections are particularly important for petrologists as they help identify minerals, determine their textural relationships, classify rocks, and locate minerals for further analysis. Sixteen thin sections were elaborated in the Lamination Laboratory of GeoAnalitica facilities in the Geoscience Institute (IGc) of the University of São Paulo. Thin sections have 4mm of thickness and 3x4cm of area.

The petrographic analysis included mineral identification according to optical properties and textural analysis, such as fractures, veins, vesicles and amygdales. Petrography was performed in the Petrographic Microscopy Laboratory of the IGc with the Olympus microscope using the 10x lens.

3.3 Litogeochemistry

According to Potts (1987), X-ray fluorescence (XRF) is a rapid and non-destructive analysis method with high accuracy. It can measure elements from beryllium to californium in powders, solids, or liquids, qualitatively or quantitatively. XRF spectrometers can analyze concentrations up to 100 % directly, without dilution, with reproducibility better than ±0.1 %. The method has typical limits of detection ranging from 0.1 to 10 ppm. Sample preparation for XRF analysis is crucial, requiring representative, homogeneous, and clean surfaces. XRF is effective for analyzing light elements with careful preparation. Glass discs are commonly used for quantitative determination of major elements in geochemical samples.

Samples of nonweathered and weathered basalts were collected for chemical analysis and petrographic description. 11 samples were analyzed for whole-rock chemical composition, including oxides and trace elements. Representative rock samples were crushed and powdered to 200 mesh size. Major elements were obtained from fused discs using wavelength dispersive X-ray spectrometry while trace elements were analyzed in pressed discs. The methods described by the XRF laboratory of the Geoscience Institute (IGc) at the University of São Paulo (USP) were followed for sample preparation and analysis. The analysis was performed

using X-ray fluorescence equipment PANalytical AXIOS MAX Advanced at IGc-USP Geoanalitica Facilities.

3.4 Scanning electron microscopy

Minerals are natural, homogeneous solids with defined chemical compositions and ordered atomic arrangements. As Ansberque et al. (2019) described, to achieve fast and accurate mineral identification, Energy Dispersive X-ray Spectrometers (EDS) integrated with Scanning Electron Microscopes (SEM) are used. SEM-EDS allows for rapid and reliable elemental analysis and chemical characterization of solid minerals. The technique involves bombarding the sample with an electron beam, which results in the emission of various particles, including X-rays. EDS detects and counts the characteristic X-rays produced during electron transitions within the sample. Obtaining elemental data through EDS is fast and facilitates accurate mineral characterization.

However, the spectral variability of EDS datasets for natural minerals and the influence of various factors on the accuracy of SEM-EDS data pose challenges in the technique's application. Analysis of basalt samples was conducted at the Electron Microscopy and Microanalysis Laboratory of the Geoscience Institute at the University of São Paulo. The analysis utilized a LEO 4401 Microscope, coupled to the EDS detector (Energy Dispersive X-Ray Spectrometer). The microscope allowed the examination of samples in the form of thin sections without any covering. The analysis involved the measurement of several X-ray intensities (cps/eV) of various elements, including Na, Mg, Al, Si, K, Ca, Ti, Mn, Fe and P. These intensities were obtained using the spot analysis method targeting the basaltic matrix, filled micro-vesicles (mainly zeolites) and major crystals of clinopyroxene and olivine, with each measurement lasting for a duration of 10-200 seconds

3.5 Experimental CO_2 reactions and mineralization

The CO_2 injection experiments are carried out in partnership with Institute of Physics of the University of São Paulo (IFUSP). In the SAMPA laboratory atomic models are performed to calculate the adsorption energy of CO_2 in the crystalline structure and the CO_2 injection tests into powdered basalt are carried out at the Materials Laboratory. Some experimental testes have already been performed and results were analyzed at the Institute of Energy and Environment (IEE) using DRX technique and at the Geoscience Institute (IGc) using SEM technique.

3.6 Geochemical data analysis

Geostatistics is a set of tools used to predict the spatial behavior of georeferenced data. In the context of geology, geostatistical analysis is conducted based on spatial relationships rather than temporal ones. This approach assumes that the area of interest consists of the same type of rock, and statistical measures remain invariant throughout the area (Matheron, 1963). A geochemical database of the Serra Geral Formation basalts was created with compositional data available all over the Paraná basin (Pacheco et al., 2018; Rossetti et al., 2018; Fernandes et al., 2018; Machado et al., 2018; Rocha-Júnior et al., 2020a; Giovanardi et al., 2022) (Map 2.2) as an exercise of geological site selection for CO_2 injection.

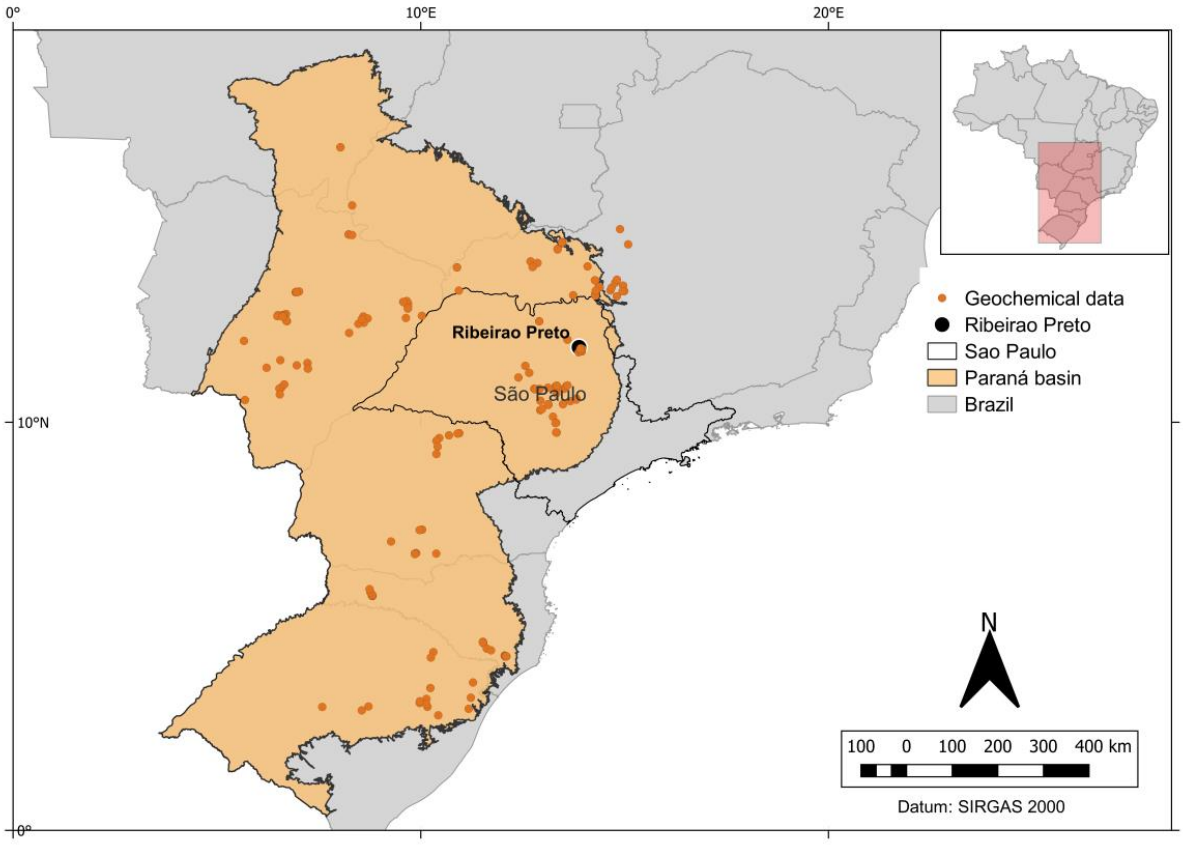

Map 3.2 - Location map of the Paraná basin with the distribution of the previously available geochemical data of basalt samples. Studied area is delimited by the Sao Paulo state.

Geochemical data base consists of 500 lines with data of the major, minor and trace elements. This data was chosen keeping in mind the cations that participate in carbon mineralization. The first step involves assessing data correlation and spatial dependence using the variogram, which calculates the semivariogram as a function of the differences in values at varying distances (Akkaş et al., 2015). The variogram provides insights into the maximum distance of influence between points and identifies the range beyond which spatial correlation diminishes. Plots such

as histograms and scatter plots were employed to display frequency distributions and explore correlations between geochemical content and depth in the case of basalt flux. To perform spatial analysis of the geochemical data, Geographic Information Systems (GIS) software like QGIS was used. The interpolation method Inverse Distance Weighting (IDW) was applied to estimate geochemical values at unknown locations based on weighted influence from neighboring sample points, not using the parameter Depth due to scarce data and being taken at surface most of the samples. However, IDW interpolation may be affected by uneven data point distribution and may produce peaks and pits around sample data points in the interpolated surface.

The results of interpolation are typically represented as 2D raster layers in GIS. With these rasters is possible to observe the geochemical distribution of the basalts within the basin and identify the areas with higher content of elements of interest for carbon mineralization, helping in the assessment for potential geological site selection for injection. In this case, the potential is proposed only from the geochemical point of view, being mandatory the evaluation of another geological characteristics as petrophysics and geomechanics (IPCC, 2005), not included in the scope of this project.

4 Results

A series of analysis and correlations were constructed with the data obtained from all the methods described. Starting from the basalts macroscopic features observed in the outcrops to their mineral and geochemical implications.

4.1 Field work

Basalt hand samples were collected from CGS, Borborema, Carrazcosa and Inderp quarries in the Ribeirão Preto –Reginópolis region, in the São Paulo state. Basalt samples were taken from massive, tabular and fractured flows.

4.1.1 CGS quarry

CGS contains outcrops of simple pahoehoe flows (Figure 4.1). The outcrop presented a length of 19m and a thickness of 7m. Samples were taken from the tabular, breach and fractured textures. Samples shows different coloration according to their alteration grade. Tabular samples have a dark gray color. Fractured samples have a very dark gray color, red to green oxidation layers and some hydrothermal veins. Breach samples have a very light grey gray and vesicles with less than 1cm of diameter.

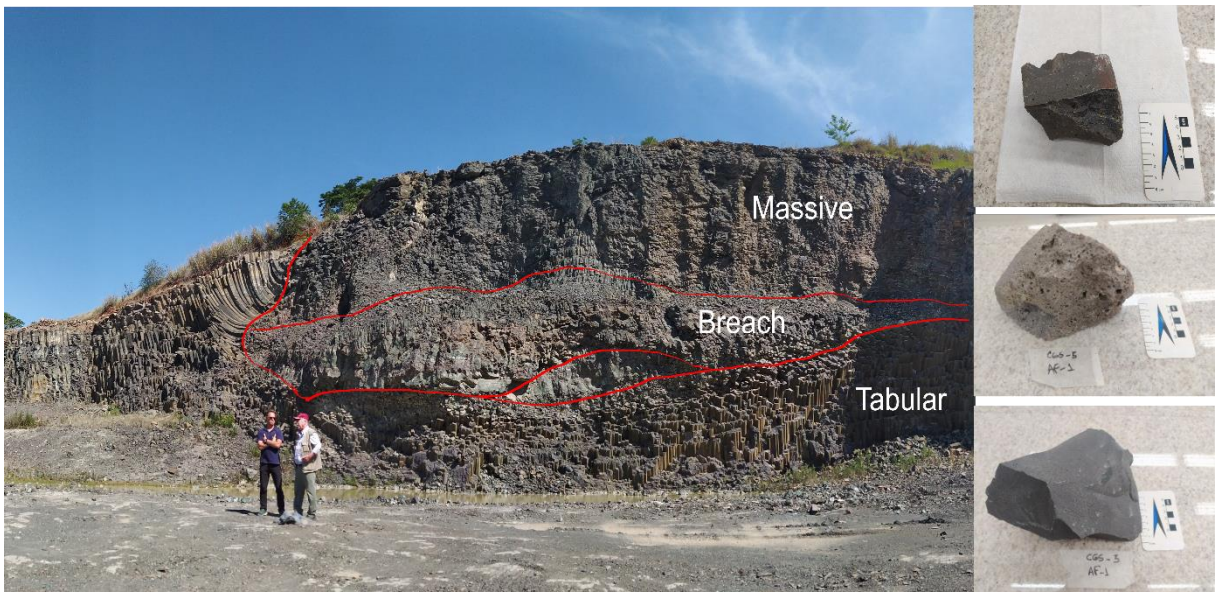

Figure 4.1 - Simple pahoehoe flow outcrop showing zones of fractured texture at the top, a breached contact zone in the middle and a tabular texture zone at the base of the flow.

4.1.2 Borborema quarry

Borborema contains outcrops of simple pahoehoe flows (Figure 4.2). The outcrop presented a length of 25m and a thickness of 8.75m. Samples were taken from the tabular and breach textures, which presented hydrothermal alterations as well. Tabular flow has a thickness of 7m, samples have a light gray coloration and presence of hydrothermal alteration veins.

Breach flow has a thickness of 1.75m, samples present a reddish light gray coloration possibly due to oxidation. Their vesicles have diameters below 1cm and a presence below 5%.

Figure 4.2 - Simple pahoehoe flow outcrop showing only a breached contact zone at the top and a tabular texture zone at the base of the flow.

4.1.3 Carrazcoza quarry

Carrazcoza contains outcrops of pounded pahoehoe flows (Figure 4.3). The outcrop presented a length of 15m and a thickness of 8.75m. Samples were taken from the tabular and fractured textures. Tabular samples have very dark grey coloration, with oxidation layers and hydrothermal veins. Massive samples have dark grey coloration, without external alterations.

Figure 4.3 - Pounded pahoehoe flow outcrop showing zones of massive texture at the top and a tabular texture zone at the base of the flow.

4.1.4 Inderp quarry

Inderp contains outcrops of pounded pahoehoe flows (Figure 4.4). The outcrop presented a length of 20m and a thickness of 5.5m. Samples were taken from massive textures, which presented oxide and pyrite layers. These samples have a very dark grey to dark grey coloration.

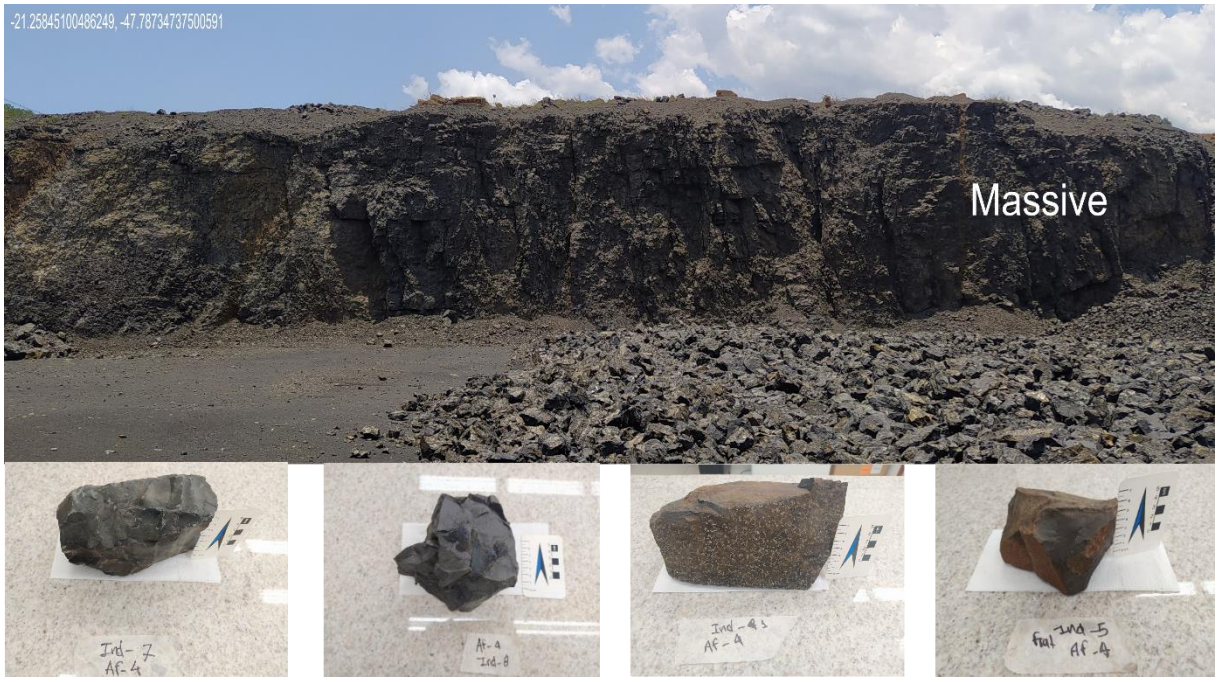

Figure 4.4 - Pounded pahoehoe flow outcrop showing only a massive texture. This basalt presents minor alteration.

4.2 Mineral composition and textures

The basalt flows in the Ribeirão Preto region presents characteristic of the simple pahoehoe and pounded pahoehoe types. These flows show vesicles and amygdalas at the top containing zeolites, celadonite, and silica, as well as aphanitic, glomeroporphyritic and diktitaxitic textures

4.2.1 Vesicular basalts

Samples from the CGS and Borborema quearries, belonging to the simple pahoehoe facies, are characterized by a hypocrystalline matrix consisting mainly of calcic plagioclase (labradorite) with average presence of 39%, calcic clinopyroxene (augite) to 33%, volcanic glass 9%, opaque minerals 5%, oxides 5%, celadonite 4% and quartz 3%. Altered olivine crystals were observed (Figure 4.5). The amygdalas in these basalts are filled with zeolites and show a high presence of celadonite (Figure 4.6). Due to meteorization caused by hydrothermal activity, the color of these basalts in outcrop varies from gray to reddish gray and there is also presence of micro-veins filled with silica.

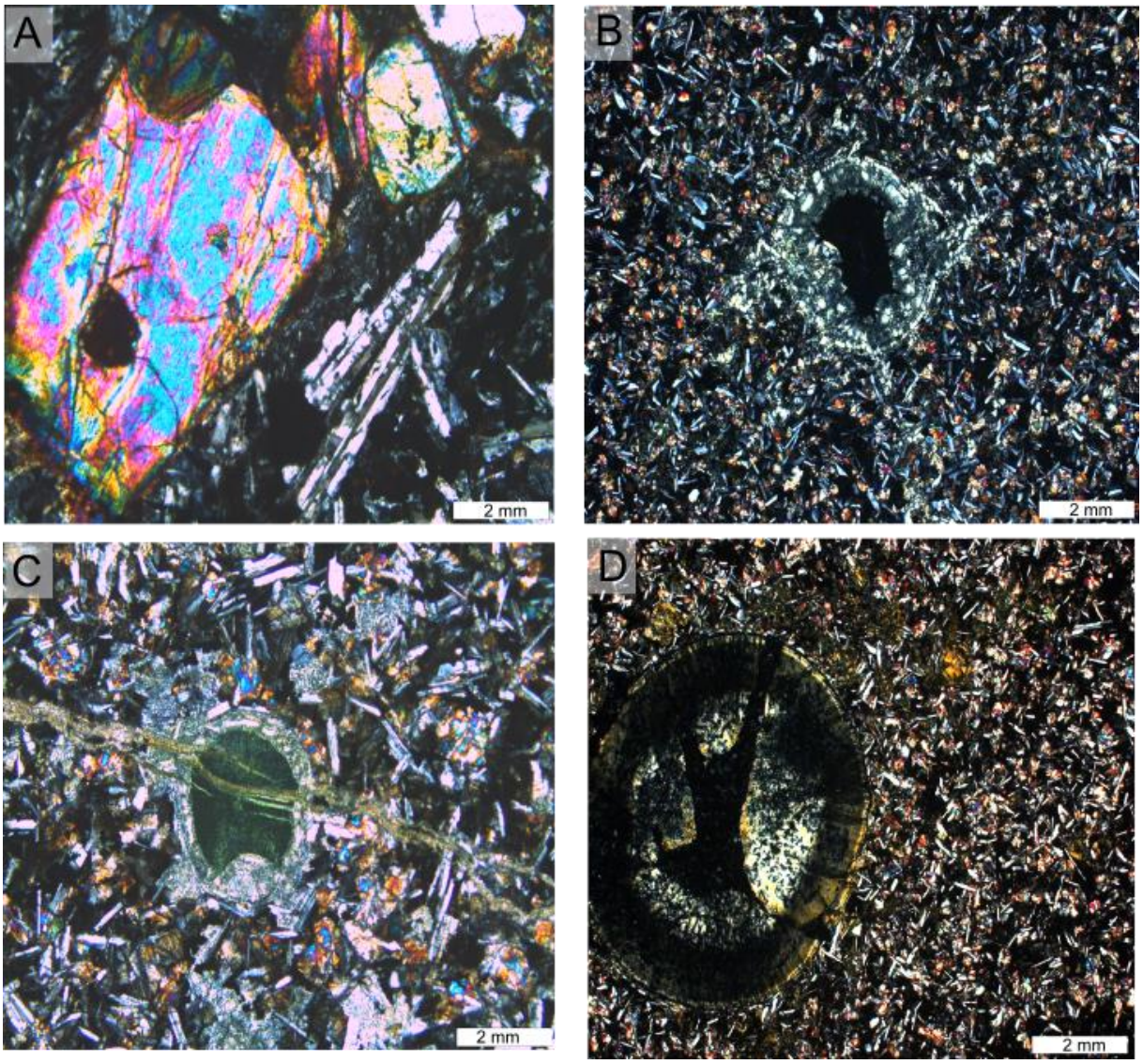

Figure 4.5 - Simple pahoehoe basalt from the vesicular zone. A) Major olivine and plagioclase crystal. B), D) Aphanitic microcrystalline texture with microvesicles filled with zeolites and quartz rims. C) Zeolite with silica rim crossed cut by a hydrothermal vein.

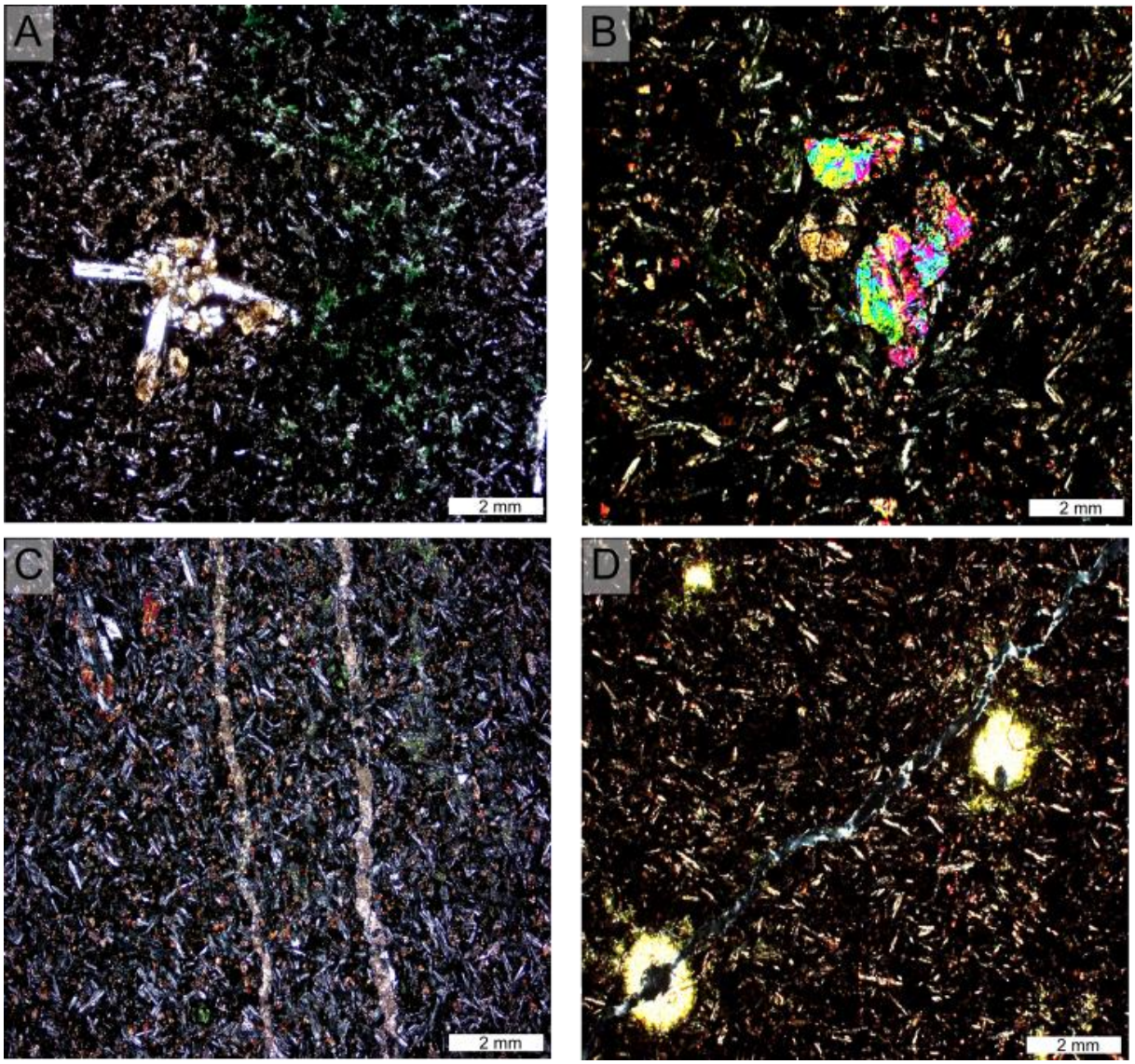

Figure 4.6. Simple pahoehoe basalt from the vesicular zone. A) Glomeroporphyritic plagioclase crystals in groundmass with celadonite (green) and oxide (brown reddish) as alteration layers. B) Altered augite crystal in highly oxide groundmass. C) Aphanitic microcrystalline texture with microvesicles filled with hydrothermal alteration veins. D) Zeolites crossed cut by quartz vein.

4.2.2 Fractured basalts

Basalt samples from the Carrazcosa quarry belong to the ponded facies of pahoehoe flows (Figure 4.6). They exhibit a hypocrystalline matrix with microvesicles composed mainly of calcic plagioclase (labradorite) 39%, calcic clinopyroxene (augite) 33%, volcanic glass 3%, opaque minerals 6%, oxides 4% and celadonite 6%. Samples present also veins composed of carbonates, silica, and celadonite are present in these samples. The color of the B3 basalts, taken from a massive flow, is preserved as dark gray to black.

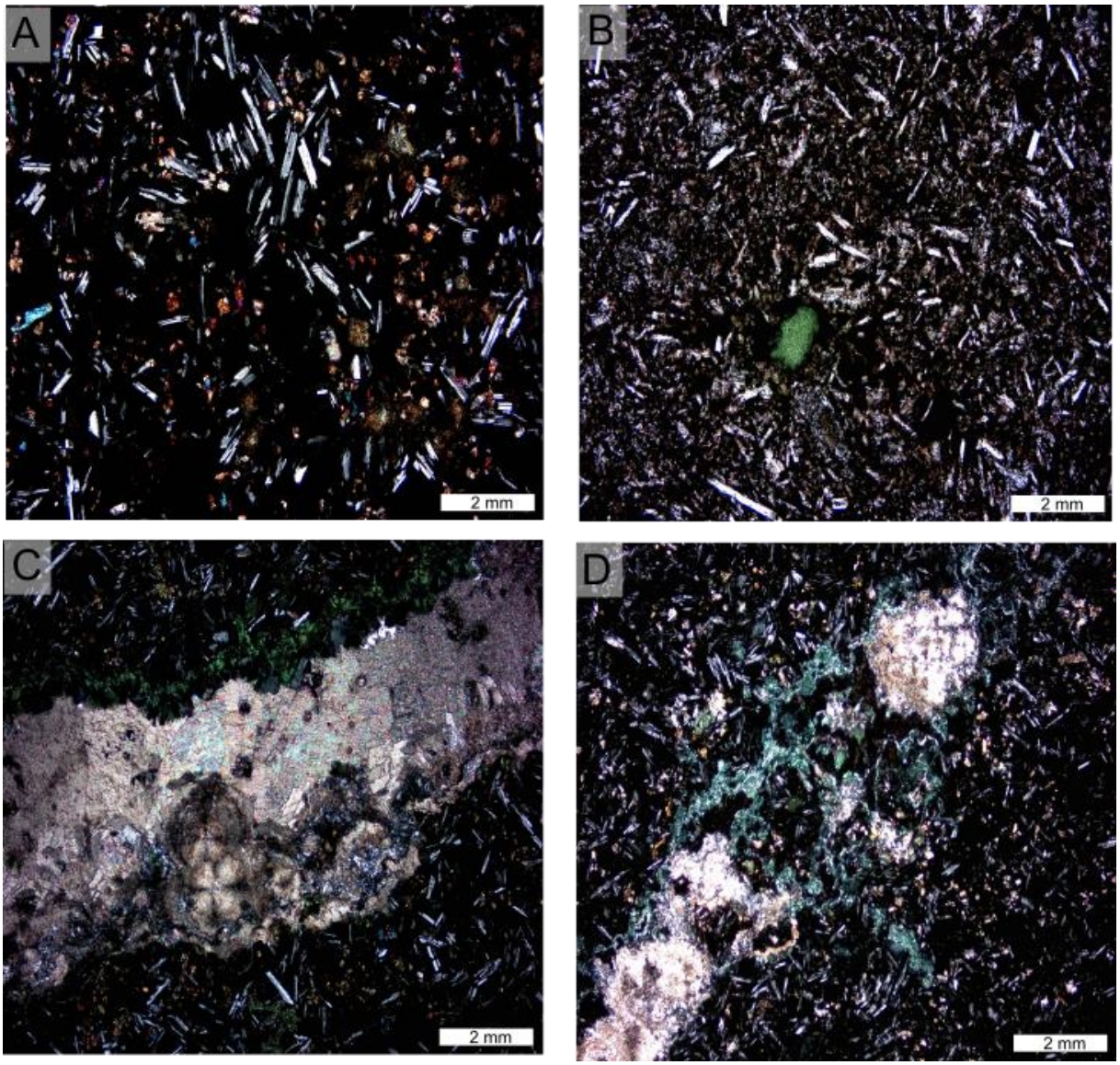

Figure 4.7 - Basalt samples from the pahoehoe pounded facies. A) Groundmass with bladed plagioclase and clinopyroxenes with high oxide alteration. B) Microvesicle filled with celadonite (green) in a groundmass with high presence of feldspars and oxide layers. C), D) Veins are composed of carbonates, silica and celadonite.

4.2.3 Massive basalts

Basalt samples from the Inderp quarry belong to the pahoehoe ponded facies (Figure 4.8). Present hypocrystalline matrix with porphyritic textures composed of calcic plagioclase mainly labradorite 42%, calcic clinopyroxene mainly augite 38%, volcanic glass 3%, opaque minerals 3%, oxides 7% and celadonite 5%. Micro-veins are composed of silica and celadonite. Because samples were taken from a massive flow, the colour is preserved dark gray to black.

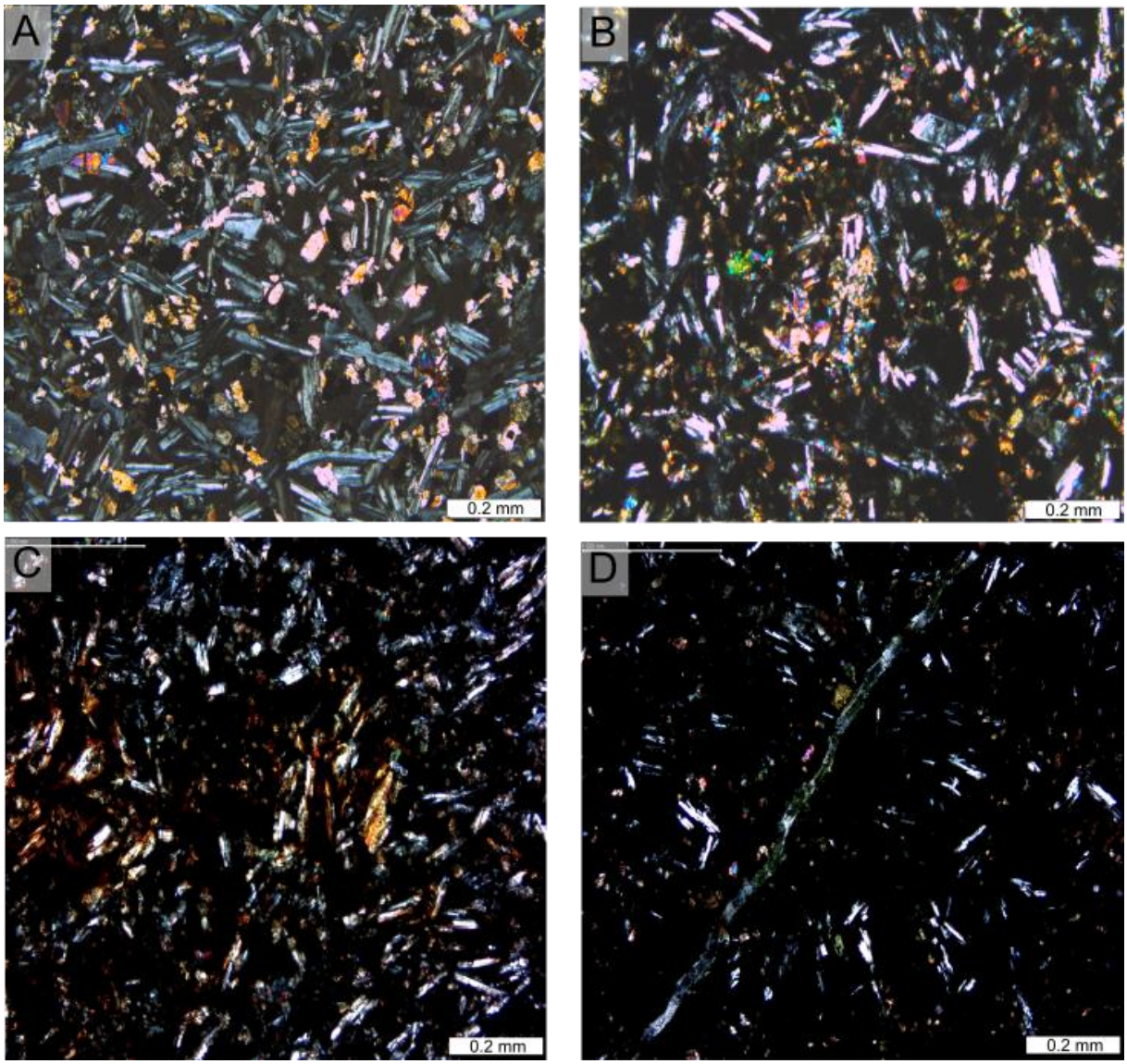

Figure 4.8 - Basalt samples from the pahoehoe pounded facies. Highlights the presence of micro-veins composed of silica and celadonite and the predominance of porphyritic textures.

4.3 Geochemical bulk composition

The whole rock geochemistry of the 11 basalt samples is presented in Table 2. The Serra Geral basalts in the Ribeirão Preto – Reginópolis region have SiO_2 concentrations between 46 and 51%. Thus, when plotted in classifications diagrams for volcanic rocks such as the TAS (Le Bas, 1986), which shows the Alkali-Silica relation, samples yield in the Basalt field with some samples close to the limit of Trachy basalt (Figure 4.9).

Table 2 - Whole rock geochemistry of Serra Geral basalts in the studied area.

Samples	Major oxides wt%										LoI
	SiO_2	TiO_2	Al_2O_3	Fe_2O_3	MnO	MgO	CaO	Na_2O	K_2O	P_2O_5	
CGS-1	47.03	3.699	12.20	15.91	0.242	5.21	7.76	2.48	2.25	0.500	2.14
CGS-3	47.75	3.712	12.41	15.70	0.256	5.26	8.29	2.50	2.03	0.494	1.71
CGS-4	46.13	3.665	12.10	15.36	0.324	6.07	7.11	2.49	2.27	0.570	4.22
CGS-5	47.85	3.777	12.53	15.49	0.274	5.28	8.94	2.39	1.73	0.480	1.93
BORB-1	50.75	2.001	13.32	14.40	0.219	5.44	10.11	2.29	0.57	0.227	1.47
BORB-2	50.27	1.948	13.35	13.47	0.205	5.89	10.10	2.28	0.54	0.226	1.22
BORB-5	50.24	1.959	13.29	14.13	0.217	5.88	10.67	2.07	0.71	0.249	1.60
BORB-7	51.17	2.814	12.72	13.96	0.180	3.73	7.02	3.04	3.64	0.383	1.29
CARR-6	49.81	3.896	12.30	15.57	0.237	4.10	7.94	2.44	1.38	0.627	1.30
IND-1	50.96	3.727	12.57	15.53	0.221	3.85	7.99	2.69	1.49	0.697	0.79
IND-9	50.58	3.887	12.31	15.71	0.216	3.90	7.93	2.52	1.51	0.625	0.95

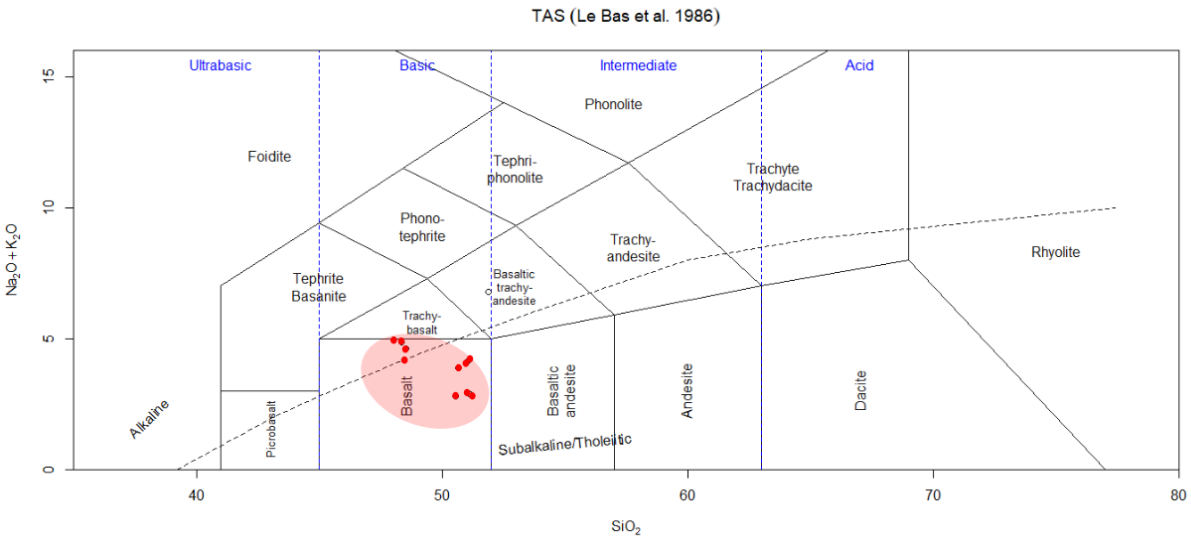

Figure 4.9 - Geochemical classification for mafic rocks based on total alkali vs silica (TAS diagram), proposed by Le Bas, 1986.

FRX analysis show a highly enrichment in Fe_2O_3 (13.7%), Al_2O_3 (13.6%), CaO (10.3%) and MgO (6%) for the Borborema quarry. Meanwhile for the CGS quarry, the abundance is very similar, with a slightly higher content of Fe_2O_3 (15.7%) and K_2O (1.6%). FRX analysis show a highly enrichment in Fe_2O_3 (15.8%), Al_2O_3 (~12.4%), CaO (~8%), MgO (~4%) and Na_2O (2.5%) for the Carrazcosa and Inderp quarries (Figure 4.10).

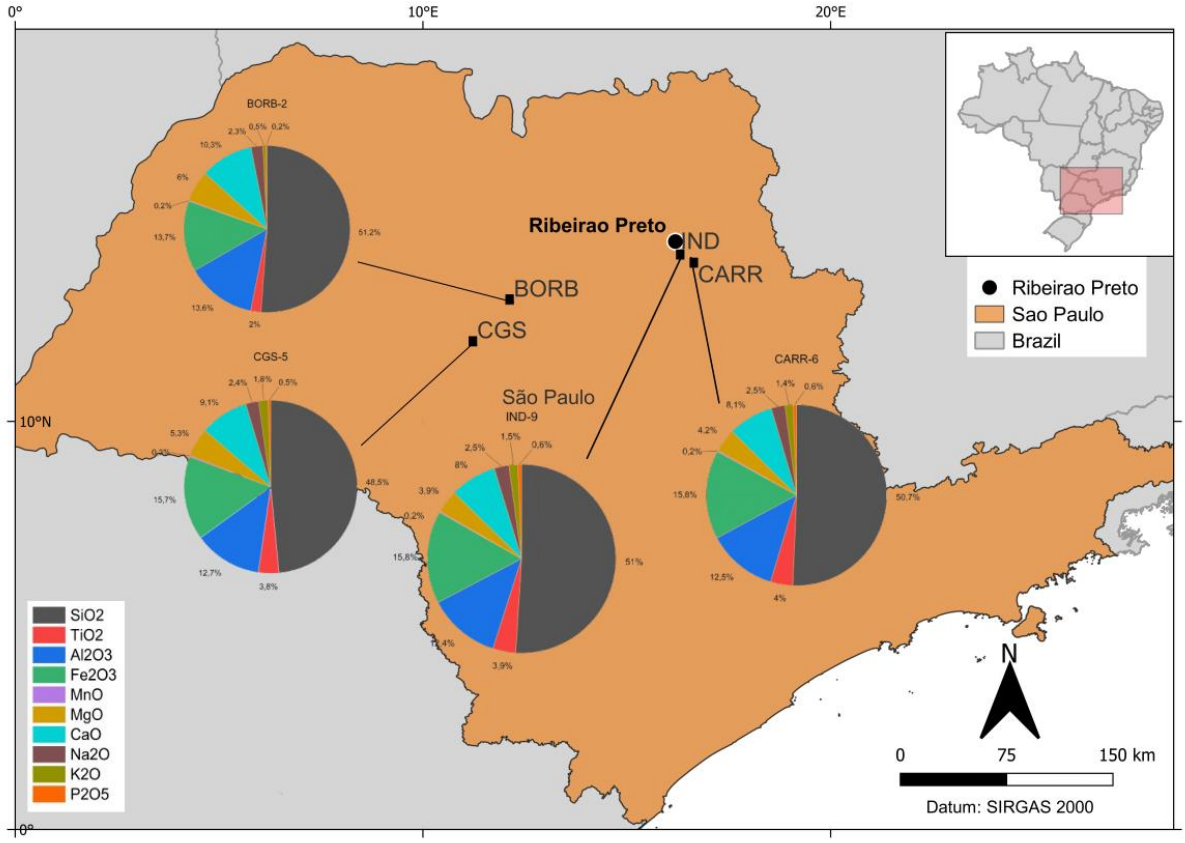

Figure 4.10 - Oxides percents of the elements in the basalt minerals.

4.4 Primary and secondary products element composition

SEM-EDS analysis of Serra Geral basalts has yielded chemical insights about elemental composition and mineral identification of primary and secondary mineral products. It is possible to observed the alteration grade of the rock due to the element's distribution. SEM-EDS analysis was performed on five representative samples of each basaltic texture.

4.4.1 CGS-1 Sample:

Geochemical data shows enrichment in iron (4 atoms) and aluminum (3 atoms), with significant levels of calcium, titanium, and magnesium (Table 3). The SEM image targets two amygdalas filled with silica surrounded by a basaltic mass, including the analysis of the basalt's hypocrystalline matrix as can be observed in Figure 4.11 and Figure 4.12. Similar to the CGS-5 sample, the elevated levels of iron, aluminum, and other elements are attributed to mineral sources within the rock, such as altered pyroxenes and plagioclase.

The presence of iron, magnesium, manganese, and titanium suggests the occurrence of the oxide ilmenite, and the widespread presence of manganese may indicate basalt oxidation.

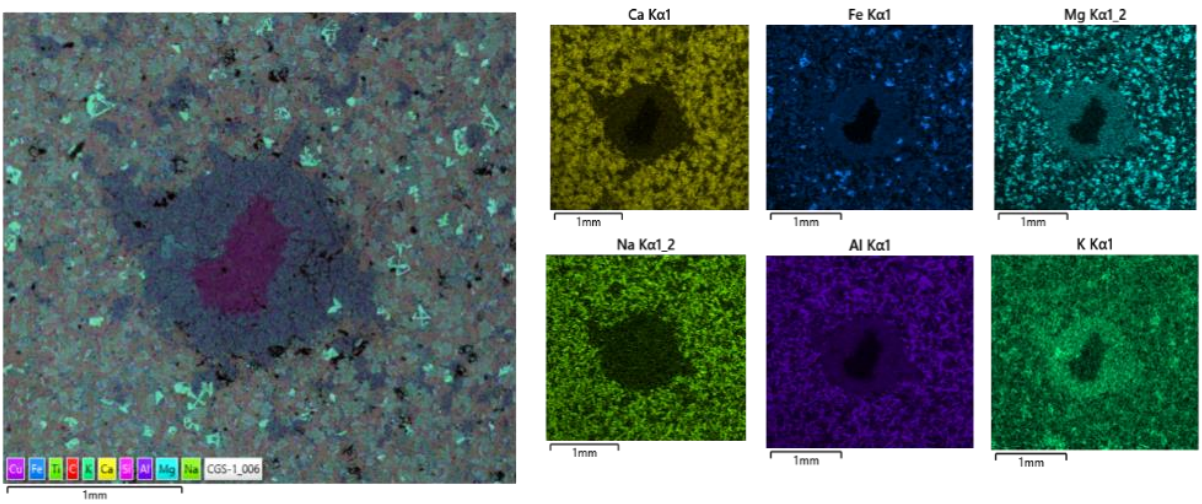

Figure 4.11 - SEM-EDS elements map of the vesicular basalt, targeting an amygdala with an aluminum rich rim.

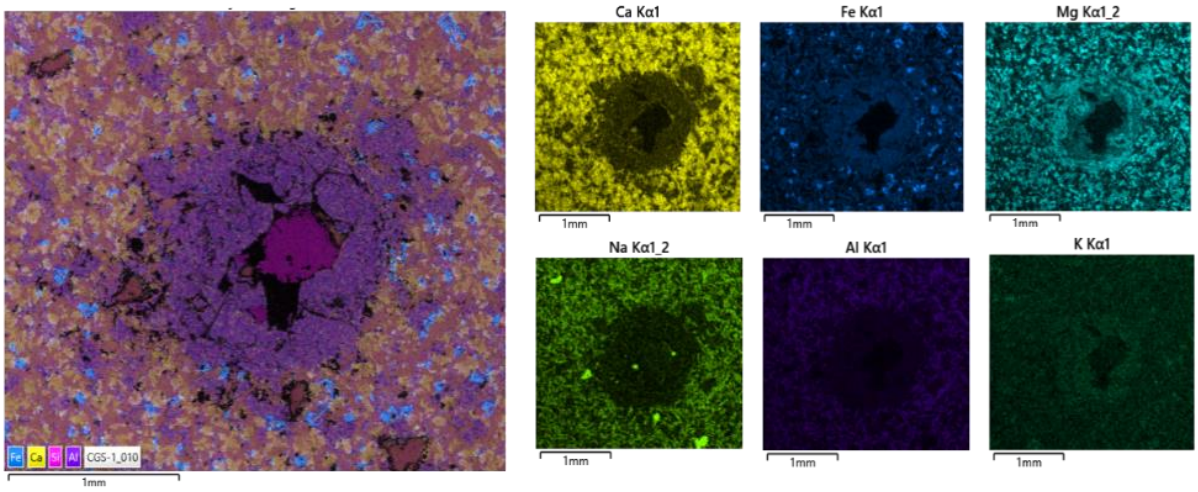

Figure 4.12 - SEM-EDS elements map of the vesicular basalt, targeting an amygdala with a magnesium rich rim.

4.4.2 CGS-5 Sample:

Geochemical data shows enrichment in iron (3 atoms) compared to CGS-1, and an increase in aluminum (3 atoms) (Table 3). Calcium, magnesium, and titanium are also present, albeit in lower amounts than CGS-1. The SEM Image targets two microvesicles partially filled with Na-Al zeolite and a K-rich alteration border. The basalt's hypocrystalline matrix appears to be more altered as can be observed in Figure 4.13 and Figure 4.14

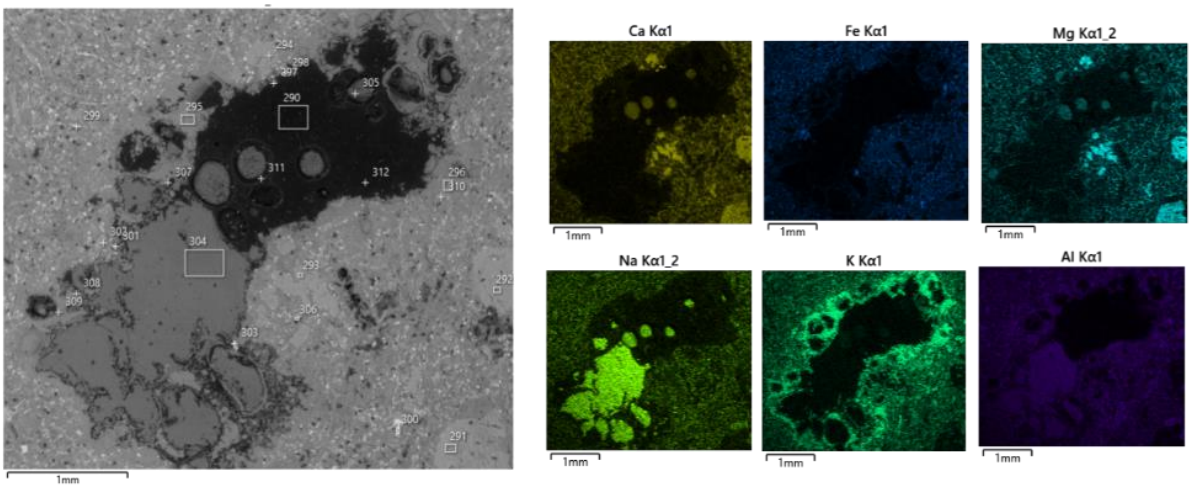

Figure 4.13 - SEM-EDS elements map of the vesicular basalt, targeting a microvesicle filled with a sodic rich zeolite and a potassium rich rim.

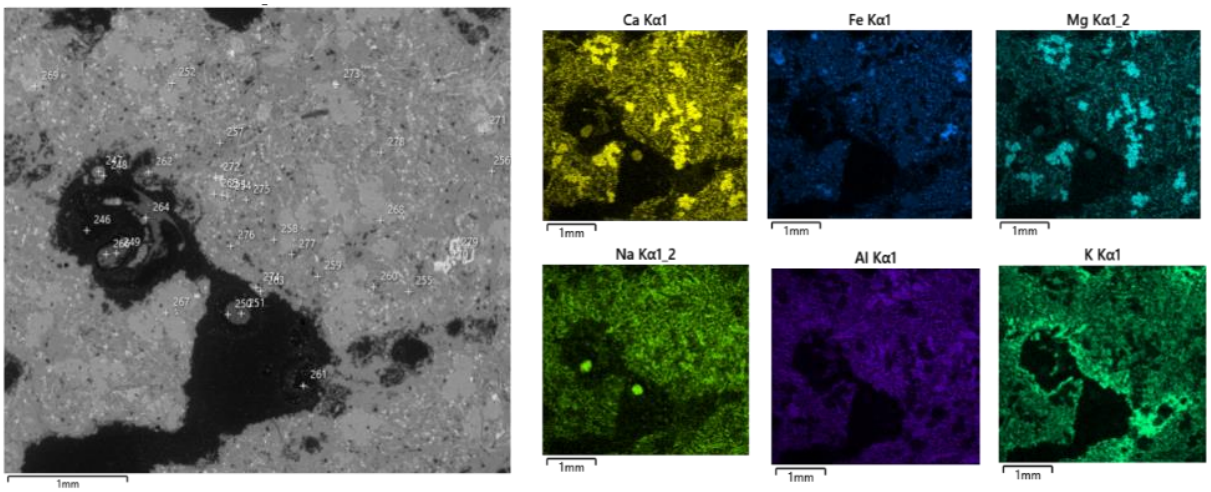

Figure 4.14 - SEM-EDS elements map of the vesicular basalt, targeting a microvesicle with a potassium rich rim.

The elevated levels of iron, aluminum, and other elements are attributed to various mineral sources within the rock. Iron, magnesium, and titanium may originate from altered pyroxenes, while calcium and aluminum likely come from plagioclase. Potassium is associated with sericite and celadonite, while sodium is attributed to zeolites. Presence of iron, magnesium, manganese, and titanium suggests the occurrence of the oxide ilmenite.

Table 3. Atomic percents of the minerals of Serra Geral basalts.

Samples	Elements atomic%								
	Si	Ca	Mg	Fe	Na	Al	K	Ti	Mn
CGS-1	8.74	1.92	1.39	4.06	0.66	2.79	0.13	1.29	0.13
CGS-5	9.29	1.74	1.29	3.31	0.90	2.75	0.77	1.10	0.11
BORB-2	6.63	1.70	1.44	3.72	0.77	0.38	4.11	2.09	0.62
IND-1	8.00	2.66	0.91	4.87	1.20	3.47	0.27	1.90	0.10
IND-9	11.04	2.11	2.08	8.97	1.00	3.06	0.52	3.18	0.17

4.4.3 BORB-2 Sample:

Geochemical data shows higher enrichment in aluminum (4 atoms) and iron (4 atoms), with significant levels of titanium, calcium, and magnesium (Table 3). The SEM Image targets an altered olivine crystal within a basaltic mass as can be observed in Fig. 3.26. The elevated levels of iron, aluminum, and other elements are attributed to mineral sources within the rock, including altered pyroxenes and plagioclase. The presence of iron, magnesium, manganese, and titanium may be reinforced by the occurrence of the oxide ilmenite (Figure 4.15).

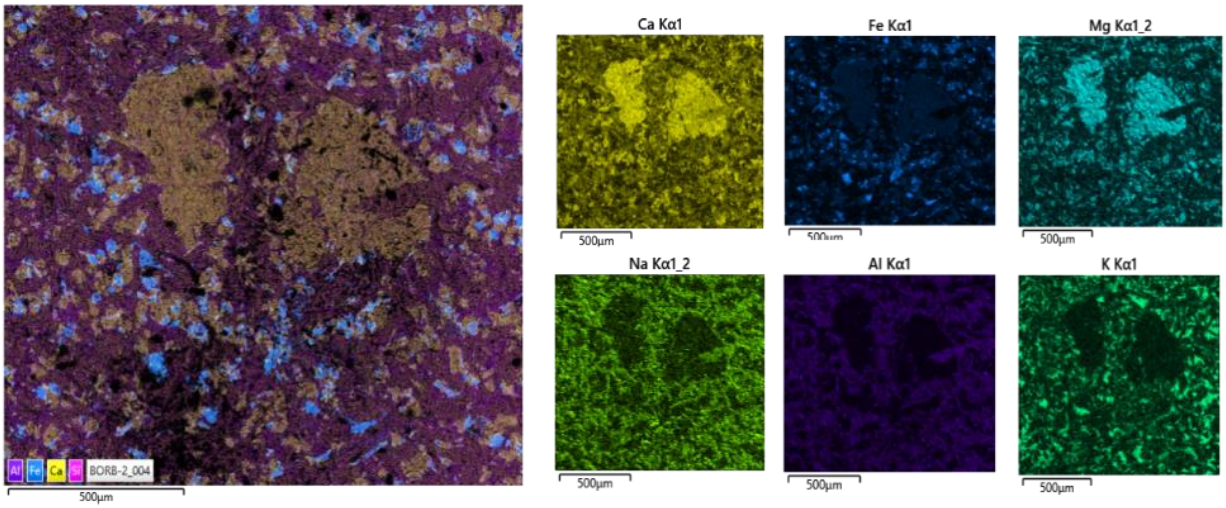

Figure 4.15 - SEM-EDS elements map of the vesicular basalt, targeting an altered olivine crystal embedded in a hypocrystalline matrix rich in sodium and potassium.

4.4.4 IND-1 Sample

Geochemical data shows the highest content of iron (5 atoms), with significant amounts of aluminum, calcium, and titanium, and lower levels of magnesium and sodium (Table 3). The SEM Images target an amygdala filled with a sodic zeolite, surrounded by a K-rich border and a micro-fracture within the matrix as can be observed in Figure 4.16 and Figure 4.17. The basalt's hypocrystalline matrix appears to be more altered. The elevated iron content is prominent in this sample, along with other elements originating from various minerals in the rock. The presence of iron, magnesium, manganese, and titanium may be reinforced by the occurrence of the oxide ilmenite. The micro-vesicle contains sodic zeolites, including analcite, and the basalt matrix appears to have undergone alteration.

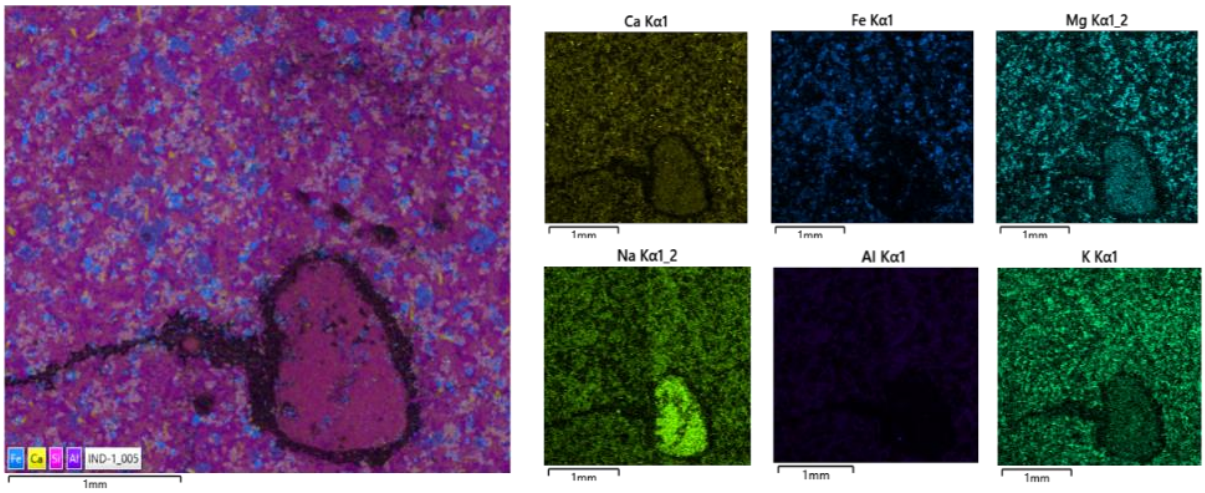

Figure 4.16 - SEM-EDS elements map of an amygdala filled with a sodic zeolite and a sodic alteration border

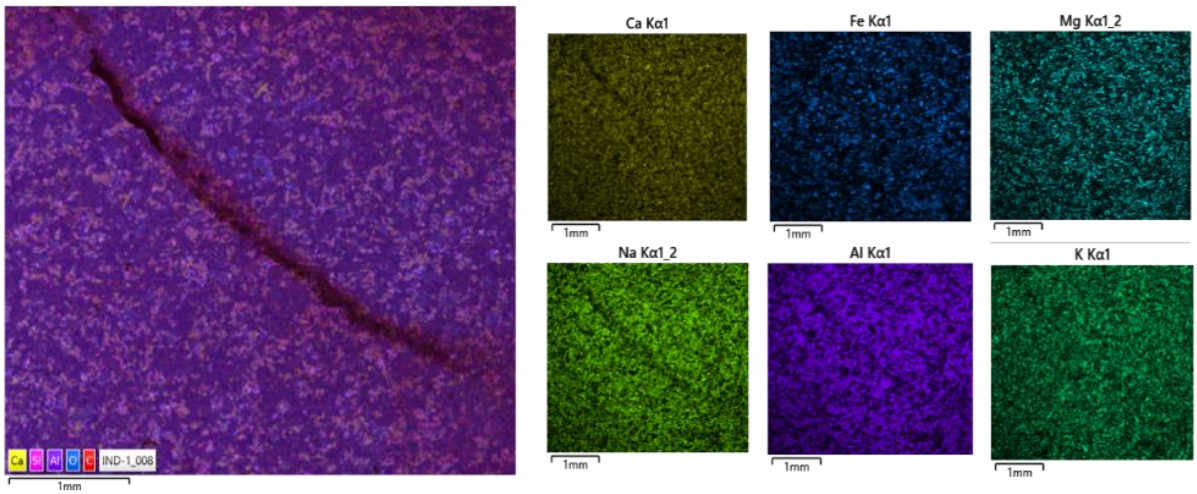

Figure 4.17 - SEM-EDS elements map of a microfractured within the basaltic matrix, especially poor in calcium.

4.4.5 IND-9 Sample

Geochemical shows the highest content of iron (9 atoms), with significant levels of titanium, aluminum, calcium, and magnesium (Table 3). The SEM Image targets a more altered hypocrystalline matrix. Presence of ilmenite is highlighted, along with blade-shaped K-Na-rich crystals. P is also present, possibly associated with a hydrothermal fluid (Figure 4.18).

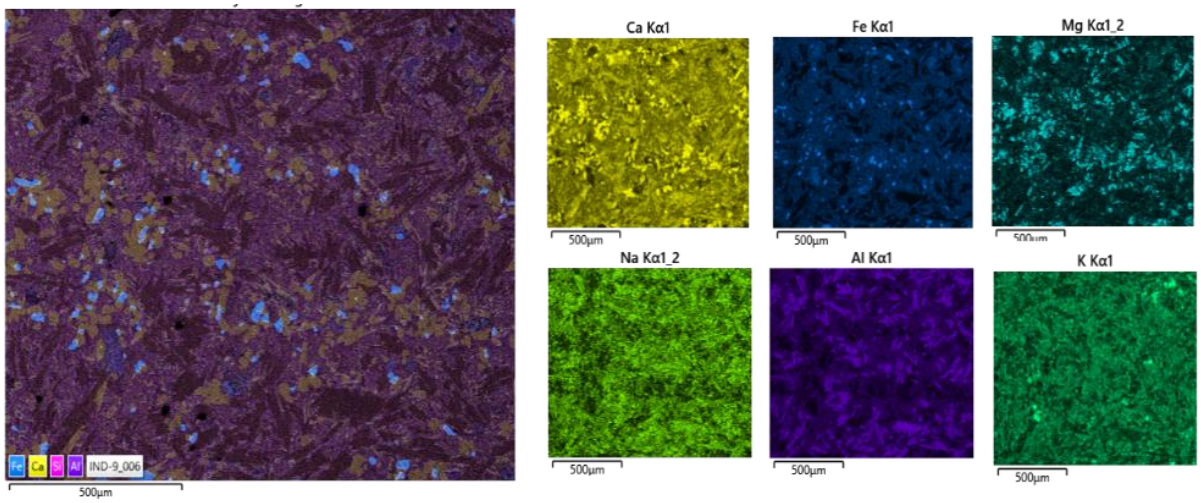

Figure 4.18 - SEM-EDS elements map of the basaltic matriz, characteristic of rocks with textures. Matrix shows high presence of sodium and potassium.

Similar to IND-1, this sample exhibits elevated iron content, along with other elements sourced from minerals within the rock. The presence of iron, magnesium, manganese, and titanium may be reinforced by the occurrence of the oxide ilmenite. The observation of ilmenite and K-Na-rich crystals suggests specific mineral formations, and the presence of phosphorus may be linked to hydrothermal activity.

Through the analysis of five representative basalt samples using Scanning Electron Microscopy with Energy Dispersive X-ray Spectroscopy (SEM-EDS), it was determined the atomic content of the minerals rock (Figure 4.19). This atomic composition is important for understanding the available atoms that might play a significant role in dissolution and precipitation reactions during the carbon mineralization process. Notably, the Serra Geral basalts showcase a substantial potential, providing between 4 to 8 atoms of iron (Fe), 2 to 3 atoms of aluminum (Al), approximately 2 atoms of calcium (Ca), and roughly 1.3 atoms of magnesium (Mg).

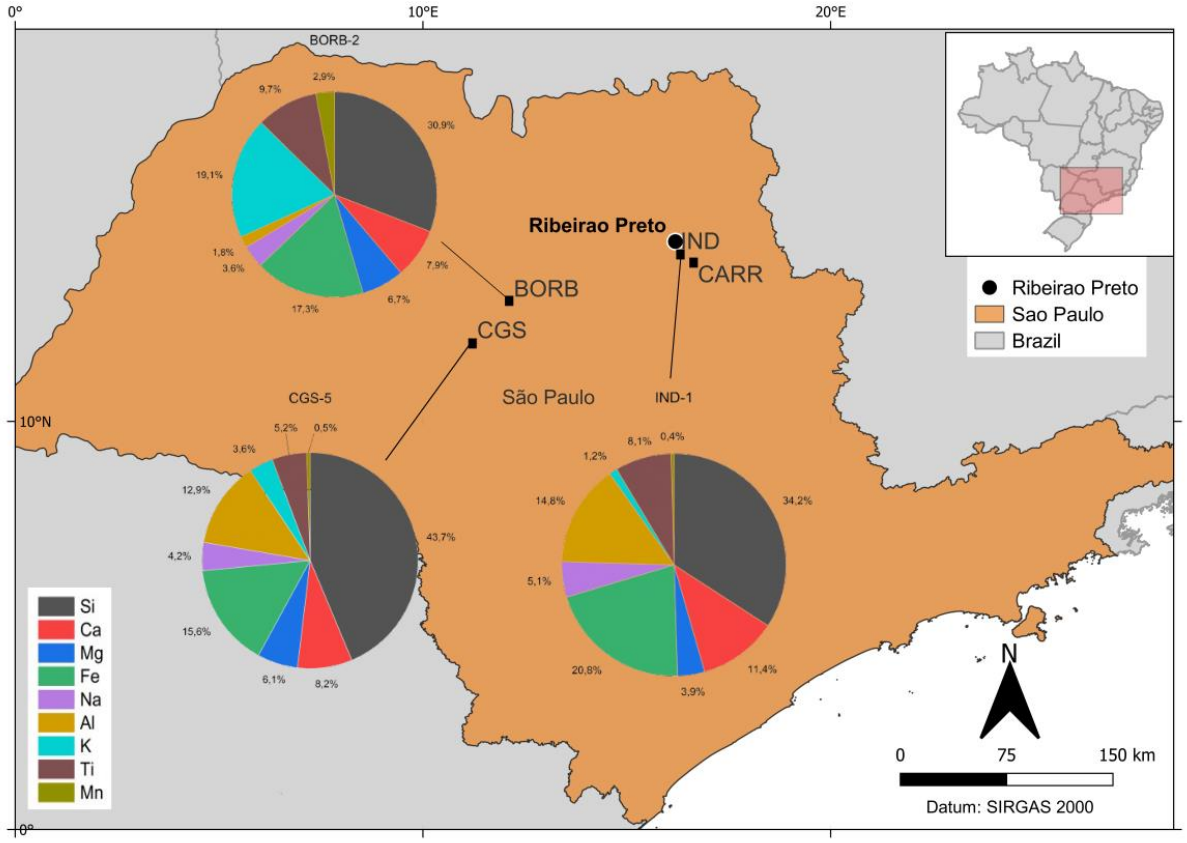

Figure 4.19 - Atomic percents of the elements in the basalt minerals

4.5 Experimental reactions

The experiments are carried out in partnership with Institute of Physics of the University of São Paulo (IFUSP). In the SAMPA laboratory atomic models were performed to calculate the adsorption energy of CO_2 in the crystalline structure and the CO_2 injection tests into powdered basalt were carried out at the Materials Laboratory. Some experimental testes have already been performed and results were analyzed at the Institute of Energy and Environment (IEE) using DRX technique and at the Geoscience Institute (IGc) using SEM technique. Precipitation of dolomite and calcite was observed.

4.5.1 Atomistic Approach

First principles calculations were carried out, based on density functional theory, in order to evaluate the catalytic activity of the minerals that make up the basaltic rocks of the Serra Geral Formation by PhD. Alvaro Torres Baptista. These minerals correspond to the plagioclase group of Ca-rich feldspars (anorthite, bytownite and labradorite). The adsorption process of CO_2 molecules was evaluated. The results showed that, in all cases, the calculated adsorption energy was negative, suggesting that the adsorption processes are favorable from a thermodynamic

point of view. These values were between -0.5 and -3.0 eV, remembering that more negative values indicate a strong interaction between adsorbate and surface mineral. On the other hand, adsorption energies close to -0.5 eV correspond to a weak interaction, called physisorption. Labradorite presented the values closest to physisorption, followed by bytownite and finally anorthite. Complementary analyzes are necessary to suggest an order of catalytic activity of the studied minerals.

4.5.2 Experimental set up

Laboratory facilities for CO_2 injection were set up at the SAMPA-Laboratory of Materials of the Institute of Physics of the University of São Paulo by PhD. Saulo de Tarso Alves dos Passos. The set up consists of reactors cylinders, CO_2 line, water line, boiling system and precipitation beakers. Basalt samples of the Serra Geral Formation were tested with CO_2 fluids at different concentrations of this gas and NaCl to vary the pH of the solution. Temperature was also varied between 30 and 90°C. It was not possibly to set up a pressure system.

4.5.3 Characterization post reaction

Once the injection experiments concluded, the precipitated products were analyzed at the X-ray Diffraction Laboratory of the IEE-USP by PhD Gabriel Capistrano Godinho. Results shows the presence of mineral carbonate species such as dolomite, aragonite and calcite. At the SEM Laboratory of the IGc, the precipitates were visually analyzed. The actual formation of the carbonates was verified by the image analyses of the textures and geometry of these products.

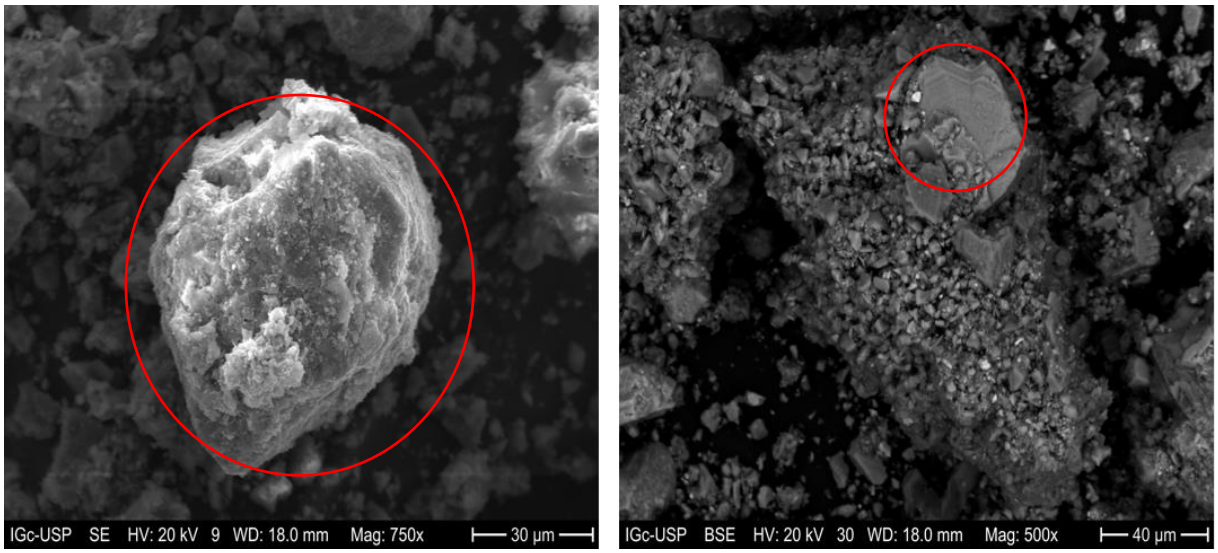

Figure 20. SEM-EDS image showing anorthite and dolomite formed by the CO_2 injection experiments. Images acquire by PhD Gabriel Capistrano Godinho

4.6 Geochemical database of the Paraná basin and descriptive analysis

The analysis of a set of 500 basalt samples from available published works reveals interesting insights into the concentrations of various compounds (Pacheco et al., 2018; Machado et al., 2018; Rocha-Júnior et al., 2020a; Giovanardi et al., 2022). The samples have been categorized based on the concentration ranges for CaO, Fe_2O_3, MgO, SiO_2, and Sr.

1. CaO Concentration: The CaO concentrations in the samples vary between 8 and 10 w%. Approximately 80 to 140 samples fall within this concentration range (Figure 4.21).
2. Fe_2O_3 Concentration: The Fe_2O_3 concentrations in the samples range from 13 to 16 w%. This concentration range is observed in approximately 160 to 210 samples (Figure 4.21). It indicates a relatively wider range compared to CaO, and a substantial portion of the samples falls within this range.
3. MgO Concentration: The MgO concentrations in the samples vary between 4 and 5 w%. Approximately 60 to 140 samples exhibit this concentration range (Figure 4.21). The range is narrower compared to CaO and Fe_2O_3, suggesting a more consistent concentration for MgO.

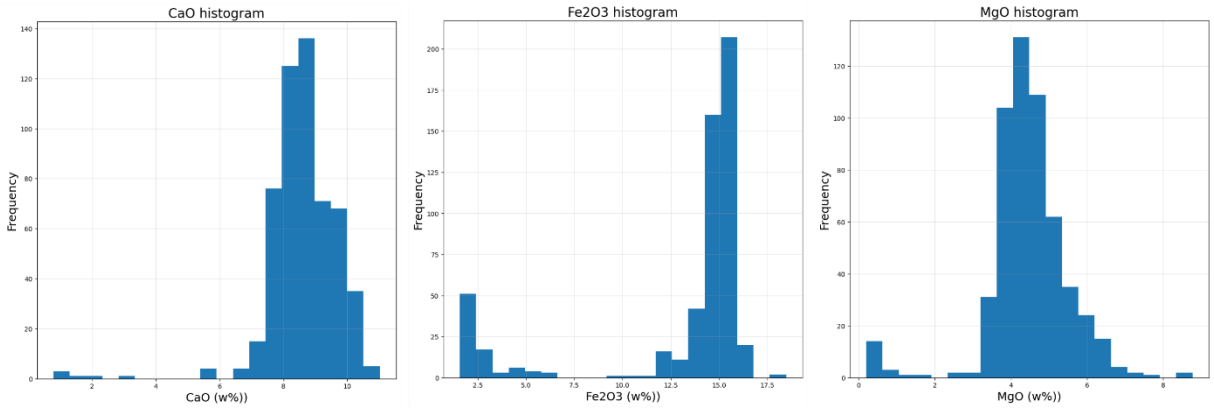

Figure 4.21 - Frequency of calcium, iron and magnesium concentrations of the basalt sample.

4. SiO_2 Concentration: Over 200 samples in the dataset display a SiO_2 content of approximately 53 w% (Figure 4.22). This concentration appears to be predominant in the dataset, indicating a common composition in a significant number of samples.
5. Sr Concentration: More than 150 samples contain 400 ppm (parts per million) of Sr (Figure 4.22). This suggests that a substantial portion of the samples set has a consistent Sr content at this specific concentration level.

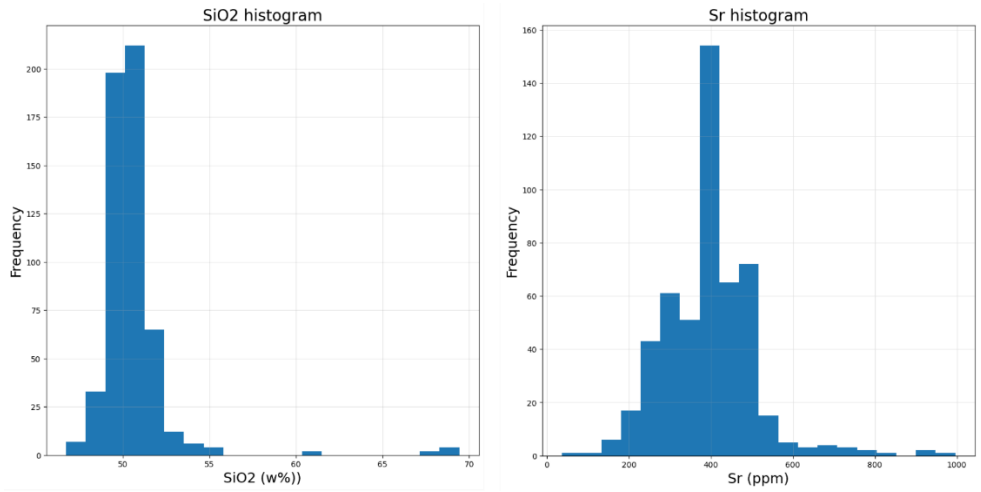

Figure 4.22 - Frequency of silica oxide and strontium concentrations of the basalt samples.

4.6.1 Geochemical behavior at depth

In terms of the possible cations' abundance at different depths, there is no discernible correlation among them. The variations in depth do not significantly impact the relative abundances of these cations. However, there is a notable consistency in the layered distribution of their abundances across different depths (Figure 4.23).

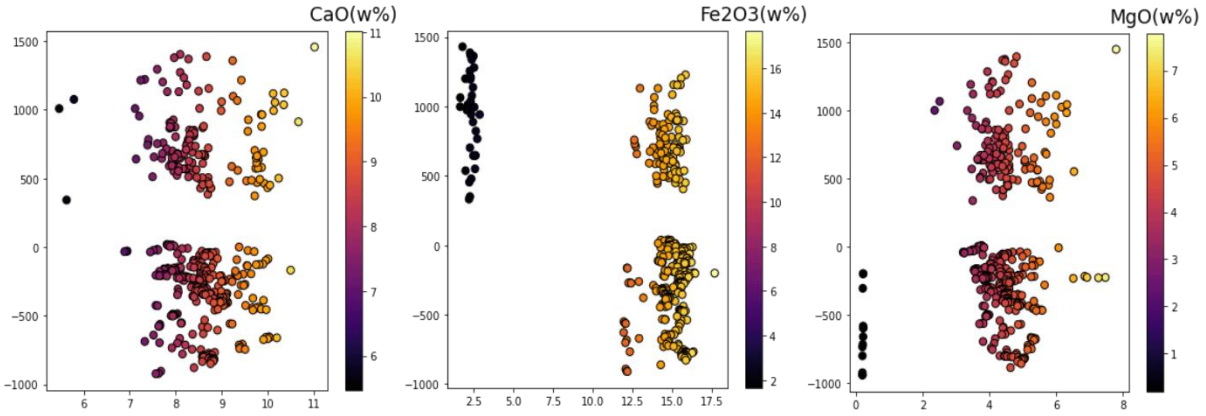

Figure 4.23 - Dispersion graph showing the behavior at depth of calcium, iron and magnesium oxide in the basalt samples.

MnO displays a higher abundance at greater depths within the basin. Concentrations of MnO range from 15 to 17 w% in these deeper sections. The abundance of Sr, demonstrates a correlation with depth. Higher elevations within the basin correspond to greater abundance, with Sr concentrations exceeding 900 ppm (Figure 4.24). Overall, the concentration patterns of various cations, the degree of alteration, and the relationship between cation abundance and

depth provide valuable insights into the composition and characteristics of the basaltic flows within the basin.

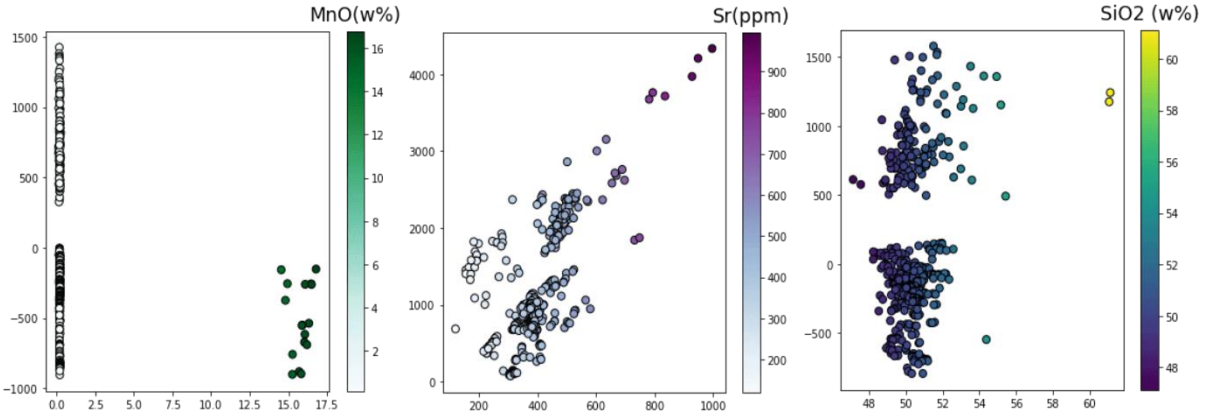

Figure 4.24 - Dispersion graphs showing the behavior at depth of manganese and silica oxide, and strontium in the basalt samples.

4.6.2 Geochemical distribution in the Paraná basin

After the statistical analysis and refinement of the geochemical data base, a series of maps were constructed in order to observed the oxide composition distribution within the basin. With focus in the São Paulo state, is presented the abundance of the oxides containing the main elements that may turn into available cations for the carbon mineralization reactions. These maps account as geochemical layers for a potential geological site selection for CO_2 injection.

The distribution of concentration areas within the basin exhibits distinct patterns for different elements. CaO concentrations exceeding 8.9 w% are predominantly found in the central to northern regions of the basin (Map 3.1). These areas showcase a higher presence of calcium oxide in the rock composition.

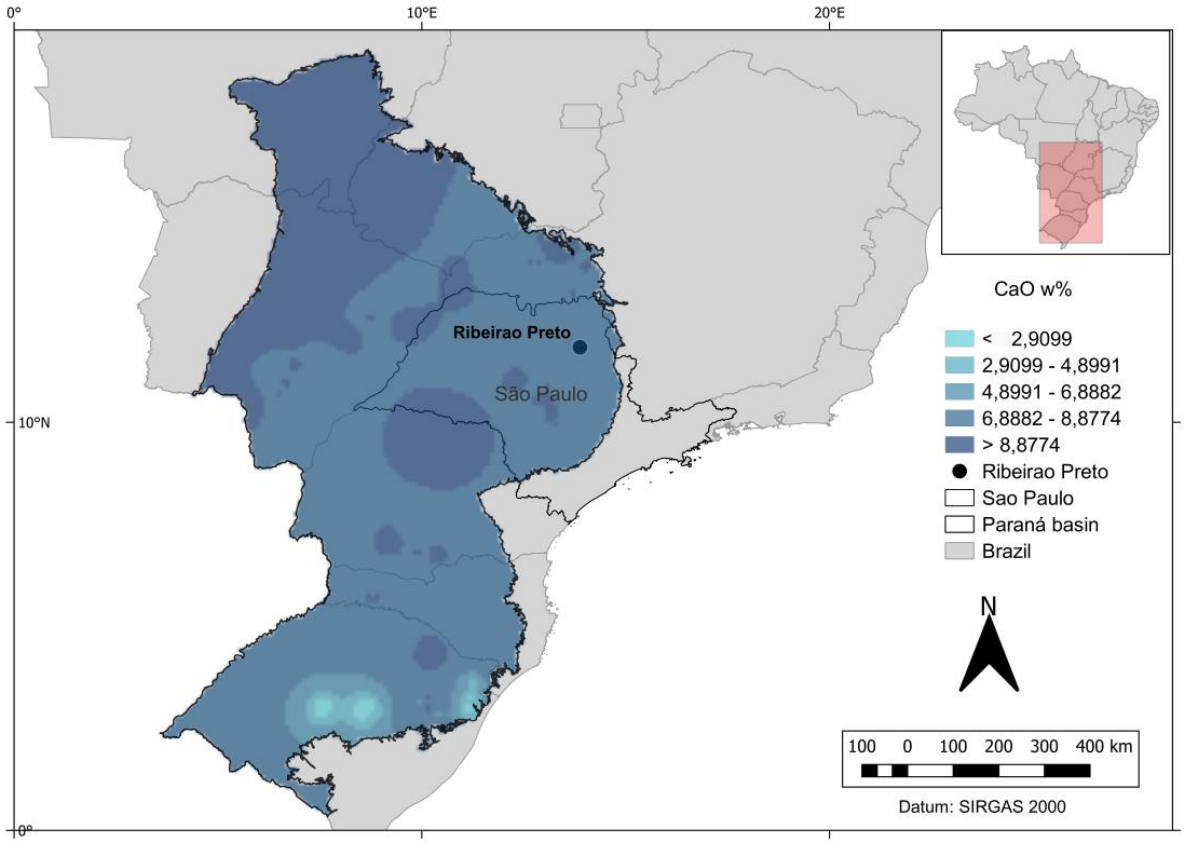

Map 4.1 - Chemical distribution of calcium oxide concentrations in the Paraná basin.

Fe_2O_3 concentrations do not exhibit a specific trend in relation to other cations. When Fe_2O_3 exceeds 12 w%, it is predominantly found in the southwestern area of the basin, while being depleted in the central to south area and the northern corner (Map 3.2). This implies that iron oxide concentration is not directly influenced by the distribution of other cations in the rock formation.

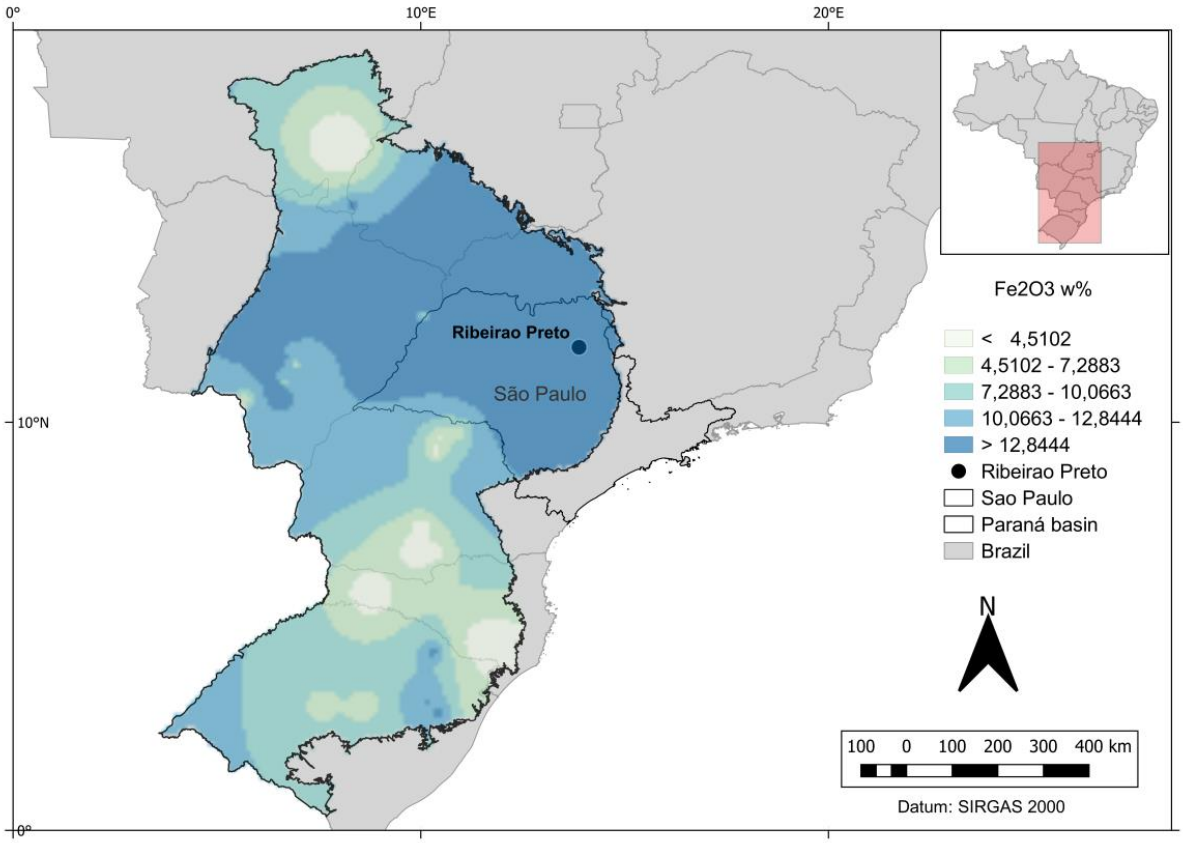

Map 4.2 - Chemical distribution of iron oxide concentrations in the Paraná basin.

On the other hand, MgO concentrations above 5.8 w% are observed in smaller areas, primarily located in the northern part, with some portions extending to the central and southern regions (Map 3.3). The concentration of magnesium oxide demonstrates less extent compared to CaO.

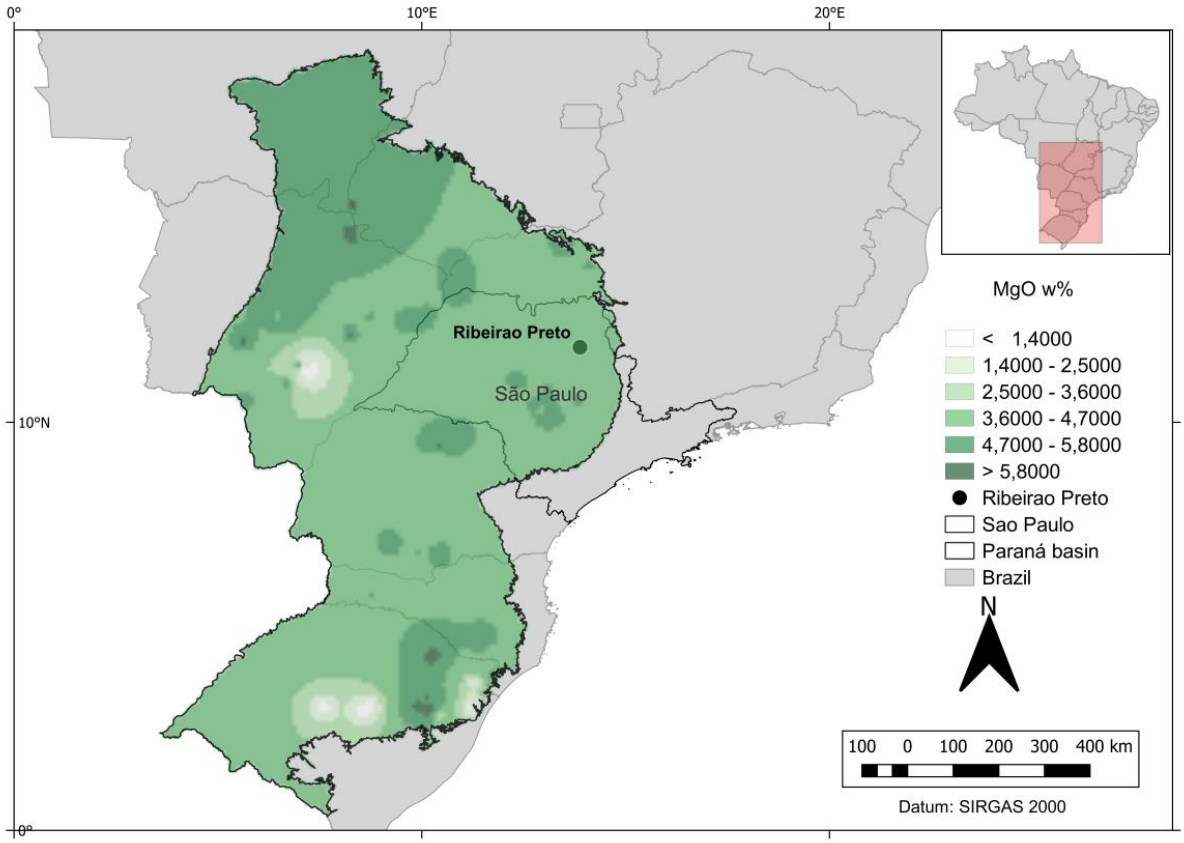

Map 4.3 - Chemical distribution of magnesium oxide concentrations in the Paraná basin.

TiO concentrations are higher in the western side of the basin, spread mainly in the São Paulo and Minas Gerais state (Map 3.4). TiO is less than 1 w% especially in the southern portions of the basin in the Paraná and Rio Grande do Sul states.

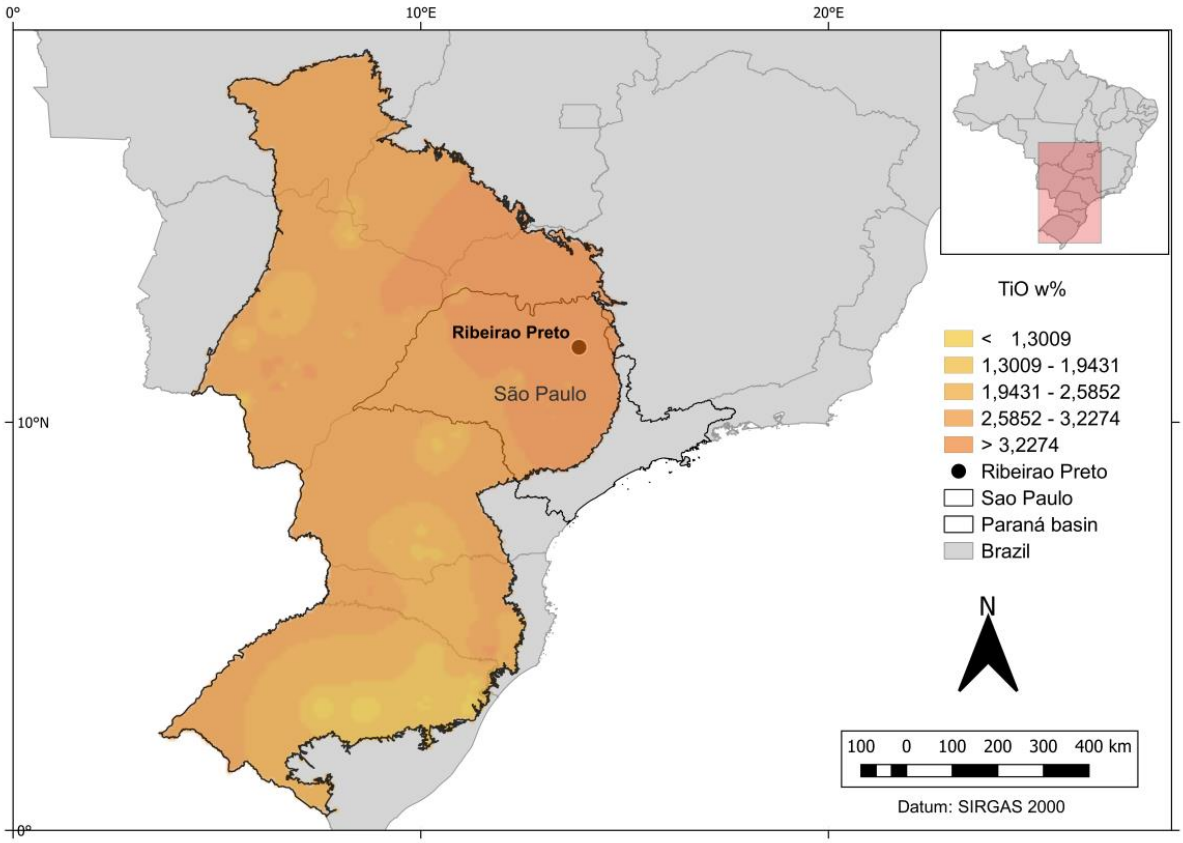

Map 4.4 - Chemical distribution of titanium oxide concentrations in the Paraná basin.

Sr concentration is particularly low in the northeastern part of the basin and in the Paraná state, with less than 340 ppm. In the rest of the basin, Sr concentration ranges from 540 to 734 ppm (Map 3.5).

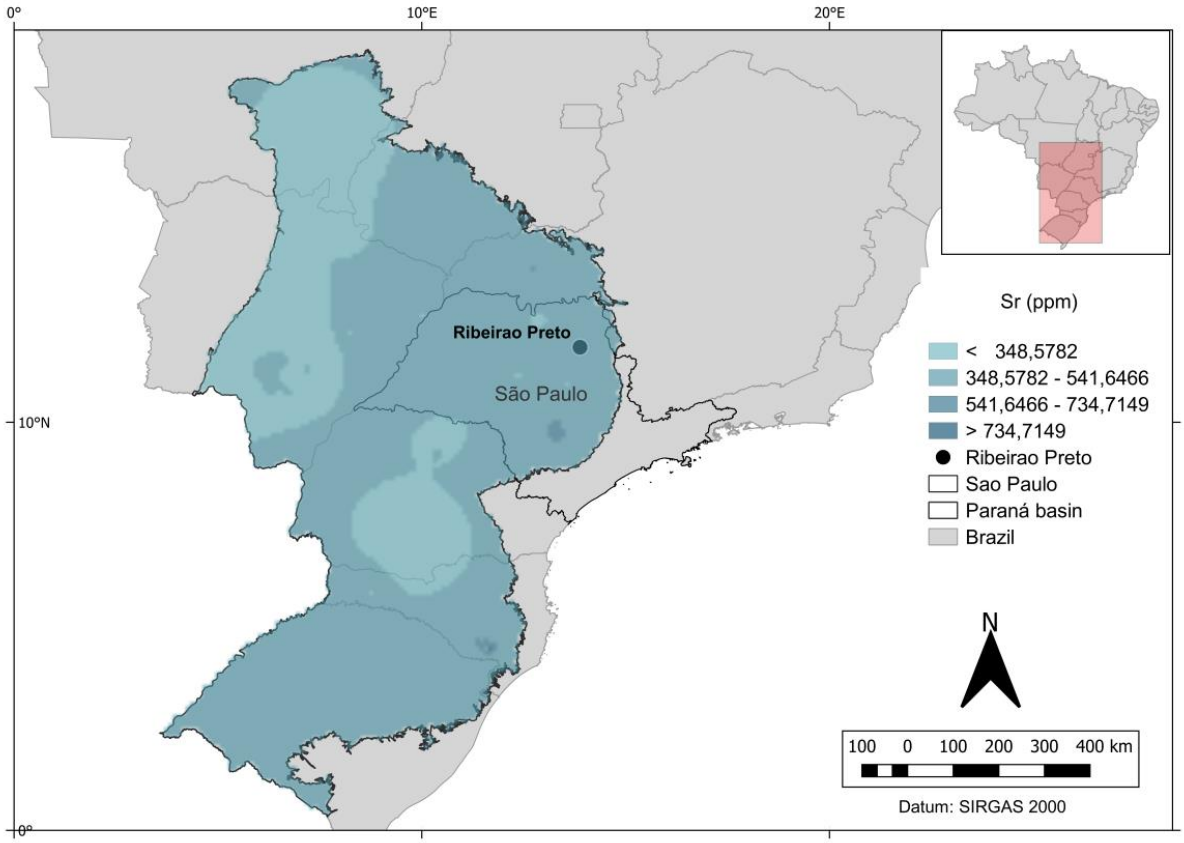

Map 4.5 - Chemical distribution of strontium concentrations in the Paraná basin.

Lost on ignition, which indicates the level of rock alteration, reveals that the main areas of altered basalt are spread in the southeastern region and the south corner of the basin (Map 3.6). As one moves from São Paulo state to Santa Catarina state, the outcrop basalts exhibit lesser degrees of meteorization. This suggests that the alteration grade of the rock gradually decreases from the south towards the center of the basin.

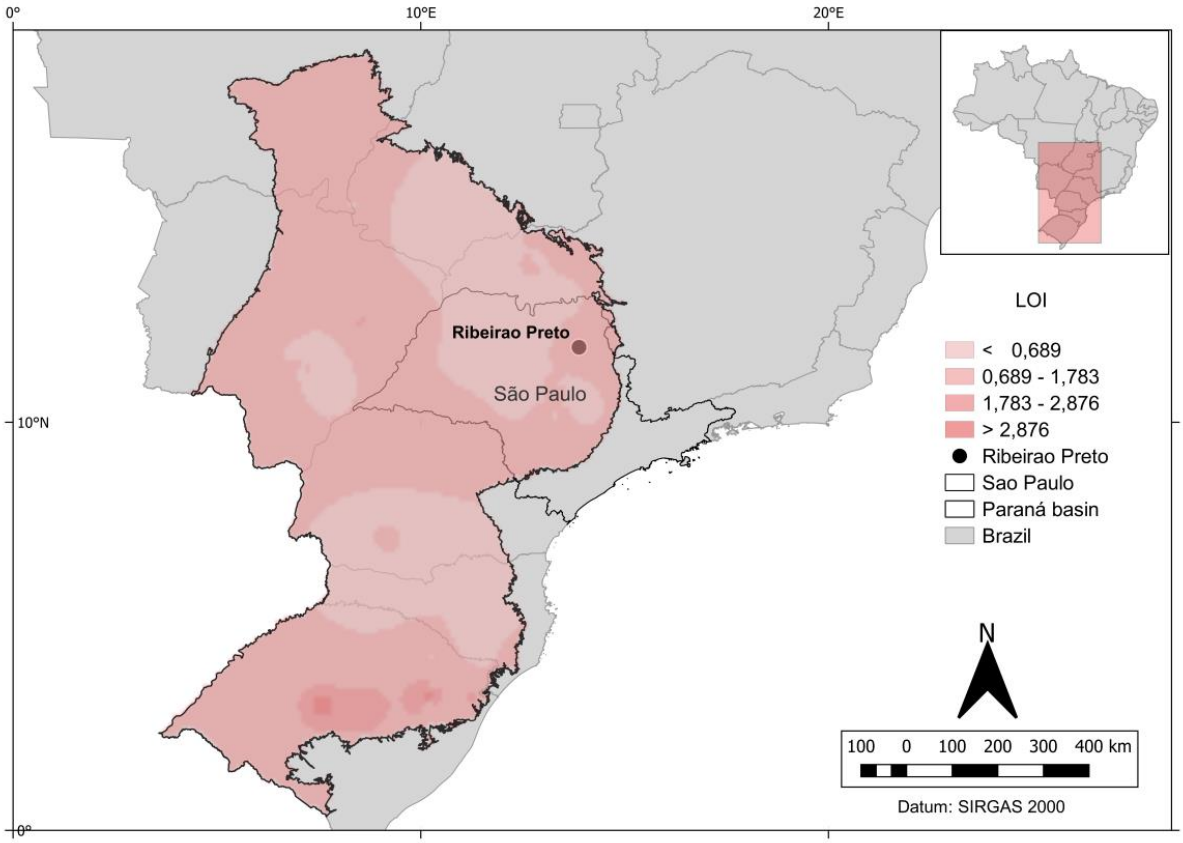

Map 4.6 - Distribution of the basalts lost on ignition values in the Paraná basin.

In conclusion, the São Paulo state as location of interest is showcasing the higher contents of the main geochemical elements for carbon mineralization. With a composition of iron oxide over 12%, about 8% of calcium oxide, from 4 to 6% of magnesium oxide, titanium oxide superior to 3%, strontium over 500 ppm and lost on ignition below 2 among lithological textures of microvesiculated and fractured basalt.

5 Discussion

5.1.1 Mineral review

The basalts of the Serra Geral Formation have a general mineralogy of 39% of Ca-Palgioclase, 35% of Ca-clinopyroxene and 3% of Celadonite, an age of 134My and an extension of 1600km^2, that provides them with great potential as a reservoir for CO_2 mineralization. Especially if the characteristics of other volcanic provinces such as Central American Magmatic Province-CAMP, Columbia River Basalt-CR and the Mid- Ocean Ridge Basalts-MORB of Iceland are taken into account. These basalts have already been successfully tested for carbon mineralization. Table 4 presents the characteristics described for mentions basalts.

Table 4. Magmatic provinces tested for carbon mineralization.

Magmatic Province	Type	Age	Reference
Serra Geral	Continental flood basalt	> 135My	Machado et al. (2018)
CAMP	Continental flood basalt	>200My	Schaef et al. (2010)
CR	Continental flood basalt	<10My	Schaef et al. (2010)
Stapafell Mountain	Mid-ocean ridge basalt	< 1My	Marieni et al. (2018)

CAMP is a continental flood basalt older than 200 My, especially rich in Ca-Plagioclase (43%) and glass (31%). CR is a continental flood basalt as well, younger than 10 My, with higher presence of Ca-Plagioclase (35%) and glass (45%). Finally, the Stapafell Mountain is a MORB type basaltic province, younger than 1 My and has an elevated content of Ca-Plagioclase (41%) and Olvine (16%).

When Serra Geral is compared with these provinces lot of similarities can be noticed (Figure 5.1). Regarding the presence of plagioclase, they have a difference between 2 and 5%. For pyroxene, a difference between 1 and 17%. For olivine, a difference of 15%, being present only in the MORB, the other continental basalts do not include olivine in their mineral content descriptions. For the oxide content, a difference between 5 and 9%. For glass, a difference between 2 and 39%. The occurrence of celadonite counts as unique among these basalts.

Therefore, a great mineralizing potential can be expected from the basalts in Brazil. Since the source of calcium for the fluid enrichment and carbonates precipitation in this case would be plagioclase and pyroxene minerals.

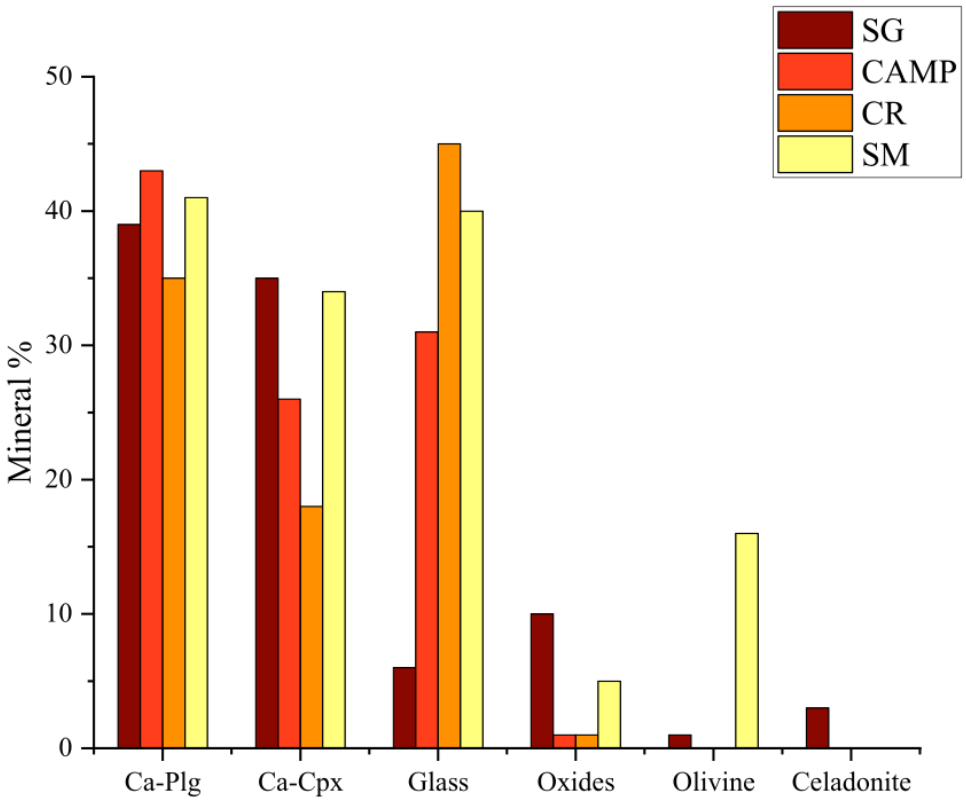

Figure 5.1 - Mineral comparison related to other continental basalts that have already been tested and mineralized.

5.1.2 Geochemical review

As it was presented in the Mineral review section, continental basalts as the Columbia River, Central America Magmatic Province, Newark Basin basalts in North America, the Deccan traps in India, the Karoo basalts in Africa and the MORB basalts in Iceland, share a very similar mineral content with the Serra Geral Formation in Brazil (Figure).

Therefore, beyond mineral, its geochemical bulk composition is very similar as well. In the experiments performed by Schaef et al. (2010), before injecting the supercritical CO_2 into the continental basalts of United States, India and South Africa, their geochemical characterization was determined. Showing a bulk composition expressed in oxide (wt%), these basalts have a

content of SiO_2 greater than 50%, Fe_2O_3 superior to 14%, Al_2O_3 of ~13% and CaO of ~10%. After three years of injection and different reaction rates, they got to precipitate carbonate nodules, clays and sulfurs. Concluding that the formation of products is going to depend on the composition of the injection fluid over the rock composition.

On the other hand, the geochemical characterization performed by Marieni and Oelkers (2018) in the basalts of the Stapafell Mountain, before the injection experiments with CO_2 dissolved in seawater, show similar values as well. With a SiO_2 content of ~48%, it already indicates is a MORB type basalt, Al_2O_3 of 15%, CaO superior to 11% and Fe_2O_3 superior to 10%. In this case, authors investigated the dissolution rates of the minerals on glass, crystalline basalt and altered basalt, performing reaction experiments at different pH and a maximum temperature of 100°C. Conclusion was that plagioclase appeared to be more reactive than pyroxene, and the dissolution and released of cations from natural secondary mineral products have the potential to form carbonate precipitated as well.

Acknowledging the characteristics and properties of these tested basalts, allows to expect a positive potential for the CO_2 injection experiments in the Serra Geral Formation basalts. As it can be seen in the Figure 5.2, geochemical composition values present differences below 5% and as performed experiments indicates, mineralization potential does not depend on the geological setting, leaving the door open for infinite possibilities of use in carbon mineralization and storage for the basalt in Brazil.

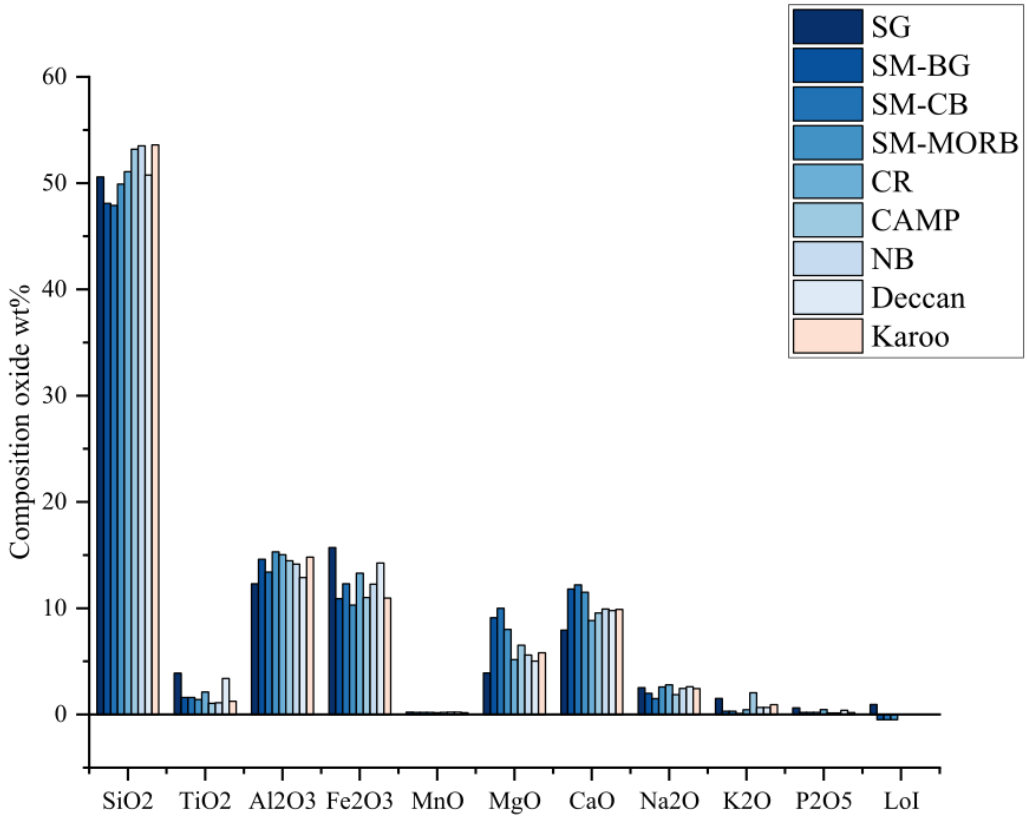

Figure 5.2 - Comparative oxide composition between Serra Geral Formation (SG), Stapafell Mountain (SM), Columbia River basalts (CR), Central American Magmatic Province (CAMP), Newark basin (NB), Deccan and Karoo.

Through the analysis of five representative basalt samples using Scanning Electron Microscopy with Energy Dispersive X-ray Spectroscopy (SEM-EDS), it was determined the atomic content of the minerals rock (Figure 4.19). This atomic composition is important for understanding the available atoms that might play a significant role in dissolution and precipitation reactions during the carbon mineralization process. Notably, the Serra Geral basalts showcase a substantial potential, providing between 4 to 8 atoms of iron (Fe), 2 to 3 atoms of aluminum (Al), approximately 2 atoms of calcium (Ca), and roughly 1.3 atoms of magnesium (Mg).

5.1.2.1 Geochemical site selection

The São Paulo state qualified as a favorable injection site from the geochemical and textural point of view. With a composition of iron oxide over 12%, about 8% of calcium oxide, from 4 to 6% of magnesium oxide, titanium oxide superior to 3%, strontium over 500 ppm and lost on ignition below 2 among lithological textures of microvesiculated and fractured basalt, the basaltic flows of this state is promissory for CO_2 injection and carbon mineralization.

5.2 Carbon mineralization in the Serra Geral Basalts

The CO_2 injection experiments conducted by SAMPA Laboratories at the Institute of Physics (USP) on basalt samples have yielded insights into the Serra Geral Formation mineralization potential of CO_2. These experiments have shed light on the critical role that basalt texture plays in the process. It appears that the areas of massive or fractured basalt exhibit the greatest capacity to enrich the carbonate fluid with cations through mineral dissolution. As it is proved by the precipitation of dolomite, aragonite and calcite. This underscores the importance of understanding the geological characteristics of the subsurface when considering carbon capture and storage strategies.

Vesicular levels, typically found either below or at the top of these enriched massive areas, present an interesting dynamic. Once the carbonate-enriched fluid infiltrates these spaces, it can initiate the precipitation of various carbonate species within the pore spaces. The heterogeneity of flows, marked by fractures and faults within the basalt, offers additional conduits for fluid movement and carbonate precipitation.

It is worth noting that the dissolution of secondary products within the basalt formation may also come into play. This could either promote carbon mineralization or, on the contrary, lead to the formation of other clay species that might clog the pore spaces. Moreover, to mitigate potential clogging effects, the circulation of deep aquifer waters emerges as a key factor. These waters can facilitate the movement and transportation of the injected fluid, reducing the risk of pore space obstruction.

In conclusion, the mineralization potential of CO_2 in basalt formations is influenced by various factors, including basalt texture, geological heterogeneity, and the dissolution of secondary products. Understanding these intricacies is crucial for developing effective carbon capture and storage strategies. Moreover, harnessing the circulation of deep aquifer waters can prove instrumental in optimizing these processes and mitigating potential challenges.

6 Conclusions

The studied basalt flows from the Ribeirão Preto – Reginópolis regions presents dimensions bigger than 15x15m in average. In this region, the flow types predominantly found are simple pahoehoe and pounded pahoehoe. These basalt flows are characterized by microvesiculated-amygdaloidal and massive-glomeroporphyritic textures, respectively. In the basin. its cretaceous flows are widespread over an area of ~1600km^2 and reaches depths greater than 1700m, accounting as a good geometry for an igneous reservoir targeting mineral trapping

The mineral content that makes up these textures represent the chemical source for carbon mineralization. Serra Geral Formation basalt have an average mineralogy for Ca-plagioclase, Ca-clinopyroxene and celadonite of 39%, 35% and 3%. Moreover, acknowledging the geological similarities that the Serra Geral basalt shares with other continental basalts already successfully tested for carbon mineralization, such as the Central American Magmatic Province (CAMP), Columbia River Basalt (CR) and even the Mid- Ocean Ridge Basalts-MORB of Iceland provides these basalts as good candidates at reservoir scale for CO_2 mineralization.

The Serra Geral Formation in Brazil shares a strikingly similar geochemical composition with various continental basalts worldwide. Experiments with similar basalts revealed the formation of carbonate nodules, clays, and sulfurs upon injecting supercritical CO_2. The type of products formed depended on the injection fluid's composition relative to the rock. Another study on MORB basalts at Stapafell Mountain yielded analogous results, indicating that plagioclase was more reactive than pyroxene. Acknowledging these characteristics suggests a positive potential for CO_2 injection in Serra Geral Formation basalts. Geochemical composition differences below 5% and successful experiments imply that mineralization potential does not depend strongly on geology, open possibilities for carbon mineralization and storage in Brazil.

The atomic composition representing the potential available atoms that may participate in dissolution and precipitation reactions during carbon mineralization process appears to be sufficient for carbonates formation. Carbonates typically form through reactions involving divalent cations such as Ca^{2+} and Mg^{2+}, along with $CO3^{2-}$ ions.

Experiments conducted by SAMPA Laboratories on Serra Geral Formation basalt samples highlight the influence of basalt texture on CO_2 mineralization potential. Massive and fractured basalt areas seem to be most effective at enriching carbonate fluids with cations through mineral

dissolution, leading to the precipitation of carbonates like dolomite, aragonite, and calcite, as occurred in the CO_2 injection testes. Vesicular levels within these areas would enable further carbonate species precipitation. However, in realistic reservoir conditions, the basalt's heterogeneity, marked by fractures and faults, may affect fluid movement and mineralization. Dissolution of secondary products could promote or hinder mineralization. Deep aquifer waters play a vital role in preventing pore space obstruction by facilitating fluid movement.

Finally, São Paulo state is identified as potential location for CO_2 injection and carbon mineralization based on the basalt flows geochemical and textural characteristics. These regions boast basaltic flows with good composition percents of iron oxide, calcium oxide, magnesium oxide, titanium oxide, strontium concentrations, and lost on ignition values indicating low weathering. In conclusion, the lithological textures of microvesiculated and fractured basalt in this state make it a promising candidate for CO_2 injection and subsequent carbon mineralization.

6.1 Further work

In order to advance in the understanding and feasibility of carbon capture and geological storage in the Serra Geral basalts, contributing to sustainable carbon management efforts in Brazil, it is yet necessary research on the following matters:

1. Quantifying Mineralization at Reservoir Scale: Future research should focus on quantifying the carbon dioxide (CO_2) mineralization potential at a reservoir scale within the Serra Geral basalts. This involves assessing the extent to which CO_2 can be permanently converted into stable mineral forms, such as carbonates, providing valuable insights into long-term storage capacity.

2. Evaluating Carbon Mineralization in Fractures: Understanding the role of fractures within the basalts in the carbon mineralization process is essential. Further investigations should delve into how fractures influence the speed and efficiency of CO_2 mineralization, as well as their impact on long-term storage integrity.

3. Estimating Permeability Changes: Assessing changes in permeability induced by injected CO_2 fluid is critical to ensure the safety and feasibility of geological storage. Research should aim to quantify how CO_2 injection alters the rock's permeability and porosity, which is essential for predicting fluid migration and containment.

4. Pilot Injection Impact on Aquifer System: Modelling a pilot injection of CO_2 provides a valuable opportunity to assess its potential impacts on the Serra Geral-Guarani aquifer system. Future work should focus on monitoring changes in groundwater quality, aquifer pressure, and potential migration of CO_2 or brine fluids to ensure the integrity of the aquifer and its long-term protection.

References

Akkaş, E., Akin, L., Evren Çubukçu, H., and Artuner, H., 2015, Application of Decision Tree Algorithm for classification and identification of natural minerals using SEM–EDS: Computers & Geosciences, v. 80, p. 38–48, doi:10.1016/j.cageo.2015.03.015.

Al Hameli, F., Belhaj, H., and Al Dhuhoori, M., 2022, CO2 Sequestration Overview in Geological Formations: Trapping Mechanisms Matrix Assessment: Energies, v. 15, p. 7805, doi:10.3390/en15207805.

Alfredsson, H.A., Oelkers, E.H., Hardarsson, B.S., Franzson, H., Gunnlaugsson, E., and Gislason, S.R., 2013, The geology and water chemistry of the Hellisheidi, SW-Iceland carbon storage site: International Journal of Greenhouse Gas Control, v. 12, p. 399–418, doi:10.1016/j.ijggc.2012.11.019.

Al-Mutairi, S.M., and Kokal, S.L., 2011, EOR Potential in the Middle East: Current and Future Trends, *in* All Days, Vienna, Austria, SPE, p. SPE-143287-MS, doi:10.2118/143287-MS.

Ampomah, W., Balch, R., Will, R., Cather, M., Gunda, D., and Dai, Z., 2017, Co-optimization of CO2-EOR and Storage Processes under Geological Uncertainty: Energy Procedia, v. 114, p. 6928–6941, doi:10.1016/j.egypro.2017.03.1835.

Anchliya, A.., Ehlig-Economides, C.., and Jafarpour, B.., 2012, Aquifer Management To Accelerate CO2 Dissolution and Trapping: SPE Journal, v. 17, p. 805–816, doi:10.2118/126688-PA.

Ansberque, C., Mark, C., Caulfield, J.T., and Chew, D.M., 2019, Combined in-situ determination of halogen (F, Cl) content in igneous and detrital apatite by SEM-EDS and LA-Q-ICPMS: A potential new provenance tool: Chemical Geology, v. 524, p. 406–420, doi:10.1016/j.chemgeo.2019.07.012.

Askarova, A., Mukhametdinova, A., Markovic, S., Khayrullina, G., Afanasev, P., Popov, E., and Mukhina, E., 2023, An Overview of Geological CO2 Sequestration in Oil and Gas Reservoirs: Energies, v. 16, p. 2821, doi:10.3390/en16062821.

Bachu, S., Gunter, W.D., and Perkins, E.H., 1994, Aquifer disposal of CO2: Hydrodynamic and mineral trapping: Energy Conversion and Management, v. 35, p. 269–279, doi:10.1016/0196-8904(94)90060-4.

Benson, S.M., and Cole, D.R., 2008, CO2 Sequestration in Deep Sedimentary Formations: Elements, v. 4, p. 325–331, doi:10.2113/gselements.4.5.325.

Bergamaschi, S., Duarte, A.C.D.F., Serrano, J.S., Figueiredo, A.D.M.B., Vasconcelos, L.C., Oliveira, R.M.A.G.D., Ade, M.V.B., Pinheiro, A.E.P., and Martins, M.V.A., 2016, REGIONAL OUTCROPS WITH DIDACTIC INTEREST AND SEDIMENTARY FACIES ASSOCIATION OF THE ITARARÉ GROUP AT SÃO PAULO (BRAZIL): Journal of Sedimentary Environments, v. 1, p. 159–170, doi:10.12957/jse.2016.21964.

Berger, G., Claparols, C., Guy, C., and Daux, V., 1994, Dissolution rate of a basalt glass in silica-rich solutions: Implications for long-term alteration: Geochimica et Cosmochimica Acta, v. 58, p. 4875–4886, doi:10.1016/0016-7037(94)90218-6.

Bickle, M., Chadwick, A., Huppert, H.E., Hallworth, M., and Lyle, S., 2007, Modelling carbon dioxide accumulation at Sleipner: Implications for underground carbon storage: Earth and Planetary Science Letters, v. 255, p. 164–176, doi:10.1016/j.epsl.2006.12.013.

Blum, A.E., and Stillings, L.L., 1995, Chapter 7. FELDSPAR DISSOLUTION KINETICS, *in* White, A.F. and Brantley, S.L. eds., Chemical Weathering Rates of Silicate Minerals, De Gruyter, p. 291–352, doi:10.1515/9781501509650-009.

Bolster, D., 2014, The fluid mechanics of dissolution trapping in geologic storage of CO_2: Journal of Fluid Mechanics, v. 740, p. 1–4, doi:10.1017/jfm.2013.531.

Bongiolo, A.D.B.E.S., Ferreira, F.J.F., Bittencourt, A.V.L., and Salamuni, E., 2014, CONNECTIVITY AND MAGNETIC-STRUCTURAL COMPARTMENTALIZATION OF THE SERRA GERAL AND GUARANI AQUIFER SYSTEMS IN CENTRAL STATE OF PARANÁ (PARANÁ BASIN, BRAZIL): Revista Brasileira de Geofísica, v. 32, p. 141, doi:10.22564/rbgf.v32i1.402.

Bradshaw, J., Bachu, S., Bonijoly, D., Burruss, R., Holloway, S., Christensen, N.P., and Mathiassen, O.M., 2007, CO2 storage capacity estimation: Issues and development of standards: International Journal of Greenhouse Gas Control, v. 1, p. 62–68, doi:10.1016/S1750-5836(07)00027-8.

Busch, A., and Gensterblum, Y., 2011, CBM and CO2-ECBM related sorption processes in coal: A review: International Journal of Coal Geology, v. 87, p. 49–71, doi:10.1016/j.coal.2011.04.011.

Callow, B., Falcon-Suarez, I., Ahmed, S., and Matter, J., 2018, Assessing the carbon sequestration potential of basalt using X-ray micro-CT and rock mechanics: International Journal of Greenhouse Gas Control, v. 70, p. 146–156, doi:10.1016/j.ijggc.2017.12.008.

Cañón-Tapia, E., 2018, The Paraná-Etendeka Continental Flood Basalt Province: A historical perspective of current knowledge and future research trends: Journal of Volcanology and Geothermal Research, v. 355, p. 287–303, doi:10.1016/j.jvolgeores.2017.11.011.

Cao, X., Li, Q., Xu, L., and Tan, Y., 2023, A review of in-situ carbon mineralization in basalt: Journal of Rock Mechanics and Geotechnical Engineering, p. S1674775523003372, doi:10.1016/j.jrmge.2023.11.010.

Carneiro, P., Dullius, J., Ligabue, R., Machado, C., Ketzer, J.M., and Einloft, S., 2013, Basalt carbonation and its potential use in C[O.sub.2] storage/Carbonatacao do basalto e seu potencial uso no armazenamento de C[O.sub.2]: Tecnologia em Metalurgia e Materiais, v. 10, p. 43+.

Ciotta, M., 2022, CO2 Geological Storage in Santos Basin: Potential and Best Suitable Sites, *in* Perspectives to CO2 Geological Storage and Greenhouse Gas Negative Emissions in South-Southeastern Brazil: Paraná and Santos Sedimentary Basins, Editora Blucher, p. 27–40, doi:10.5151/9786555501346-02.

Clark, D.E., Oelkers, E.H., Gunnarsson, I., Sigfússon, B., Snæbjörnsdóttir, S.Ó., Aradóttir, E.S., and Gíslason, S.R., 2020, CarbFix2: CO2 and H2S mineralization during 3.5 years of continuous injection into basaltic rocks at more than 250 °C: Geochimica et Cosmochimica Acta, v. 279, p. 45–66, doi:10.1016/j.gca.2020.03.039.

Côrtes, A.R.P., and Perinotto, J.A.D.J., 2015, Facies and facies association of Piramboia Formation in the region of Descalvado (SP): Geologia USP. Série Científica, v. 15, p. 23, doi:10.11606/issn.2316-9095.v15i3-4p23-40.

Cunha, G.G.D., Roisenberg, A., Pulgati, F.H., and Freitas, M.A., 2016, Hidrogeoquímica do Sistema Aquífero Serra Geral na região do Alto Rio Uruguai, Noroeste do Rio Grande do Sul e sua

relação espacial com a tectônica rúptil: Pesquisas em Geociências, v. 43, p. 55, doi:10.22456/1807-9806.78192.

Dang, W., Zhang, J., Wei, X., Tang, X., Chen, Q., Li, Z., Zhang, M., and Liu, J., 2017, Geological controls on methane adsorption capacity of Lower Permian transitional black shales in the Southern North China Basin, Central China: Experimental results and geological implications: Journal of Petroleum Science and Engineering, v. 152, p. 456–470, doi:10.1016/j.petrol.2017.03.017.

De Paula E Silva, F., Kiang, C.H., and Caetano-Chang, M.R., 2009, Sedimentation of the Cretaceous Bauru Group in São Paulo, Paraná Basin, Brazil: Journal of South American Earth Sciences, v. 28, p. 25–39, doi:10.1016/j.jsames.2009.02.008.

Doble, R., Mallants, D., Huddlestone-Holmes, C., Peeters, L.J.M., Kear, J., Turnadge, C., Wu, B., Noorduijn, S., and Arjomand, E., 2023, A multi-stage screening approach to evaluate risks from inter-aquifer leakage associated with gas well and water bore integrity failure: Journal of Hydrology, v. 618, p. 129244, doi:10.1016/j.jhydrol.2023.129244.

Eiken, O., Ringrose, P., Hermanrud, C., Nazarian, B., Torp, T.A., and Høier, L., 2011, Lessons learned from 14 years of CCS operations: Sleipner, In Salah and Snøhvit: Energy Procedia, v. 4, p. 5541–5548, doi:10.1016/j.egypro.2011.02.541.

Ernst, R.E., 2021, Large Igneous Provinces, *in* Encyclopedia of Geology, Elsevier, p. 60–68, doi:10.1016/B978-0-12-409548-9.12528-X.

Fernandes, L.A., Giannini, P.C.F., and Góes, A.M., 2003, Araçatuba Formation: palustrine deposits from the initial sedimentation phase of the Bauru Basin: Anais da Academia Brasileira de Ciências, v. 75, p. 173–187, doi:10.1590/S0001-37652003000200006.

Fernandes, A.J., Maldaner, C.H., Sobrinho, J.M.A., Pressinotti, M.M.N., and Wahnfried, I., 2010, Estratigrafia dos Derrames de Basaltos da Formação Serra Geral (Ribeirão Preto - SP) Baseada na Geologia Física, Petrografia e Geoquímica: Geologia USP. Série Científica, v. 10, p. 73–99, doi:10.5327/Z1519-874X2010000200006.

Fernandes, A.J., Negri, F. de A., Azevedo Sobrinho, J.M., and Janasi, V. de A., 2018, Local geological sections and regional stratigraphy based on physical geology and chemical stratigraphy of the Serra Geral Group from Araraquara to Avaré, SP: Brazilian Journal of Geology, v. 48, p. 243–261, doi:10.1590/2317-4889201720180093.

Fisher, A.T., 1998, Permeability within basaltic oceanic crust: Reviews of Geophysics, v. 36, p. 143–182, doi:10.1029/97RG02916.

Flett, M., Brantjes, J., Gurton, R., McKenna, J., Tankersley, T., and Trupp, M., 2009, Subsurface development of CO2 disposal for the Gorgon Project: Energy Procedia, v. 1, p. 3031–3038, doi:10.1016/j.egypro.2009.02.081.

Furre, A.-K., Eiken, O., Alnes, H., Vevatne, J.N., and Kiær, A.F., 2017, 20 Years of Monitoring CO2-injection at Sleipner: Energy Procedia, v. 114, p. 3916–3926, doi:10.1016/j.egypro.2017.03.1523.

Gastmans, D., Hutcheon, I., Menegário, A.A., and Chang, H.K., 2016, Geochemical evolution of groundwater in a basaltic aquifer based on chemical and stable isotopic data: Case study from the Northeastern portion of Serra Geral Aquifer, São Paulo state (Brazil): Journal of Hydrology, v. 535, p. 598–611, doi:10.1016/j.jhydrol.2016.02.016.

Gastmans, D., Menegário, A.A., and Moura, C.C., 2013, HIDROGEOQUÍMICA DAS ÁGUAS SUBTERRÂNEAS DO AQUÍFERO SERRA GERAL NA PORÇÃO CENTRO SUL DO ESTADO DE SÃO PAULO: Águas Subterrâneas, v. 27, doi:10.14295/ras.v27i3.27391.

Gauteplass, J., Almenningen, S., Barth, T., and Ersland, G., 2020, Hydrate Plugging and Flow Remediation during CO2 Injection in Sediments: Energies, v. 13, p. 4511, doi:10.3390/en13174511.

Giacomel, P., Spagnuolo, E., Nazzari, M., Marzoli, A., Passelegue, F., Youbi, N., and Di Toro, G., 2018, Frictional Instabilities and Carbonation of Basalts Triggered by Injection of Pressurized H_2O- and CO_2 - Rich Fluids: Geophysical Research Letters, doi:10.1029/2018GL078082.

Giovanardi, T., Da Costa, P.C.C., Girardi, V.A.V., Weska, R.K., Vasconcelos, P.M., Thiede, D.S., Mazzucchelli, M., and Cipriani, A., 2022, Age, geochemistry and mantle source of the Alto Diamantino basalts: Insights on NW Paraná Magmatic Province: Lithos, v. 426–427, p. 106797, doi:10.1016/j.lithos.2022.106797.

Gislason, S.R., and Oelkers, E.H., 2014, Carbon Storage in Basalt: Science, v. 344, p. 373–374, doi:10.1126/science.1250828.

Gislason, S.R., and Oelkers, E.H., 2003, Mechanism, rates, and consequences of basaltic glass dissolution: II. An experimental study of the dissolution rates of basaltic glass as a function of pH and temperature: Geochimica et Cosmochimica Acta, v. 67, p. 3817–3832, doi:10.1016/S0016-7037(03)00176-5.

Gislason, S.R., Wolff-Boenisch, D., Stefansson, A., Oelkers, E.H., Gunnlaugsson, E., Sigurdardottir, H., Sigfusson, B., Broecker, W.S., Matter, J.M., and Stute, M., 2010, Mineral sequestration of carbon dioxide in basalt: A pre-injection overview of the CarbFix project: International Journal of Greenhouse Gas Control, v. 4, p. 537–545, doi:10.1016/j.ijggc.2009.11.013.

Godec, M., Koperna, G., and Gale, J., 2014, CO2-ECBM: A Review of its Status and Global Potential: Energy Procedia, v. 63, p. 5858–5869, doi:10.1016/j.egypro.2014.11.619.

Goldberg, D.S., Kent, D.V., and Olsen, P.E., 2010, Potential on-shore and off-shore reservoirs for CO_2 sequestration in Central Atlantic magmatic province basalts: Proceedings of the National Academy of Sciences, v. 107, p. 1327–1332, doi:10.1073/pnas.0913721107.

Golding, S.D., Uysal, I.T., Boreham, C.J., Kirste, D., Baublys, K.A., and Esterle, J.S., 2011, Adsorption and mineral trapping dominate CO2 storage in coal systems: Energy Procedia, v. 4, p. 3131–3138, doi:10.1016/j.egypro.2011.02.227.

Gudbrandsson, S., Wolff-Boenisch, D., Gislason, S.R., and Oelkers, E.H., 2011, An experimental study of crystalline basalt dissolution from $2 \leqslant pH \leqslant 11$ and temperatures from 5 to 75 °C: Geochimica et Cosmochimica Acta, v. 75, p. 5496–5509, doi:10.1016/j.gca.2011.06.035.

Haldar, S.K., and Tišljar, J., 2014, Introduction to Mineralogy and Petrology: Elsevier, doi:10.1016/C2012-0-03337-6.

Hamza, A., Hussein, I.A., Al-Marri, M.J., Mahmoud, M., Shawabkeh, R., and Aparicio, S., 2021, CO2 enhanced gas recovery and sequestration in depleted gas reservoirs: A review: Journal of Petroleum Science and Engineering, v. 196, p. 107685, doi:10.1016/j.petrol.2020.107685.

Hannis, S., Lu, J., Chadwick, A., Hovorka, S., Kirk, K., Romanak, K., and Pearce, J., 2017, CO2 Storage in Depleted or Depleting Oil and Gas Fields: What can We Learn from Existing Projects? Energy Procedia, v. 114, p. 5680–5690, doi:10.1016/j.egypro.2017.03.1707.

Hernandez, G.A., Bello, R.O., McVay, D.A., Ayers, W.B., Rushing, J.A., Ruhl, S.K., Hoffmann, M.F., and Ramazanova, R.I., 2006, Evaluation of the Technical and Economic Feasibility of CO2 Sequestration and Enhanced Coalbed-Methane Recovery in Texas Low-Rank Coals, *in* All Days, Calgary, Alberta, Canada, SPE, p. SPE-100584-MS, doi:10.2118/100584-MS.

Hirata, R., and Foster, S., 2021, The Guarani Aquifer System – from regional reserves to local use: Quarterly Journal of Engineering Geology and Hydrogeology, v. 54, p. qjegh2020- 091, doi:10.1144/qjegh2020-091.

Hoch, A.R., Reddy, M.M., and Drever, J.I., 1996, The effect of iron content and dissolved O2 on dissolution rates of clinopyroxene at pH 5.8 and 25°C: preliminary results: Chemical Geology, v. 132, p. 151–156, doi:10.1016/S0009-2541(96)00050-2.

Hughes, D.S., 2009, Carbon storage in depleted gas fields: Key challenges: Energy Procedia, v. 1, p. 3007–3014, doi:10.1016/j.egypro.2009.02.078.

Iglauer, S., 2017, CO_2 –Water–Rock Wettability: Variability, Influencing Factors, and Implications for CO_2 Geostorage: Accounts of Chemical Research, v. 50, p. 1134–1142, doi:10.1021/acs.accounts.6b00602.

Jamekhorshid, A., and Azin, R., 2023, Application of life cycle assessment on enhanced oil recovery processes, *in* Challenges and Recent Advances in Sustainable Oil and Gas Recovery and Transportation, Elsevier, p. 227–242, doi:10.1016/B978-0-323-99304-3.00013-3.

Jin, L. et al., 2017, Advancing CO2 enhanced oil recovery and storage in unconventional oil play—Experimental studies on Bakken shales: Applied Energy, v. 208, p. 171–183, doi:10.1016/j.apenergy.2017.10.054.

Johnson, J.W., Nitao, J.J., and Knauss, K.G., 2004, Reactive transport modelling of CO_2 storage in saline aquifers to elucidate fundamental processes, trapping mechanisms and sequestration partitioning: Geological Society, London, Special Publications, v. 233, p. 107–128, doi:10.1144/GSL.SP.2004.233.01.08.

Junior, A.N., Queiroz, G.N., Godoy, M.G., Cardoso, V.D.S., Cedrola, S.M.L., Mansoldo, F.R.P., Firpo, R.M., Gomes Paiva, L.M., Sohrabi, M., and Vermelho, A.B., 2023, Assessing EOR strategies for application in Brazilian pre-salt reservoirs: Geoenergy Science and Engineering, v. 223, p. 211508, doi:10.1016/j.geoen.2023.211508.

Khosrokhavar, R., Griffiths, S., and Wolf, K.-H., 2014, Shale Gas Formations and Their Potential for Carbon Storage: Opportunities and Outlook: Environmental Processes, v. 1, p. 595–611, doi:10.1007/s40710-014-0036-4.

Koppers, A.A.P., and Sager, W.W., 2014, Large-Scale and Long-Term Volcanism on Oceanic Lithosphere, *in* Developments in Marine Geology, Elsevier, v. 7, p. 553–597, doi:10.1016/B978-0-444-62617-2.00019-0.

Kristjánsdóttir, H., and Kristjánsdóttir, S., 2021, CARBFIX AND SULFIX IN GEOTHERMAL PRODUCTION, AND THE BLUE LAGOON IN ICELAND: GRINDAVÍK URBAN SETTLEMENT, AND VOLCANIC ACTIVITY: Baltic Journal of Economic Studies, v. 7, p. 1–9, doi:10.30525/2256-0742/2021-7-1-1-9.

Lashgari, H.R., Sun, A., Zhang, T., Pope, G.A., and Lake, L.W., 2019, Evaluation of carbon dioxide storage and miscible gas EOR in shale oil reservoirs: Fuel, v. 241, p. 1223–1235, doi:10.1016/j.fuel.2018.11.076.

Leiss, W., and Larkin, P., 2019, Risk communication and public engagement in CCS projects: the foundations of public acceptability: International Journal of Risk Assessment and Management, v. 22, p. 384, doi:10.1504/IJRAM.2019.103339.

Leite, C.M.D.C., Wendland, E., and Gastmans, D., 2021, Caracterização hidrogeoquímica de águas subterrâneas utilizadas para abastecimento público na porção nordeste do Sistema Aquífero Guarani: Engenharia Sanitaria e Ambiental, v. 26, p. 29–43, doi:10.1590/s1413-415220190087.

Li, Y.-H., Shen, C.-H., Wu, C.-Y., and Hsieh, B.-Z., 2020, Numerical Study of CO2 Geological Storage in Saline Aquifers without the Risk of Leakage: Energies, v. 13, p. 5259, doi:10.3390/en13205259.

Liu, M., and Grana, D., 2020, Petrophysical characterization of deep saline aquifers for CO2 storage using ensemble smoother and deep convolutional autoencoder: Advances in Water Resources, v. 142, p. 103634, doi:10.1016/j.advwatres.2020.103634.

L′Orange Seigo, S., Dohle, S., and Siegrist, M., 2014, Public perception of carbon capture and storage (CCS): A review: Renewable and Sustainable Energy Reviews, v. 38, p. 848–863, doi:10.1016/j.rser.2014.07.017.

Machado, F.B., Rocha-Júnior, E.R.V., Marques, L.S., Nardy, A.J.R., Zezzo, L.V., and Marteleto, N.S., 2018, Geochemistry of the Northern Paraná Continental Flood Basalt (PCFB) Province: implications for regional chemostratigraphy: Brazilian Journal of Geology, v. 48, p. 177–199, doi:10.1590/2317-4889201820180098.

Mahzari, P. et al., 2021, Characterizing fluid flow paths in the Hellisheidi geothermal field using detailed fault mapping and stress-dependent permeability: Geothermics, v. 94, p. 102127, doi:10.1016/j.geothermics.2021.102127.

Marieni, C., and Oelkers, E., 2018, Carbon sequestration potential of altered mafic reservoirs: Energy Procedia, v. 146, p. 68–73, doi:10.1016/j.egypro.2018.07.010.

Marques Dos Santos, C.A., Batezelli, A., Nakasuga, W.M., Resende, R.S., Tello Saenz, C.A., and Nunes, J.O.R., 2020, Sedimentary provenance of the Marília Formation (Bauru Basin), Southeast Brazil (I. Somerville, Ed.): Geological Journal, v. 55, p. 2834–2850, doi:10.1002/gj.3576.

Marsh, B.D., 2015, Magmatism, Magma, and Magma Chambers, *in* Treatise on Geophysics, Elsevier, p. 273–323, doi:10.1016/B978-0-444-53802-4.00116-0.

Martens, S., Liebscher, A., Möller, F., Würdemann, H., Schilling, F., and Kühn, M., 2011, Progress report on the first european on-shore CO2 storage site at ketzin (Germany) — Second year of injection: Energy Procedia, v. 4, p. 3246–3253, doi:10.1016/j.egypro.2011.02.243.

Matheron, G., 1963, Principles of geostatistics: Economic Geology, v. 58, p. 1246–1266, doi:10.2113/gsecongeo.58.8.1246.

Matter, J.M. et al., 2011, The CarbFix Pilot Project–Storing carbon dioxide in basalt: Energy Procedia, v. 4, p. 5579–5585, doi:10.1016/j.egypro.2011.02.546.

Mazzotti, M., Pini, R., and Storti, G., 2009, Enhanced coalbed methane recovery: The Journal of Supercritical Fluids, v. 47, p. 619–627, doi:10.1016/j.supflu.2008.08.013.

McGrail, B.P., Schaef, H.T., Spane, F.A., Cliff, J.B., Qafoku, O., Horner, J.A., Thompson, C.J., Owen, A.T., and Sullivan, C.E., 2017a, Field Validation of Supercritical CO_2 Reactivity with Basalts: Environmental Science & Technology Letters, v. 4, p. 6–10, doi:10.1021/acs.estlett.6b00387.

McGrail, B.P., Schaef, H.T., Spane, F.A., Horner, J.A., Owen, A.T., Cliff, J.B., Qafoku, O., Thompson, C.J., and Sullivan, E.C., 2017b, Wallula Basalt Pilot Demonstration Project: Post-injection Results and Conclusions: Energy Procedia, v. 114, p. 5783–5790, doi:10.1016/j.egypro.2017.03.1716.

Md Yusof, M.A., Mohamed, M.A., Md Akhir, N.A., Ibrahim, M.A., Saaid, I.M., Idris, A.K., Idress, M., and Awangku Matali, A.A.A., 2022, Influence of Brine–Rock Parameters on Rock Physical Changes During CO2 Sequestration in Saline Aquifer: Arabian Journal for Science and Engineering, v. 47, p. 11345–11359, doi:10.1007/s13369-021-06110-8.

Medina Ketzer, J.M., Xavier Machado, C., Camboim Rockett, G., and Iglesias, R.S., 2015, Brazilian atlas of CO2 capture and geological storageAtlas brasileiro de captura e armazenamento geológico de CO2: Edipucrs.

Merey, S., and Sinayuc, C., 2016, Analysis of carbon dioxide sequestration in shale gas reservoirs by using experimental adsorption data and adsorption models: Journal of Natural Gas Science and Engineering, v. 36, p. 1087–1105, doi:10.1016/j.jngse.2016.02.052.

Michael, K., Golab, A., Shulakova, V., Ennis-King, J., Allinson, G., Sharma, S., and Aiken, T., 2010, Geological storage of CO2 in saline aquifers—A review of the experience from existing storage operations: International Journal of Greenhouse Gas Control, v. 4, p. 659–667, doi:10.1016/j.ijggc.2009.12.011.

Morelatto, R. BACIA DO PARANÁ Sumário Geológico e Setores em Oferta:

Nehru, C.E., 1989, Petrographic methods, *in* Petrology, Dordrecht, Kluwer Academic Publishers, Encyclopedia of Earth Science, p. 447–449, doi:10.1007/0-387-30845-8_178.

Netto, A.L.A., Alves, V.H., Peyerl, D., Jacobi, P.R., and Santos, E.M. dos, 2021, Panorama das políticas públicas e estratégias para desenvolvimento da captura e armazenamento de carbono: reflexões para o Brasil: Revista de Gestão Ambiental e Sustentabilidade, v. 10, p. e19305, doi:10.5585/geas.v10i1.19305.

Niu, B., Al-Menhali, A., and Krevor, S.C., 2015, The impact of reservoir conditions on the residual trapping of carbon dioxide in B erea sandstone: Water Resources Research, v. 51, p. 2009–2029, doi:10.1002/2014WR016441.

Oelkers, E.H., 2001, An experimental study of forsterite dissolution rates as a function of temperature and aqueous Mg and Si concentrations: Chemical Geology, v. 175, p. 485–494, doi:10.1016/S0009-2541(00)00352-1.

Oelkers, E.H., and Gislason, S.R., 2001, The mechanism, rates and consequences of basaltic glass dissolution: I. An experimental study of the dissolution rates of basaltic glass as a function of aqueous Al, Si and oxalic acid concentration at 25°C and pH = 3 and 11: Geochimica et Cosmochimica Acta, v. 65, p. 3671–3681, doi:10.1016/S0016-7037(01)00664-0.

Oelkers, E.H., and Schott, J., 2001, An experimental study of enstatite dissolution rates as a function of pH, temperature, and aqueous Mg and Si concentration, and the mechanism of pyroxene/pyroxenoid dissolution: Geochimica et Cosmochimica Acta, v. 65, p. 1219–1231, doi:10.1016/S0016-7037(00)00564-0.

Oelkers, E.H., and Schott, J., 1995, Experimental study of anorthite dissolution and the relative mechanism of feldspar hydrolysis: Geochimica et Cosmochimica Acta, v. 59, p. 5039–5053, doi:10.1016/0016-7037(95)00326-6.

Ogawa, T., Nakanishi, S., Shidahara, T., Okumura, T., and Hayashi, E., 2011, Saline-aquifer CO2 sequestration in Japan-methodology of storage capacity assessment: International Journal of Greenhouse Gas Control, v. 5, p. 318–326, doi:10.1016/j.ijggc.2010.09.009.

Okoli, A.E., Kolawole, O., Akaolisa, C.Z., Ikoro, D.O., and Ozotta, O., 2024, Alterations in petrophysical and mechanical properties due to basaltic rock-CO2 interactions: comprehensive review: Arabian Journal of Geosciences, v. 17, p. 10, doi:10.1007/s12517-023-11800-8.

Pacheco, F.E.R.C., Caxito, F.D.A., Moraes, L.C.D., Marangoni, Y.R., Santos, R.P.Z.D., and Pedrosa-Soares, A.C., 2018, Basaltic ring structures of the Serra Geral Formation at the southern Triângulo Mineiro, Água Vermelha region, Brazil: Journal of Volcanology and Geothermal Research, v. 355, p. 136–148, doi:10.1016/j.jvolgeores.2017.06.019.

Pan, Z., and Wood, D.A., 2015, Coalbed methane (CBM) exploration, reservoir characterisation, production, and modelling: A collection of published research (2009–2015): Journal of Natural Gas Science and Engineering, v. 26, p. 1472–1484, doi:10.1016/j.jngse.2015.07.049.

Pearce, J., Raza, S., Baublys, K., Hayes, P., Firouzi, M., and Rudolph, V., 2022, Unconventional CO2 Storage: CO2 Mineral Trapping Predicted in Characterized Shales, Sandstones, and Coal Seam Interburden: SPE Journal, v. 27, p. 3218–3239, doi:10.2118/209791-PA.

Peuble, S., Godard, M., Luquot, L., Andreani, M., Martinez, I., and Gouze, P., 2015, CO2 geological storage in olivine rich basaltic aquifers: New insights from reactive-percolation experiments: Applied Geochemistry, v. 52, p. 174–190, doi:10.1016/j.apgeochem.2014.11.024.

Pinto, M.L., 2019, Arcabouço tectônico da Bacia do Paraná, uma nova abordagem com base em dados de métodos potenciais:

Pogge von Strandmann, P.A.E., Burton, K.W., Snæbjörnsdóttir, S.O., Sigfússon, B., Aradóttir, E.S., Gunnarsson, I., Alfredsson, H.A., Mesfin, K.G., Oelkers, E.H., and Gislason, S.R., 2019, Rapid CO2 mineralisation into calcite at the CarbFix storage site quantified using calcium isotopes: Nature Communications, v. 10, p. 1983, doi:10.1038/s41467-019-10003-8.

Potts, P.J., 1987, X-ray fluorescence analysis: principles and practice of wavelength dispersive spectrometry, *in* A Handbook of Silicate Rock Analysis, Dordrecht, Springer Netherlands, p. 226–285, doi:10.1007/978-94-015-3988-3_8.

Prasad, S.K., Sangwai, J.S., and Byun, H.-S., 2023, A review of the supercritical CO2 fluid applications for improved oil and gas production and associated carbon storage: Journal of CO2 Utilization, v. 72, p. 102479, doi:10.1016/j.jcou.2023.102479.

Pratikna, K., Rahman, M.J., and Mondol, N.H., 2022, Characterization of Utsira Formation around the Sleipner CO2 storage site, central North Sea, *in* Second International Meeting for Applied Geoscience & Energy, Houston, Texas, Society of Exploration Geophysicists and American Association of Petroleum Geologists, p. 552–556, doi:10.1190/image2022-3750949.1.

Pruess, K., and Müller, N., 2009, Formation dry-out from CO_2 injection into saline aquifers: 1. Effects of solids precipitation and their mitigation: FORMATION DRY-OUT FROM CO_2 INJECTION, 1: Water Resources Research, v. 45, doi:10.1029/2008WR007101.

Rämö, O.T., Heikkilä, P.A., and Pulkkinen, A.H., 2016, Geochemistry of Paraná-Etendeka basalts from Misiones, Argentina: Some new insights into the petrogenesis of high-Ti continental

flood basalts: Journal of South American Earth Sciences, v. 67, p. 25–39, doi:10.1016/j.jsames.2016.01.008.

Rasmusson, K., Rasmusson, M., Tsang, Y., Benson, S., Hingerl, F., Fagerlund, F., and Niemi, A., 2018, Residual trapping of carbon dioxide during geological storage—Insight gained through a pore-network modeling approach: International Journal of Greenhouse Gas Control, v. 74, p. 62–78, doi:10.1016/j.ijggc.2018.04.021.

Rasool, M.H., Ahmad, M., and Ayoub, M., 2023, Selecting Geological Formations for CO2 Storage: A Comparative Rating System: Sustainability, v. 15, p. 6599, doi:10.3390/su15086599.

Ratouis, T.M.P., Snæbjörnsdóttir, S.Ó., Voigt, M.J., Sigfússon, B., Gunnarsson, G., Aradóttir, E.S., and Hjörleifsdóttir, V., 2022, Carbfix 2: A transport model of long-term CO2 and H2S injection into basaltic rocks at Hellisheidi, SW-Iceland: International Journal of Greenhouse Gas Control, v. 114, p. 103586, doi:10.1016/j.ijggc.2022.103586.

Raza, A., Gholami, R., Rezaee, R., Bing, C.H., Nagarajan, R., and Hamid, M.A., 2017, Assessment of CO 2 residual trapping in depleted reservoirs used for geosequestration: Journal of Natural Gas Science and Engineering, v. 43, p. 137–155, doi:10.1016/j.jngse.2017.04.001.

Raza, A., Gholami, R., Rezaee, R., Bing, C.H., Nagarajan, R., and Hamid, M.A., 2018, CO2 storage in depleted gas reservoirs: A study on the effect of residual gas saturation: Petroleum, v. 4, p. 95–107, doi:10.1016/j.petlm.2017.05.005.

Raza, A., Glatz, G., Gholami, R., Mahmoud, M., and Alafnan, S., 2022, Carbon mineralization and geological storage of CO2 in basalt: Mechanisms and technical challenges: Earth-Science Reviews, v. 229, p. 104036, doi:10.1016/j.earscirev.2022.104036.

Riccomini, C., 1997, Considerações sobre a posição estratigráfica e tectonismo deformador da formação Itaqueri na porção centro-leste do Estado de São Paulo: Revista do Instituto Geológico, v. 18, p. 41–48, doi:10.5935/0100-929X.19970003.

Rocha-Júnior, E.R.V., Marques, L.S., Babinski, M., Machado, F.B., Petronilho, L.A., and Nardy, A.J.R., 2020a, A telltale signature of Archean lithospheric mantle in the Paraná continental flood basalts genesis: Lithos, v. 364–365, p. 105519, doi:10.1016/j.lithos.2020.105519.

Rocha-Júnior, E.R.V., Marques, L.S., Babinski, M., Machado, F.B., Petronilho, L.A., and Nardy, A.J.R., 2020b, A telltale signature of Archean lithospheric mantle in the Paraná continental flood basalts genesis: Lithos, v. 364–365, p. 105519, doi:10.1016/j.lithos.2020.105519.

Rochelle, C.A., Czernichowski-Lauriol, I., and Milodowski, A.E., 2004, The impact of chemical reactions on CO_2 storage in geological formations: a brief review: Geological Society, London, Special Publications, v. 233, p. 87–106, doi:10.1144/GSL.SP.2004.233.01.07.

Romanak, K., and Dixon, T., 2022, CO2 storage guidelines and the science of monitoring: Achieving project success under the California Low Carbon Fuel Standard CCS Protocol and other global regulations: International Journal of Greenhouse Gas Control, v. 113, p. 103523, doi:10.1016/j.ijggc.2021.103523.

Rosenqvist, M.P., Meakins, M.W.J., Planke, S., Millett, J.M., Kjøll, H.J., Voigt, M.J., and Jamtveit, B., 2023, Reservoir properties and reactivity of the Faroe Islands Basalt Group: Investigating the potential for CO2 storage in the North Atlantic Igneous Province: International Journal of Greenhouse Gas Control, v. 123, p. 103838, doi:10.1016/j.ijggc.2023.103838.

Rossetti, L., Lima, E.F., Waichel, B.L., Hole, M.J., Simões, M.S., and Scherer, C.M.S., 2018, Lithostratigraphy and volcanology of the Serra Geral Group, Paraná-Etendeka Igneous

Province in Southern Brazil: Towards a formal stratigraphical framework: Journal of Volcanology and Geothermal Research, v. 355, p. 98–114, doi:10.1016/j.jvolgeores.2017.05.008.

Ryu, J.-S., Vigier, N., Decarreau, A., Lee, S.-W., Lee, K.-S., Song, H., and Petit, S., 2016, Experimental investigation of Mg isotope fractionation during mineral dissolution and clay formation: Chemical Geology, v. 445, p. 135–145, doi:10.1016/j.chemgeo.2016.02.006.

Sant'Anna, L.G., Clauer, N., Cordani, U.G., Riccomini, C., Velázquez, V.F., and Liewig, N., 2006, Origin and migration timing of hydrothermal fluids in sedimentary rocks of the Paraná Basin, South America: Chemical Geology, v. 230, p. 1–21, doi:10.1016/j.chemgeo.2005.11.009.

Schaef, H.T., McGrail, B.P., and Owen, A.T., 2011, Basalt Reactivity Variability with Reservoir Depth in Supercritical CO2 and Aqueous Phases: Energy Procedia, v. 4, p. 4977–4984, doi:10.1016/j.egypro.2011.02.468.

Schaef, H.T., McGrail, B.P., and Owen, A.T., 2010, Carbonate mineralization of volcanic province basalts: International Journal of Greenhouse Gas Control, v. 4, p. 249–261, doi:10.1016/j.ijggc.2009.10.009.

Schott, J., Mavromatis, V., Fujii, T., Pearce, C.R., and Oelkers, E.H., 2016, The control of carbonate mineral Mg isotope composition by aqueous speciation: Theoretical and experimental modeling: Chemical Geology, v. 445, p. 120–134, doi:10.1016/j.chemgeo.2016.03.011.

Shabani, B., Lu, P., Kammer, R., and Zhu, C., 2022, Effects of Hydrogeological Heterogeneity on CO2 Migration and Mineral Trapping: 3D Reactive Transport Modeling of Geological CO2 Storage in the Mt. Simon Sandstone, Indiana, USA: Energies, v. 15, p. 2171, doi:10.3390/en15062171.

Shehata, A.M., El-Banbi, A.H., and Sayyouh, M.H., 2012, Guidelines to Optimize CO2 EOR in Heterogeneous Reservoirs, *in* All Days, Cairo, Egypt, SPE, p. SPE-151871-MS, doi:10.2118/151871-MS.

Shukla, R., Ranjith, P., Haque, A., and Choi, X., 2010a, A review of studies on CO2 sequestration and caprock integrity: Fuel, v. 89, p. 2651–2664, doi:10.1016/j.fuel.2010.05.012.

Shukla, R., Ranjith, P., Haque, A., and Choi, X., 2010b, A review of studies on CO2 sequestration and caprock integrity: Fuel, v. 89, p. 2651–2664, doi:10.1016/j.fuel.2010.05.012.

Silva, B.A.D., Calegari, M.R., Pinheiro, M.R., and Fujita, R.H., 2021, Lithostructural and tectonic determinants in the geomorphic evolution of the Basalt Plateau – Southern Brazil: Journal of South American Earth Sciences, v. 110, p. 103351, doi:10.1016/j.jsames.2021.103351.

Silva Ramos, G.M., Barbosa, J.A., De Araújo, A.F.L., Correia Filho, O.J., Barreto, C.J.S., Cruz Oliveira, J.T., and De Medeiros, R.S., 2023, Potential for permanent CO2 sequestration in depleted volcanic reservoirs in the offshore Campos Basin, Brazil: International Journal of Greenhouse Gas Control, v. 128, p. 103942, doi:10.1016/j.ijggc.2023.103942.

Snæbjörnsdóttir, S.Ó., Oelkers, E.H., Mesfin, K., Aradóttir, E.S., Dideriksen, K., Gunnarsson, I., Gunnlaugsson, E., Matter, J.M., Stute, M., and Gislason, S.R., 2017, The chemistry and saturation states of subsurface fluids during the in situ mineralisation of CO2 and H2S at the CarbFix site in SW-Iceland: International Journal of Greenhouse Gas Control, v. 58, p. 87–102, doi:10.1016/j.ijggc.2017.01.007.

Stockmann, G., Wolff-Boenisch, D., Gíslason, S.R., and Oelkers, E.H., 2008, Dissolution of diopside and basaltic glass: the effect of carbonate coating: Mineralogical Magazine, v. 72, p. 135–139, doi:10.1180/minmag.2008.072.1.135.

Stockmann, G.J., Wolff-Boenisch, D., Gislason, S.R., and Oelkers, E.H., 2011, Do carbonate precipitates affect dissolution kinetics? 1: Basaltic glass: Chemical Geology, v. 284, p. 306–316, doi:10.1016/j.chemgeo.2011.03.010.

Suekane, T., Nobuso, T., Hirai, S., and Kiyota, M., 2008, Geological storage of carbon dioxide by residual gas and solubility trapping: International Journal of Greenhouse Gas Control, v. 2, p. 58–64, doi:10.1016/S1750-5836(07)00096-5.

Sun, Y., Li, S., Sun, R., Liu, X., Pu, H., and Zhao, J., 2020, Study of CO_2 Enhancing Shale Gas Recovery Based on Competitive Adsorption Theory: ACS Omega, v. 5, p. 23429–23436, doi:10.1021/acsomega.0c03383.

Szulczewski, M.L., Hesse, M.A., and Juanes, R., 2013, Carbon dioxide dissolution in structural and stratigraphic traps: Journal of Fluid Mechanics, v. 736, p. 287–315, doi:10.1017/jfm.2013.511.

Tambaria, T.N., Sugai, Y., and Nguele, R., 2022, Adsorption Factors in Enhanced Coal Bed Methane Recovery: A Review: Gases, v. 2, p. 1–21, doi:10.3390/gases2010001.

Temizel, C.., Betancourt, D.J., Tiwari, A.., Zhang, M.., Aktas, S.S., and Quiros, F.., 2016, Optimization of Enhanced Coalbed Methane Recovery With C02 Injection, *in* Day 3 Fri, June 03, 2016, Buenos Aires, Argentina, SPE, p. D032S003R001, doi:10.2118/180973-MS.

Tian, J., Liu, J., Elsworth, D., Leong, Y.-K., Li, W., and Zeng, J., 2022, Shale gas production from reservoirs with hierarchical multiscale structural heterogeneities: Journal of Petroleum Science and Engineering, v. 208, p. 109380, doi:10.1016/j.petrol.2021.109380.

Van Den Broek, M., Ramírez, A., Groenenberg, H., Neele, F., Viebahn, P., Turkenburg, W., and Faaij, A., 2010, Feasibility of storing CO2 in the Utsira formation as part of a long term Dutch CCS strategy: International Journal of Greenhouse Gas Control, v. 4, p. 351–366, doi:10.1016/j.ijggc.2009.09.002.

Van Pham, T.H., Aagaard, P., and Hellevang, H., 2012, On the potential for CO2mineral storage in continental flood basalts – PHREEQC batch- and 1D diffusion–reaction simulations: Geochemical Transactions, v. 13, p. 5, doi:10.1186/1467-4866-13-5.

Voigt, M., Marieni, C., Baldermann, A., Galeczka, I.M., Wolff-Boenisch, D., Oelkers, E.H., and Gislason, S.R., 2021, An experimental study of basalt–seawater–CO2 interaction at 130 °C: Geochimica et Cosmochimica Acta, v. 308, p. 21–41, doi:10.1016/j.gca.2021.05.056.

Wallquist, L., Seigo, S.L., Visschers, V.H.M., and Siegrist, M., 2012, Public acceptance of CCS system elements: A conjoint measurement: International Journal of Greenhouse Gas Control, v. 6, p. 77–83, doi:10.1016/j.ijggc.2011.11.008.

Wang, Y., Vuik, C., and Hajibeygi, H., 2022, CO2 Storage in deep saline aquifers: impacts of fractures on hydrodynamic trapping: International Journal of Greenhouse Gas Control, v. 113, p. 103552, doi:10.1016/j.ijggc.2021.103552.

Wang, X.-C., Wilde, S.A., Li, Q.-L., and Yang, Y.-N., 2015, Continental flood basalts derived from the hydrous mantle transition zone: Nature Communications, v. 6, p. 7700, doi:10.1038/ncomms8700.

White, S.K., Spane, F.A., Schaef, H.T., Miller, Q.R.S., White, M.D., Horner, J.A., and McGrail, B.P., 2020, Quantification of CO_2 Mineralization at the Wallula Basalt Pilot Project: Environmental Science & Technology, v. 54, p. 14609–14616, doi:10.1021/acs.est.0c05142.

Williams, G., and Chadwick, A., 2012, Quantitative seismic analysis of a thin layer of CO2 in the Sleipner injection plume: GEOPHYSICS, v. 77, p. R245–R256, doi:10.1190/geo2011-0449.1.

Wimpenny, J., Gíslason, S.R., James, R.H., Gannoun, A., Pogge Von Strandmann, P.A.E., and Burton, K.W., 2010, The behaviour of Li and Mg isotopes during primary phase dissolution and secondary mineral formation in basalt: Geochimica et Cosmochimica Acta, v. 74, p. 5259–5279, doi:10.1016/j.gca.2010.06.028.

Witte, K., 2021, Social Acceptance of Carbon Capture and Storage (CCS) from Industrial Applications: Sustainability, v. 13, p. 12278, doi:10.3390/su132112278.

Wolff-Boenisch, D., Gislason, S.R., and Oelkers, E.H., 2006, The effect of crystallinity on dissolution rates and CO2 consumption capacity of silicates: Geochimica et Cosmochimica Acta, v. 70, p. 858–870, doi:10.1016/j.gca.2005.10.016.

Xie, W., Wang, M., and Duan, H., 2021, Adsorption Characteristics and Controlling Factors of CH4 on Coal-Measure Shale, Hedong Coalfield: Minerals, v. 11, p. 63, doi:10.3390/min11010063.

Xu, T., Apps, J.A., Pruess, K., and Yamamoto, H., 2007, Numerical modeling of injection and mineral trapping of CO2 with H2S and SO2 in a sandstone formation: Chemical Geology, v. 242, p. 319–346, doi:10.1016/j.chemgeo.2007.03.022.

Yang, J., Yang, C., Gu, Q., Zhu, C., Luo, M., and Zhong, P., 2023, Economic evaluation and influencing factors of CCUS-EOR technology: A case study from a high water-bearing oilfield in Xinjiang, China: Energy Reports, v. 10, p. 153–160, doi:10.1016/j.egyr.2023.06.013.

Zakharova, N.V., Goldberg, D.S., Sullivan, E.C., Herron, M.M., and Grau, J.A., 2012, Petrophysical and geochemical properties of Columbia River flood basalt: Implications for carbon sequestration: Geochemistry, Geophysics, Geosystems, v. 13, p. 2012GC004305, doi:10.1029/2012GC004305.

Zarrouk, S.J., and Moore, T.A., 2009, Preliminary reservoir model of enhanced coalbed methane (ECBM) in a subbituminous coal seam, Huntly Coalfield, New Zealand: International Journal of Coal Geology, v. 77, p. 153–161, doi:10.1016/j.coal.2008.08.007.

Zhang, S., and DePaolo, D.J., 2017, Rates of CO_2 Mineralization in Geological Carbon Storage: Accounts of Chemical Research, v. 50, p. 2075–2084, doi:10.1021/acs.accounts.7b00334.

Zhang, D., and Song, J., 2014, Mechanisms for Geological Carbon Sequestration: Procedia IUTAM, v. 10, p. 319–327, doi:10.1016/j.piutam.2014.01.027.

Zhao, X., Rui, Z., and Liao, X., 2016, Case studies on the CO2 storage and EOR in heterogeneous, highly water-saturated, and extra-low permeability Chinese reservoirs: Journal of Natural Gas Science and Engineering, v. 29, p. 275–283, doi:10.1016/j.jngse.2015.12.044.

APPENDIX A – PETROGRAPHIC DESCRIPTION

Sample ID	**CGS-1**
Rock type	Igneous, basalt
Outcrop name	Predreira CGS
Geological Unit	Serra Geral Formation
Province	Paraná-Etendeka, Paraná basin.
Location	SP, Brazil

Microscopic textures	
Structures	Microvesicles, amygdales
Crystallinity	Hipocrystalline
Granularity	Microcrystalline
Crystal size	Very fine
Crystal shape	Hipidiomorphic
Crystalline textures	Porphyritic

Composition (%)	
Ca-Plagioclase	40
Ca-Clinopyroxene	30
Glass	12
Opaques	10
Celadonite	5
Quartz	3

Summary
Simple pahoehoe basalt from the vesicular zone. Aphanitic microcrystalline texture with microvesicles filled with zeolites and quartz.

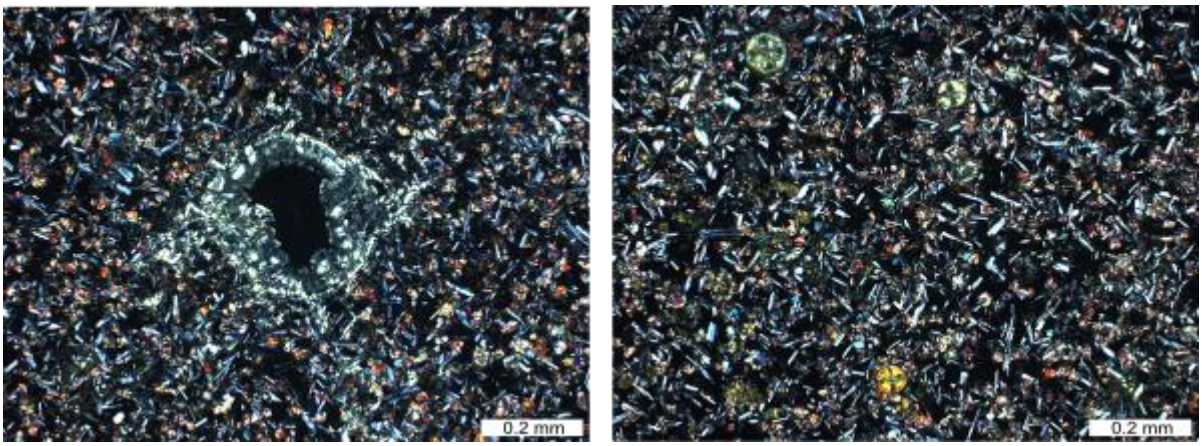

Figure 0.1. Hypocrystalline basalt with amygdales filled with zeolites. Crossed Nicols.

Sample ID	**CGS-3**
Rock type	Igneous, basalt
Outcrop name	Predreira CGS
Geological Unit	Serra Geral Formation
Province	Paraná-Etendeka, Paraná basin.
Location	SP, Brazil

Microscopic textures	
Structures	Microvesicles, amygdales
Crystallinity	Hipocrystalline
Granularity	Microcrystalline
Crystal size	Very fine
Crystal shape	Hipidiomorphic
Crystalline textures	Porphyritic

Composition (%)	
Ca-Plagioclase	35
Ca-Clinopyroxene	25
Glass	13
Opaques	10
Celadonite	2
Quartz	10
Oxides	5

Summary
Simple pahoehoe basalt from the vesicular zone. Aphanitic microcrystalline texture with microvesicles filled with zeolites and quartz.

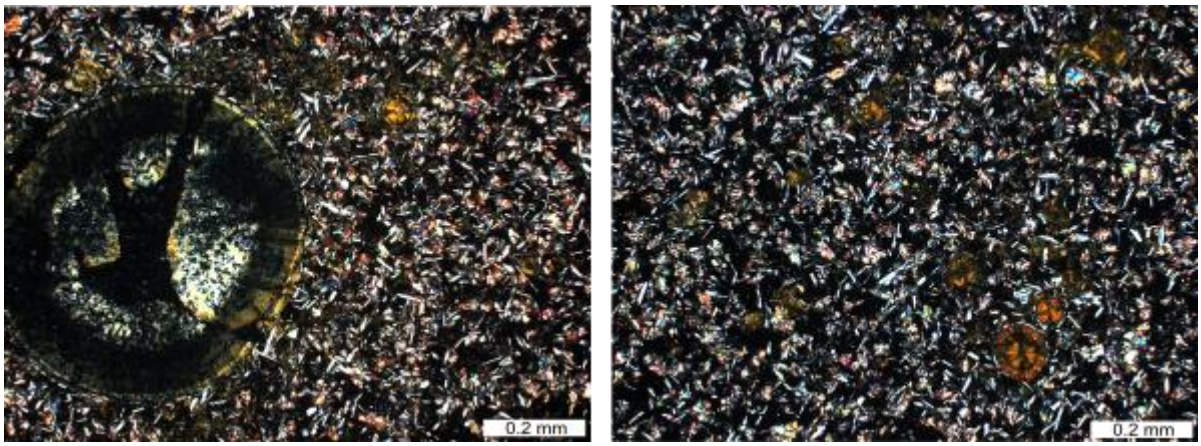

Figure 0.2. Hypocrystalline basalt with amygdales filled with altered silica and zeolites. Crossed Nicols.

Sample ID	**CGS-4**
Rock type	Igneous, basalt
Outcrop name	Predreira CGS
Geological Unit	Serra Geral Formation
Province	Paraná-Etendeka, Paraná basin.
Location	SP, Brazil

Microscopic textures	
Structures	Microvesicles, amygdales
Crystallinity	Hipocrystalline
Granularity	Microcrystalline
Crystal size	Very fine
Crystal shape	Hipidiomorphic
Crystalline textures	Porphyritic

Composition (%)	
Ca-Plagioclase	30
Ca-Clinopyroxene	25
Glass	15
Opaques	10
Celadonite	5
Quartz	10
Oxides	5

Summary
Simple pahoehoe basalt from the vesicular zone. Aphanitic microcrystalline texture with microvesicles filled with zeolites and quartz.

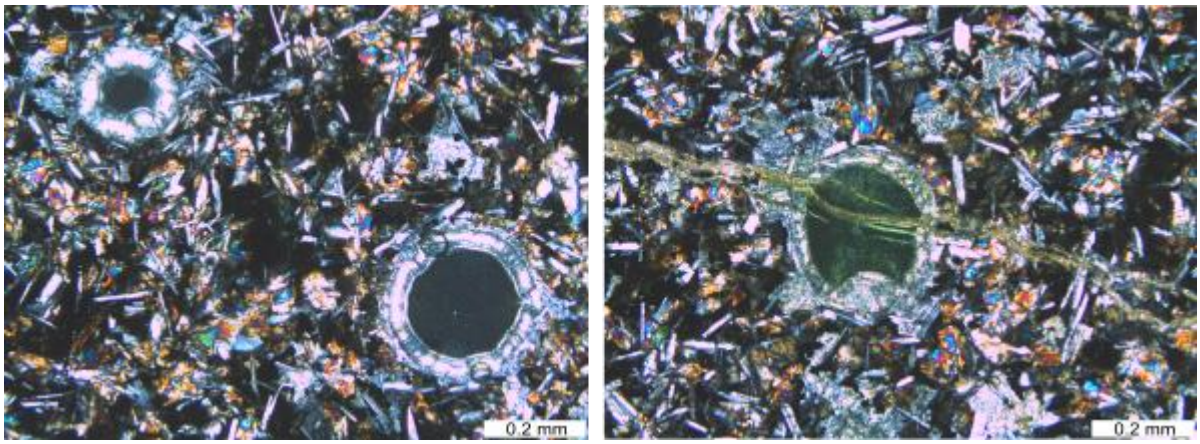

Figure 0.3Amygdaloidal texture, filling of silica and alteration products. Glomeroporphyritic texture of plagioclase crystals, and presence of hydrothermal micro-veins cutting a zeolite. Crossed Nicols.

Sample ID	**CGS-5**
Rock type	Igneous, basalt
Outcrop name	Predreira CGS
Geological Unit	Serra Geral Formation
Province	Paraná-Etendeka, Paraná basin.
Location	SP, Brazil

Microscopic textures	
Structures	Microvesicles, amygdales
Crystallinity	Hipocrystalline
Granularity	Microcrystalline
Crystal size	Very fine
Crystal shape	Hipidiomorphic
Crystalline textures	Porphyritic

Composition (%)	
Ca-Plagioclase	30
Ca-Clinopyroxene	20
Glass	15
Opaques	10
Celadonite	5
Quartz	15
Oxides	5

Summary
Simple pahoehoe basalt from the vesicular zone. Aphanitic microcrystalline texture with microvesicles filled with zeolites and quartz.

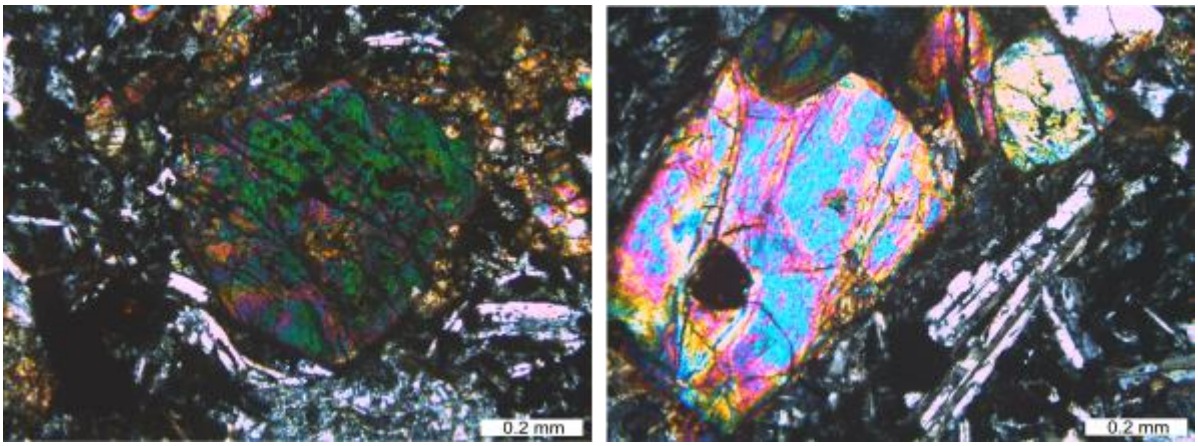

Figure 0.4. Glomeroporphyritic texture of plagioclase, with major crystal of altered olivine. Crossed Nicols.

Sample ID	**BORB-1**
Rock type	Igneous, basalt
Outcrop name	Predreira Borborema
Geological Unit	Serra Geral Formation
Province	Paraná-Etendeka, Paraná basin.
Location	SP, Brazil

Microscopic textures	
Structures	Microvesicles, amygdales
Crystallinity	Hipocrystalline
Granularity	Microcrystalline
Crystal size	Very fine
Crystal shape	Hipidiomorphic
Crystalline textures	Porphyritic

Composition (%)	
Ca-Plagioclase	30
Ca-Clinopyroxene	20
Glass	15
Opaques	15
Oxides	10
Celadonite	5
Quartz	5

Summary
Simple pahoehoe basalt from the vesicular zone. Aphanitic microcrystalline texture with microvesicles filled with zeolites and quartz.

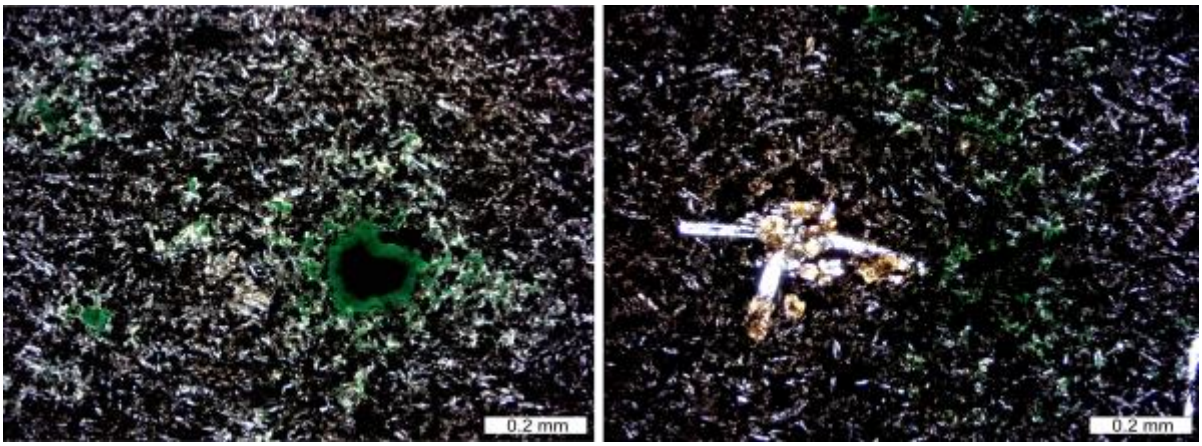

Figure 0.5. Amygdala filled with celadonite (green). Glomeroporphyritic texture characterized by the grouping of plagioclase. Crossed Nicols.

Sample ID	**BORB-2**
Rock type	Igneous, basalt
Outcrop name	Predreira Borborema
Geological Unit	Serra Geral Formation
Province	Paraná-Etendeka, Paraná basin.
Location	SP, Brazil

Microscopic textures	
Structures	Microvesicles, amygdales
Crystallinity	Hipocrystalline
Granularity	Microcrystalline
Crystal size	Very fine
Crystal shape	Hipidiomorphic
Crystalline textures	Porphyritic

Composition (%)	
Ca-Plagioclase	20
Ca-Clinopyroxene	30
Glass	15
Opaques	15
Oxides	10
Celadonite	5
Quartz	5

Summary
Simple pahoehoe basalt from the vesicular zone. Aphanitic microcrystalline texture with microvesicles filled with zeolites and quartz.

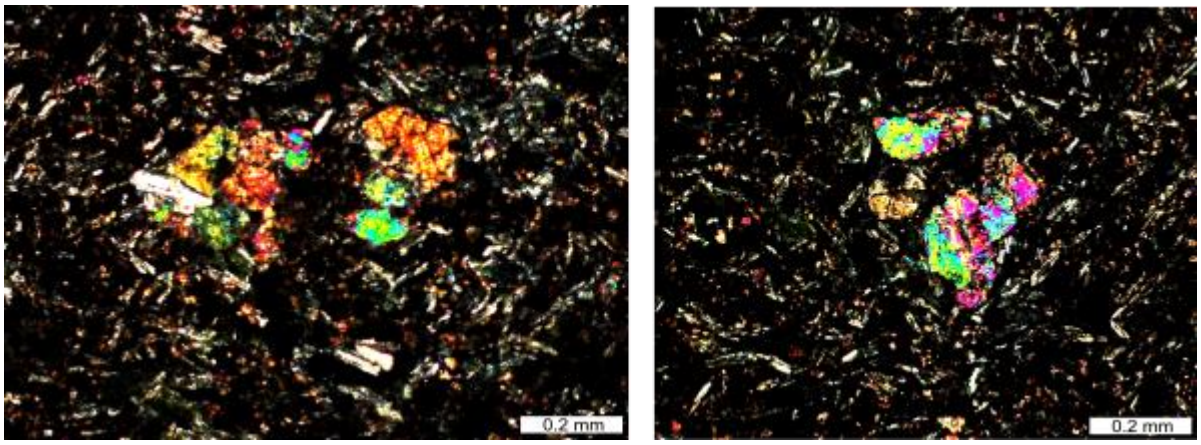

Figure 0.6. Glomeroporphyritic texture with altered augite crystals embedded in fine phanerite matrix. Crossed Nicols.

Sample ID	**BORB-5**
Rock type	Igneous, basalt
Outcrop name	Predreira Borborema
Geological Unit	Serra Geral Formation
Province	Paraná-Etendeka, Paraná basin.
Location	SP, Brazil

Microscopic textures	
Structures	Microvesicles, amygdales
Crystallinity	Hipocrystalline
Granularity	Microcrystalline
Crystal size	Very fine
Crystal shape	Hipidiomorphic
Crystalline textures	Porphyritic

Composition (%)	
Ca-Plagioclase	40
Ca-Clinopyroxene	15
Glass	10
Opaques	15
Oxides	10
Celadonite	5
Quartz	5

Summary
Simple pahoehoe basalt from the vesicular zone. Aphanitic microcrystalline texture with microvesicles filled with zeolites and quartz.

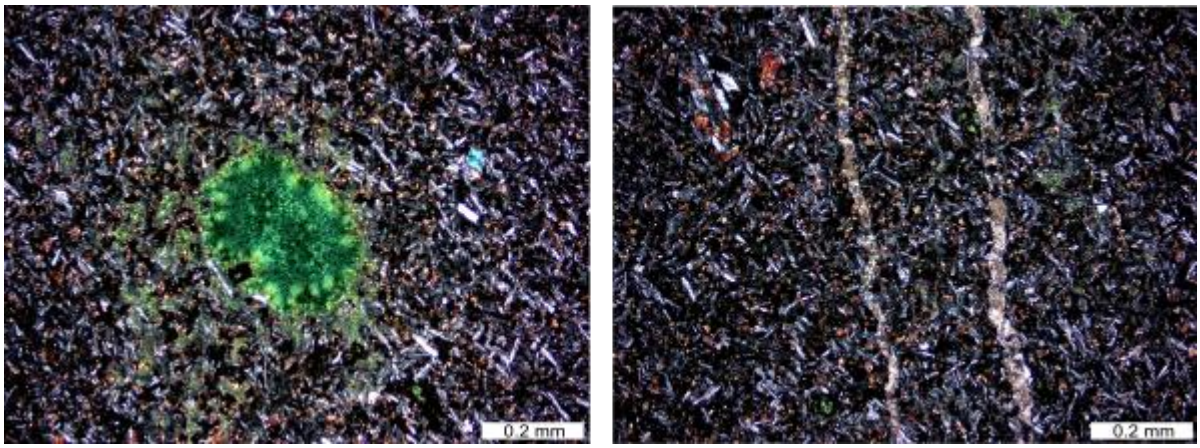

Figure 0.7. Dikititaxitic texture (microvesicular). Hypocrystalline basalt with amygdala filled with celadonite and cutting micro-veins of hydrothermal alteration products. Crossed Nicols.

Sample ID	**BORB-7**
Rock type	Igneous, basalt
Outcrop name	Predreira Borborema
Geological Unit	Serra Geral Formation
Province	Paraná-Etendeka, Paraná basin.
Location	SP, Brazil

Microscopic textures	
Structures	Microvesicles, amygdales
Crystallinity	Hipocrystalline
Granularity	Microcrystalline
Crystal size	Very fine
Crystal shape	Hipidiomorphic
Crystalline textures	Porphyritic

Composition (%)	
Ca-Plagioclase	30
Ca-Clinopyroxene	20
Glass	15
Opaques	10
Oxides	10
Celadonite	10
Quartz	5

Summary
Simple pahoehoe basalt from the vesicular zone. Aphanitic microcrystalline texture with microvesicles filled with zeolites and quartz.

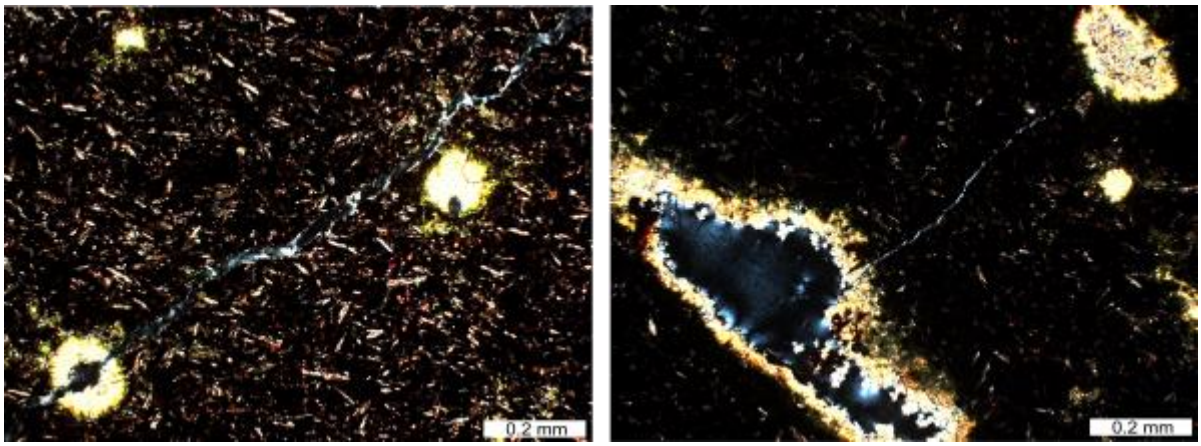

Figure 0.8. Dikititaxitic texture, characterized by microvesicles and stretched vesicles filled with silica and cutting veins of quartz.

Sample ID	**CARR-1**
Rock type	Igneous, basalt
Outcrop name	Predreira Carrazcosa
Geological Unit	Serra Geral Formation
Province	Paraná-Etendeka, Paraná basin.
Location	SP, Brazil

Microscopic textures	
Structures	Microvesicles, amygdales
Crystallinity	Hipocrystalline
Granularity	Microcrystalline
Crystal size	Very fine
Crystal shape	Hipidiomorphic
Crystalline textures	Porphyritic

Composition (%)	
Ca-Plagioclase	40
Ca-Clinopyroxene	25
Glass	15
Opaques	15
Oxides	10

Summary
Basalt samples belong to the pahoehoe ponded facies, present hypocrystalline matrix composed of calcic clinopyroxene mainly augite (15-40%), calcic plagioclase mainly labradorite (25-50%) and volcanic glass (20-40%). Veins are composed of carbonates, silica and celadonite. Because samples were taken from a massive flow, the colour is preserved dark gray to black.

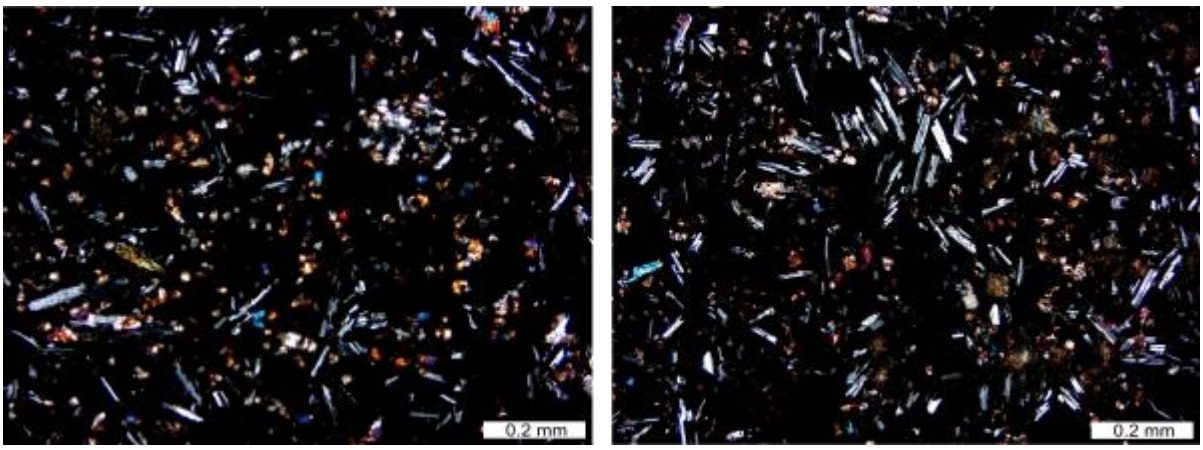

Figure 0.9. Hypocrystalline basalt, composed of plagioclase and augite. Crossed Nicols.

Sample ID	**CARR-3**
Rock type	Igneous, basalt
Outcrop name	Predreira Carrazcosa
Geological Unit	Serra Geral Formation
Province	Paraná-Etendeka, Paraná basin.
Location	SP, Brazil

Microscopic textures	
Structures	Microvesicles, amygdales
Crystallinity	Hipocrystalline
Granularity	Microcrystalline
Crystal size	Very fine
Crystal shape	Hipidiomorphic
Crystalline textures	Porphyritic

Composition (%)	
Ca-Plagioclase	40
Ca-Clinopyroxene	25
Glass	20
Opaques	8
Oxides	7

Summary
Basalt samples belong to the pahoehoe ponded facies, present hypocrystalline matrix composed of calcic clinopyroxene mainly augite (15-40%), calcic plagioclase mainly labradorite (25-50%) and volcanic glass (20-40%). Veins are composed of carbonates, silica and celadonite. Because samples were taken from a massive flow, the colour is preserved dark gray to black.

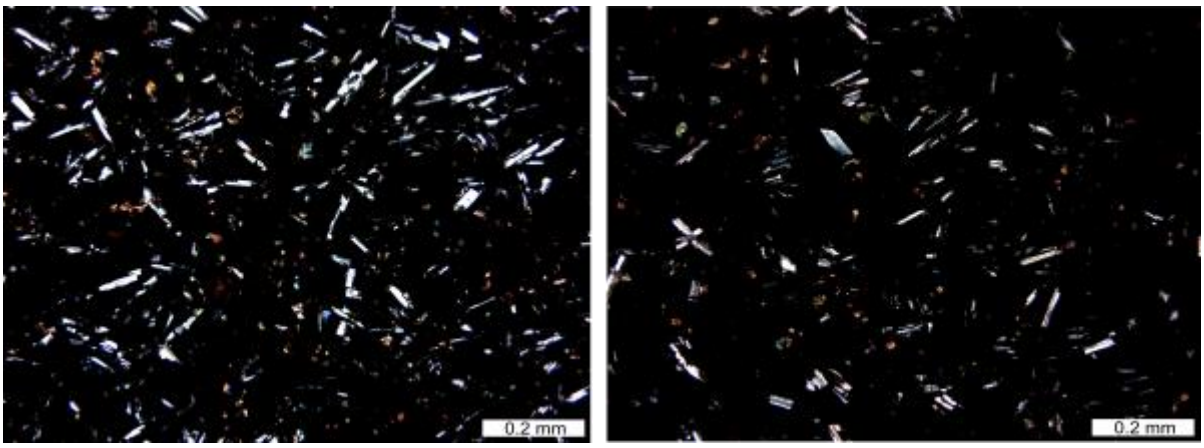

Figure 0.10. Hypocrystalline basalt, composed of microliths of plagioclase and augite. Crossed Nicols.

Sample ID	**CARR-6**
Rock type	Igneous, basalt
Outcrop name	Predreira Carrazcosa
Geological Unit	Serra Geral Formation
Province	Paraná-Etendeka, Paraná basin.
Location	SP, Brazil

Microscopic textures	
Structures	Microvesicles, amygdales
Crystallinity	Hipocrystalline
Granularity	Microcrystalline
Crystal size	Very fine
Crystal shape	Hipidiomorphic
Crystalline textures	Porphyritic

Composition (%)	
Ca-Plagioclase	35
Ca-Clinopyroxene	25
Glass	20
Opaques	10
Oxides	7
Celadonite	3

Summary
Basalt samples belong to the pahoehoe ponded facies, present hypocrystalline matrix composed of calcic clinopyroxene mainly augite (15-40%), calcic plagioclase mainly labradorite (25-50%) and volcanic glass (20-40%). Veins are composed of carbonates, silica and celadonite. Because samples were taken from a massive flow, the colour is preserved dark gray to black.

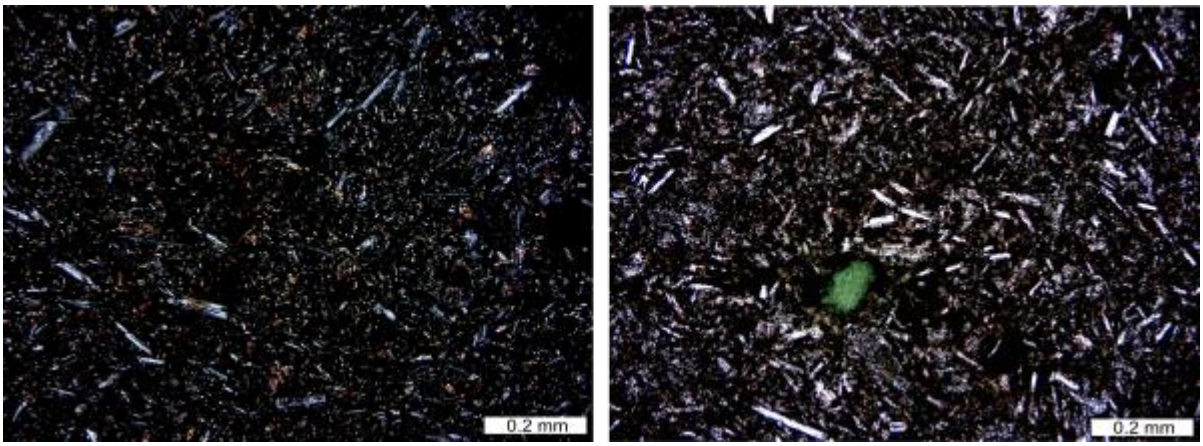

Figure 0.11. Glomeroporphyritic texture, characterized by the grouping of plagioclase and presence of a microvesicle filled with celadonite.

Sample ID	**CARR-7**
Rock type	Igneous, basalt
Outcrop name	Predreira Carrazcosa
Geological Unit	Serra Geral Formation
Province	Paraná-Etendeka, Paraná basin.
Location	SP, Brazil

Microscopic textures	
Structures	Microvesicles, amygdales
Crystallinity	Hipocrystalline
Granularity	Microcrystalline
Crystal size	Very fine
Crystal shape	Hipidiomorphic
Crystalline textures	Porphyritic

Composition (%)	
Ca-Plagioclase	30
Ca-Clinopyroxene	25
Glass	20
Opaques	15
Oxides	5
Celadonite	5

Summary

Basalt samples belong to the pahoehoe ponded facies, present hypocrystalline matrix composed of calcic clinopyroxene mainly augite (15-40%), calcic plagioclase mainly labradorite (25-50%) and volcanic glass (20-40%). Veins are composed of carbonates, silica and celadonite. Because samples were taken from a massive flow, the colour is preserved dark gray to black.

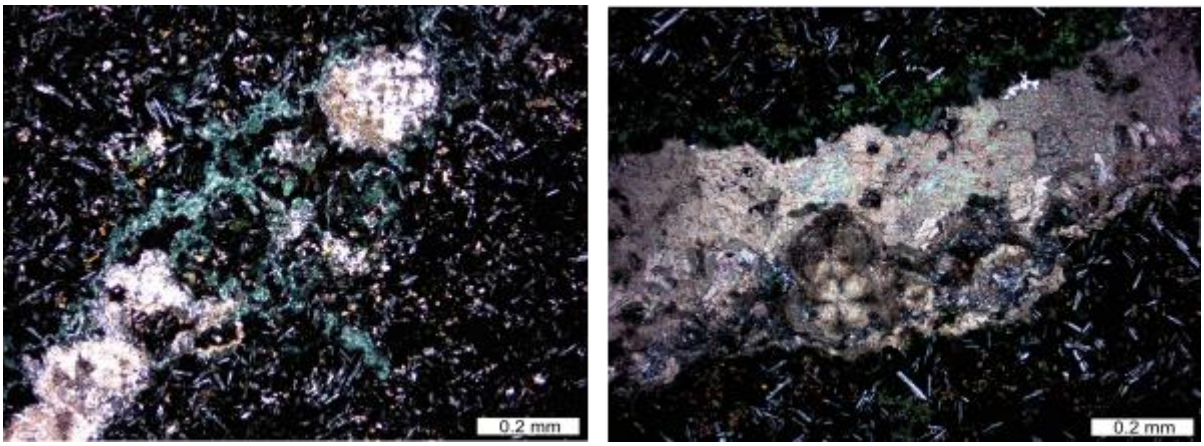

Figure 0.12. Hypocrystalline basalt with presence of hydrothermal alteration veins, filled with silica, carbonates and celadonite. Crossed Nicols.

Sample ID	**IND-1**
Rock type	Igneous, basalt
Outcrop name	Predreira Inderp
Geological Unit	Serra Geral Formation
Province	Paraná-Etendeka, Paraná basin.
Location	SP, Brazil

Microscopic textures	
Structures	Microvesicles, amygdales
Crystallinity	Hipocrystalline
Granularity	Microcrystalline
Crystal size	Very fine
Crystal shape	Hipidiomorphic
Crystalline textures	Porphyritic

Composition (%)	
Ca-Plagioclase	40
Ca-Clinopyroxene	20
Glass	15
Opaques	10
Oxides	10
Celadonite	5

Summary

Basalt samples belong to the pahoehoe ponded facies, present hypocrystalline matrix composed of calcic clinopyroxene mainly augite (15-40%), calcic plagioclase mainly labradorite (25-50%) and volcanic glass (20-40%). Veins are composed of carbonates, silica and celadonite. Because samples were taken from a massive flow, the colour is preserved dark gray to black.

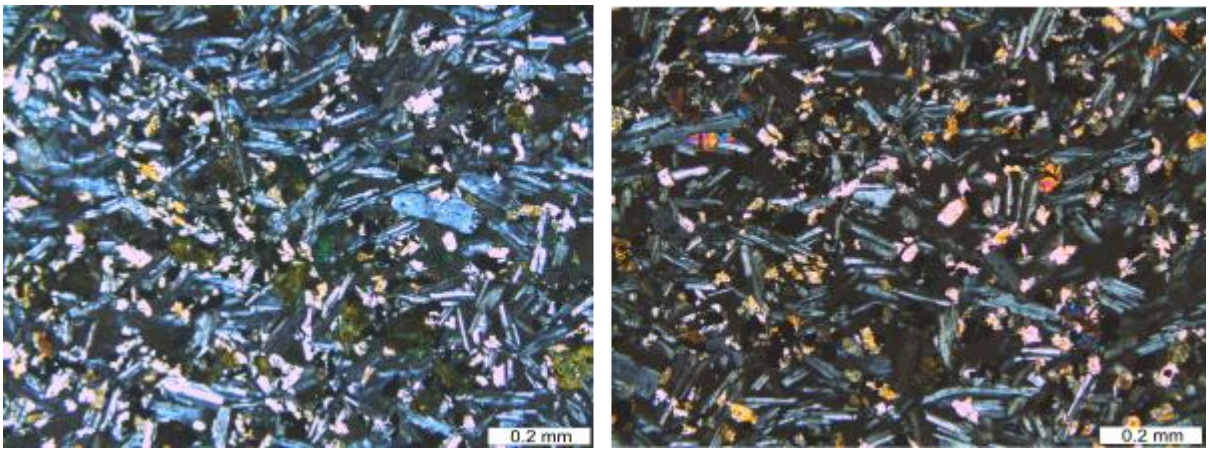

Figure 0.13. Basaltic matrix of fine phaneritic equigranular texture. Glomeroporphyritic texture of plagioclase crystals with intergranular augite. Crossed Nicols.

Sample ID	**IND-4**
Rock type	Igneous, basalt
Outcrop name	Predreira Inderp
Geological Unit	Serra Geral Formation
Province	Paraná-Etendeka, Paraná basin.
Location	SP, Brazil

Microscopic textures	
Structures	Microvesicles, amygdales
Crystallinity	Hipocrystalline
Granularity	Microcrystalline
Crystal size	Very fine
Crystal shape	Hipidiomorphic
Crystalline textures	Porphyritic

Composition (%)	
Ca-Plagioclase	30
Ca-Clinopyroxene	25
Glass	20
Opaques	15
Oxides	10

Summary
Basalt samples belong to the pahoehoe ponded facies, present hypocrystalline matrix composed of calcic clinopyroxene mainly augite (15-40%), calcic plagioclase mainly labradorite (25-50%) and volcanic glass (20-40%). Veins are composed of carbonates, silica and celadonite. Because samples were taken from a massive flow, the colour is preserved dark gray to black.

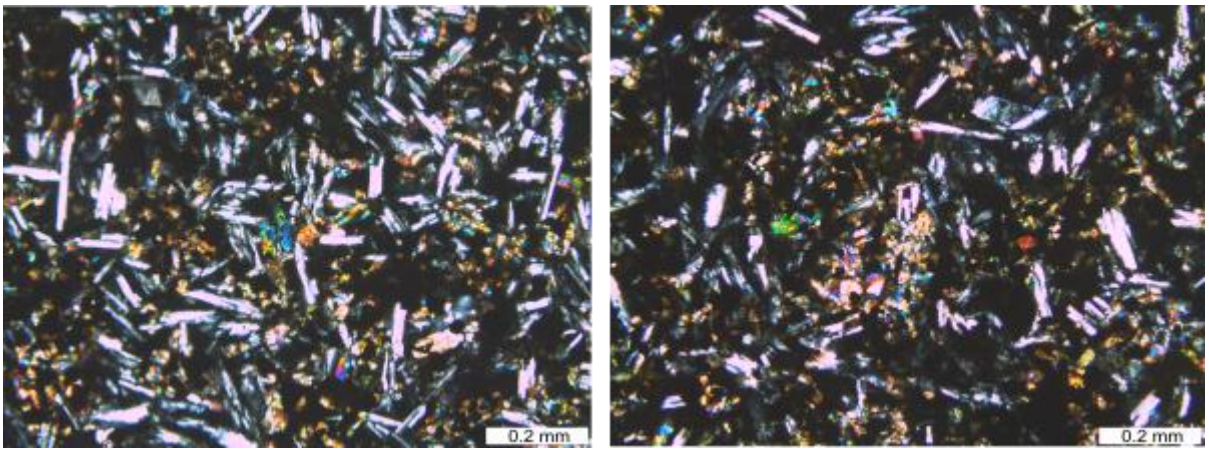

Figure 0.14. Plagioclase glomero-crystals in very fine phaneritic matrix

Sample ID	**IND-5**
Rock type	Igneous, basalt
Outcrop name	Predreira Inderp
Geological Unit	Serra Geral Formation
Province	Paraná-Etendeka, Paraná basin.
Location	SP, Brazil

Microscopic textures	
Structures	Microvesicles, amygdales
Crystallinity	Hipocrystalline
Granularity	Microcrystalline
Crystal size	Very fine
Crystal shape	Hipidiomorphic
Crystalline textures	Porphyritic

Composition (%)	
Ca-Plagioclase	35
Ca-Clinopyroxene	30
Glass	15
Opaques	15
Oxides	5

Summary
Basalt samples belong to the pahoehoe ponded facies, present hypocrystalline matrix composed of calcic clinopyroxene mainly augite (15-40%), calcic plagioclase mainly labradorite (25-50%) and volcanic glass (20-40%). Veins are composed of carbonates, silica and celadonite. Because samples were taken from a massive flow, the colour is preserved dark gray to black.

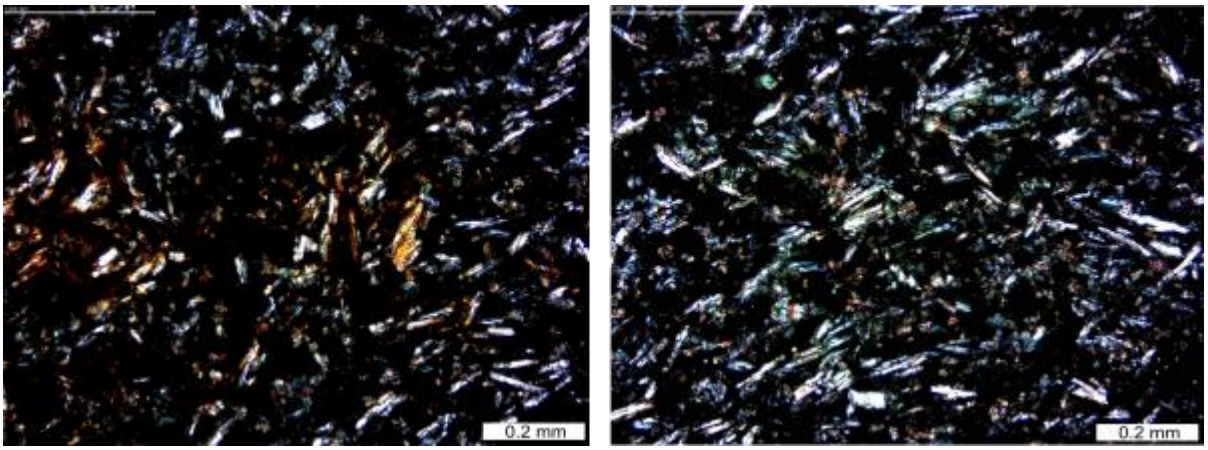

Figure 0.15. Plagioclase microliths in glassy matrix. Presence of oxide layer spread over the matrix. Crossed Nicols.

Sample ID	**IND-9**
Rock type	Igneous, basalt
Outcrop name	Predreira Inderp
Geological Unit	Serra Geral Formation
Province	Paraná-Etendeka, Paraná basin.
Location	SP, Brazil

Microscopic textures	
Structures	Microvesicles, amygdales
Crystallinity	Hipocrystalline
Granularity	Microcrystalline
Crystal size	Very fine
Crystal shape	Hipidiomorphic
Crystalline textures	Porphyritic

Composition (%)	
Ca-Plagioclase	32
Ca-Clinopyroxene	25
Glass	20
Opaques	15
Oxides	5
Celadonite	3

Summary

Basalt samples belong to the pahoehoe ponded facies, present hypocrystalline matrix composed of calcic clinopyroxene mainly augite (15-40%), calcic plagioclase mainly labradorite (25-50%) and volcanic glass (20-40%). Veins are composed of carbonates, silica and celadonite. Because samples were taken from a massive flow, the colour is preserved dark gray to black.

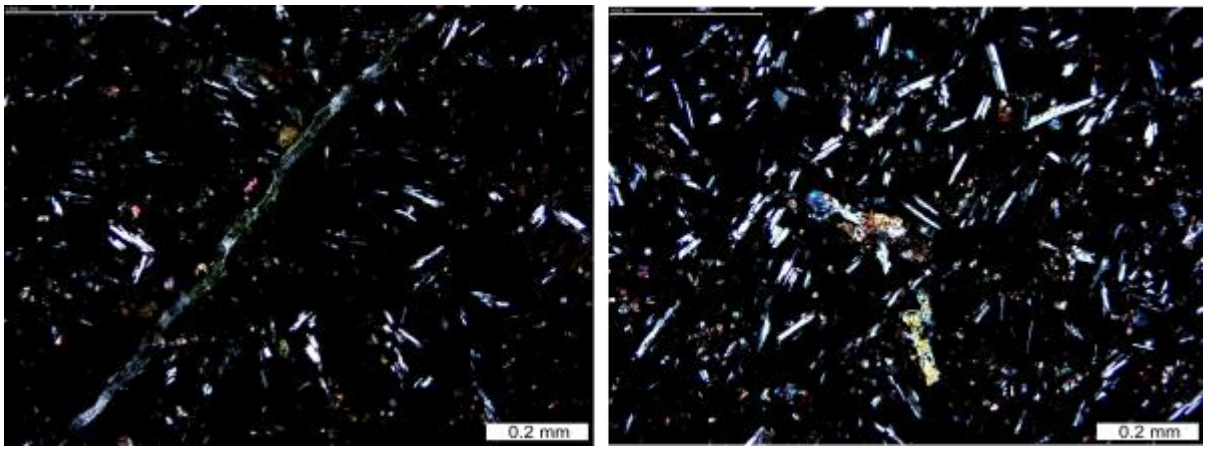

Figure 0.16. Plagioclase microliths in glassy matrix. Presence of a micro-vein of hydrothermal alteration products. Crossed Nicols.